UC Riverside

UC Riverside Electronic Theses and Dissertations

Title

Idle Resource Conversion Through Thermal and Chemical Methods Into Value-Added Products

Permalink

https://escholarship.org/uc/item/6df2d2nt

Author

Gale, Mark Mitsuo

Publication Date

2022

Copyright Information

Peer reviewed|Thesis/dissertation

UNIVERSITY OF CALIFORNIA
RIVERSIDE

Idle Resource Conversion Through Thermal and Chemical Methods Into Value-Added
Products

A Dissertation submitted in partial satisfaction
of the requirements for the degree of

Doctor of Philosophy

in

Chemical and Environmental Engineering

by

Mark Mitsuo Gale

June 2022

Dissertation Committee:
      Dr. Kandis Leslie Abdul-Aziz, Chairperson
      Dr. Charles E. Wyman
      Dr. Jianzhong Wu

The Dissertation of Mark Mitsuo Gale is approved:

_____

_____

_____

Committee Chairperson

University of California, Riverside

Acknowledgements

I would like to acknowledge and express my gratitude towards my advisor, Dr. Kandis Leslie Abdul-Aziz. Her guidance, support, and knowledge helped me grow tremendously in the past 4 years. I gained an immense amount of insight in research and in life from her. I will be forever grateful for her continuous pushes, support, and opportunities. I would like to thank Dr. Charles E. Wyman for being another mentor to me as he imparted wisdom and industry knowledge. Dr. Wyman's lab also supplied the corn stover for many of my experiments. Also, I would like to thank Dr. Charles Cai for his advice and knowledge on Parr reactors and lignin.

I have also been fortunate to have amazing labmates. Thank you; Luz Cruz, Seongbin Jo, Tu Nguyen, Soham Shah, Barnali Sutradhar, and Somchate Wasantwisut, for all their feedback and help in the laboratory. I'd like to thank, Byrce Biship, Irene Cruz-Rubio, Monica Fajardo, James Feeney, Allison Hong, Marissa Moreno, Peter Nguyen, Ogechukwu Ogbechie, Eric Song, Bradley Troung, Andrew Wassef, and Richard Yang; all who were student researchers who I mentored. I learned many invaluable lessons from them, and they helped support all the research I produced. I want to specially recognize Marissa Moreno for her hard work and dedication with the hydrothermal carbonization, slow pyrolysis, and activated carbon experiments. I'd also like to specially recognize Peter Nguyen with his hard work and dedication on PET co-pyrolysis and activation experiments.

The text of this dissertation, in part, is a reprint of the material as it appears in "Physiochemical Properties of Biochar and Activated Carbon from Biomass Residue:

A portion of the research presented in this dissertation has been previously published as:

Gale, M.; Nguyen, T.; Moreno, M.; Gilliard-AbdulAziz, K. L. Physiochemical Properties of Biochar and Activated Carbon from Biomass Residue: Influence of Process Conditions to Adsorbent Properties. *ACS Omega* **2021**, *6* (15), 10224–10233. https://doi.org/10.1021/acsomega.1c00530.

Gale, M.; Cai, C. M.; Gilliard-Abdul-Aziz, K. L. Heterogeneous Catalyst Design Principles for the Conversion of Lignin into High-Value Commodity Fuels and Chemicals. *ChemSusChem* **2020**, *13* (8), 1947–1966. https://doi.org/10.1002/cssc.202000002.

Dedication

To my family and friends.

ABSTRACT OF THE DISSERTATION

Idle Resource Conversion Through Thermal and Chemical Methods Into Value-Added
Products

by

Mark Mitsuo Gale

Doctor of Philosophy, Graduate Program in Chemical and Environmental Engineering
University of California, Riverside, June 2022
Dr. Kandis Leslie Abdul-Aziz, Chairperson

Idle resource utilization will be a part of the solution for climate change. Agricultural waste like corn stover (CS) is predominantly left on the field and can be sustainably collected. Plastic waste is a growing environmental issue that is in dire need of methods to reduce accumulation. Agricultural and plastic waste have the potential to be converted into valuable products which can offset the reliance on nonrenewable resources.

This dissertation evaluates the physiochemical properties of the solid fraction, biochar, of hydrothermal carbonization (HTC), slow pyrolysis (SP), and co-pyrolysis (CoSP). SP and CoSP utilize oxygen-free environments along with high temperatures to carbonize a carbon feedstock. HTC uses an oxygen-free environment with subcritical water and more moderate temperatures to carbonize. Furthermore, this work explores the chemical activation of the biochar generated from the aforementioned methods to create an upgraded product, activated carbon (AC). This study reports the influence of parameters during carbonization on the biochar and subsequent AC. The subcritical water in HTC played a crucial role in the more efficient degradation of biomass when compared to SP.

The ACs from the direct method and HTC removed up to 98% of the vanillin, the highest removal of any of the ACs, and produced the highest surface area.

The study of CoSP produced key insights on how polystyrene (PS) and polyethylene terephthalate (PET) interacts with CS. PS is a hydrogen donor and produces lower quality biochar and AC. PET produced high surface area biochar from the acids and oligomers formed during degradation. The oligomers are microplastics which are observed to be on the surface of the biochar and have potential environmental and health concerns. After activation, some of the CS-PET samples had a reduction of surface area due to the interactions between KOH and the products formed during thermal degradation of PET. Overall, the ACs produced from CS and plastics were lower quality in surface area and adsorption capabilities when compared with AC made from CS only. Additional idle resource utilization projects have the foundation developed and await a new researcher.

Table of Contents

List of Figures

List of Tables

Chapter 1 Introduction

1.1 Background Knowledge

The world relies on non-renewable resources that produce an inordinate amount of waste which in turn has adverse effects on the environment. Researching methods to convert idle waste streams into valuable products can create a circular resource economy which will help mitigate environmental harm by reducing the stockpiles of waste. Biomass circular economies help mitigate environmental harm by the full utilization of lignocellulosic biomass waste for energy, products, and chemical commodities[1]. When full utilization methods are not employed, the accumulation of waste and unused resources pile up. In biomass, corn stover is one of the most produced agricultural residues in the United States and is often left on the field[2]. Corn stover, the remnants of harvesting corn, removal is not a common practice and the removal can benefit future crops[3,4]. Over 4,900 million tons of plastic exist in the environment and around 380 million tons of plastic per year is produced annually[5]. There is an abundance of agricultural and plastic waste which have untapped potential that can help offset the reliance on non-renewable resources. Researching methods and processes to fully utilize idle resources are crucial to making an impact on climate change.

Products that have value and applications are essential when promoting circular economies. Biochar can be created by many forms of biomass and has several applications like soil remediation[6], energy generation[7], and adsorption[8]. Biochar is produced from carbonization of biomass. Two techniques used are hydrothermal carbonization (HTC) and pyrolysis. During carbonization, biomass is heated in an inert environment that produces three product streams- biochar (solid), bio-oil (liquid), and a gas phase. HTC uses

subcritical water as a solvent which can allow for lower temperatures when compared to pyrolysis. Pyrolysis has been studied in depth for the bio-oil production, with flash and fast pyrolysis being the preferred method to maximize bio-oil yield[9,10]. Slow pyrolysis is preferred for biochar production. Biochar can be a precursor to activated carbon, another value-added product.

In 2015, the activated carbon market was valued at \$4.7 billion USD and growth is further projected, making activated carbon (AC) a valuable product[11]. Corn stover can be a feedstock to make activated carbon[12,13]. AC has numerous uses including in catalysis, water treatment plants, and air purification[14–17]. Each application has different properties of AC that are desired, and the production of AC can be modified to best suit the specific application.

The addition of adding plastic to biomass for during pyrolysis is known as co-pyrolysis. Co-pyrolysis may be able to "kill two birds with one stone" by tackling the plastic waste challenge. Plastic waste poses many challenges with recycling not being practicable solution[18–21]. Co-pyrolysis is a form of upcycling to create value-added products from multiple feedstocks. Like many carbonization papers, the research focus of co-pyrolysis has been the oil fraction[22–24]. The biochar produced from co-pyrolysis can be a precursor to activated carbon as well. More research on the solid fraction is a necessary step to probe the viability of co-pyrolysis as a solution to idle agricultural and plastic waste.

1.2 Goals and Objectives

The overall goal of this research is to better understand methods to turn waste resources into value-added products. This research focuses on the thermal and chemical

conversion of agricultural and plastic waste into solids. There are two objectives that this work focuses on:

1. **Evaluate the physiochemical properties of biochar and activated carbon produced from corn stover**

This objective focuses on two carbonization techniques: HTC and SP, of corn stover into biochar and the subsequent chemical activation into activated carbon. The solid fraction of carbonization fractions has generally been overlooked and understudied, this work helps bridge the knowledge gap in the field. HTC and pyrolysis are two techniques that are commonly used to produce oils and have a leftover solid fraction that gets tossed aside or used as low-grade fuel. By comparing the physicochemical properties and how they relate to activated carbon, this work can open pathways to economic prosperity in rural America and the renewable energy sector. This objective assesses how different parameters in carbonization affect the end products. The activated carbon is further probed for performance in the adsorption of phenolic compounds.

2. **Evaluate the products formed from the carbonization of corn stover and plastics**

The addition of plastics to pyrolysis of biomass, co-pyrolysis, has shown benefits for the bio-oil fraction; however, the biochar fraction has been glossed over. This objective investigates how the effects of adding polystyrene and PET plastics to corn stover affects the biochar and activated carbon. This work evaluates the change in physiochemical properties of the biochar with different parameters including temperature, dwell duration, and ratio of biomass to plastic. The work will highlight the differences between products

4

of co-pyrolysis and slow pyrolysis. The biochar will further be activated to probe additional physiochemical properties and adsorption of phenolic compounds.

1.3 Organization of Dissertation

The organization of this dissertation is as follows: Chapter 2 begins with the work of carbonizing corn stover to produce biochar and activated carbon. The chapter discusses two carbonization techniques, hydrothermal carbonization and slow pyrolysis, to produce biochar. Temperature, duration, and ratio parameters were tested to determine physiochemical properties of biochar. Activated carbon was produced using a chemical activator, KOH, and the biochar produced from the carbonization technique- known as a two-step method. These activated carbons were compared to each other and a direct method. The activated carbons and biochars were characterized by SEM, XRD, BET surface area, FTIR, and XPS. The activated carbons were probed for vanillin adsorption experiments.

Chapter 3 discusses the addition of plastics to corn stover and studies the effects of co-pyrolysis. Polystyrene and polyethylene terephthalate (PET) plastics were investigated for the effects on corn stover biochar and activated carbon. The different co-pyrolysis biochars and activated carbons analyzed against each other as well as the same products from slow pyrolysis. The same characterization and vanillin experiments from Chapter 2 were conducted to help probe the distinct properties of the biochar and activated carbon.

Chapter 4 provides a literature review on heterogenous catalytic depolymerization of lignin into fuels and chemicals. Depolymerization of lignin is another technique to promote a bicircular economy. The chapter highlights different catalysis design principles

when converting lignin into value-added products. The review has a focus on bimetallic catalysts. Research furthering this was not conducted due to challenges in funding of the project.

Chapter 5 focuses on projects that did not get pursued and could have future research project developed from them. This work is comprised of Soxhlet extraction, PVC dechlorination, and orange peel biochar for plant growth. Finally, Chapter 6 highlights the findings and significance of the dissertation and the research conducted. Chapter 6 wraps up the dissertation.

1.4 References

(1)   Sherwood, J. The Significance of Biomass in a Circular Economy. *Bioresour. Technol.* **2020**, *300*, 122755. https://doi.org/10.1016/j.biortech.2020.122755.

(2)   Oak Ridge National Laboratory. US Billion Ton Update: Biomass Supply for a Bioenergy and Bioproducts Industry. *US DOE Energy Effic. Renew. Energy* **2011**, 1–195. https://doi.org/10.1089/ind.2011.7.375.

(3)   Obrycki, J. F.; Karlen, D. L. Is Corn Stover Harvest Predictable Using Farm Operation, Technology, and Management Variables? *Agron. J.* **2018**, *110* (2), 749–757. https://doi.org/10.2134/agronj2017.08.0504.

(4)   Taylor, H. M.; Welch, L. F.; Unger, P.; Stelly, M.; Kral, D. M.; Nauseef, J. H. Influence of Crop Residues on Plant Diseases. In *Crop Residue Management Systems*; 1978.

(5)   Geyer, R.; Jambeck, J. R.; Law, K. L. Production, Use, and Fate of All Plastics Ever Made. *Sci. Adv.* **2017**, *3* (7), 1–5. https://doi.org/10.1126/sciadv.1700782.

(6)   Sizmur, T.; Quilliam, R.; Puga, A. P.; Moreno-Jiménez, E.; Beesley, L.; Gomez-Eyles, J. L. Application of Biochar for Soil Remediation. *Agric. Environ. Appl. Biochar Adv. Barriers* **2015**, *63*, 295–324. https://doi.org/10.2136/sssaspecpub63.2014.0046.5.

(7)   Liu, W. J.; Jiang, H.; Yu, H. Q. Emerging Applications of Biochar-Based Materials for Energy Storage and Conversion. *Energy Environ. Sci.* **2019**, *12* (6), 1751–1779. https://doi.org/10.1039/c9ee00206e.

(8)   Gai, X.; Wang, H.; Liu, J.; Zhai, L.; Liu, S.; Ren, T.; Liu, H. Effects of Feedstock and Pyrolysis Temperature on Biochar Adsorption of Ammonium and Nitrate. *PLoS One* **2014**, *9* (12), 1–19. https://doi.org/10.1371/journal.pone.0113888.

(9)   Li, L.; Rowbotham, J. S.; Christopher Greenwell, H.; Dyer, P. W. *An Introduction to Pyrolysis and Catalytic Pyrolysis: Versatile Techniques for Biomass Conversion*; 2013. https://doi.org/10.1016/B978-0-444-53878-9.00009-6.

(10)   Park, J.; Lee, Y.; Ryu, C.; Park, Y. K. Slow Pyrolysis of Rice Straw: Analysis of Products Properties, Carbon and Energy Yields. *Bioresour. Technol.* **2014**, *155*, 63–70. https://doi.org/10.1016/j.biortech.2013.12.084.

(11)   Asimakopoulos, G.; Baikousi, M.; Salmas, C.; Bourlinos, A. B.; Zboril, R.; Karakassides, M. A. Advanced Cr(VI) Sorption Properties of Activated Carbon Produced via Pyrolysis of the "Posidonia Oceanica" Seagrass. *J. Hazard. Mater.* **2021**, *405* (September 2020). https://doi.org/10.1016/j.jhazmat.2020.124274.

(12) Ioannidou, O.; Zabaniotou, A. Agricultural Residues as Precursors for Activated Carbon Production-A Review. *Renew. Sustain. Energy Rev.* **2007**, *11* (9), 1966–2005. https://doi.org/10.1016/j.rser.2006.03.013.

(13) Zhang, T.; Walawender, W. P.; Fan, L. T.; Fan, M.; Daugaard, D.; Brown, R. C. Preparation of Activated Carbon from Forest and Agricultural Residues through CO2 Activation. *Chem. Eng. J.* **2004**, *105* (1–2), 53–59. https://doi.org/10.1016/j.cej.2004.06.011.

(14) Zhai, Y.; Xu, G.; Zhang, Y.; Liu, X.; Ma, Y.; Li, C. Depolymerization of Lignin via a Non-Precious Ni–Fe Alloy Catalyst Supported on Activated Carbon. *Green Chem.* **2017**, *19* (8), 1895–1903. https://doi.org/10.1039/c7gc00149e.

(15) Abumaizar, R. J.; Kocher, W. M.; Smith, E. H. Biofiltration of Benzene Contaminated Air Streams Using Compost-Activated Carbon Filter Media. *J. Hazard. Mater.* **1998**, *60* (2), 111–126. https://doi.org/https://doi.org/10.1016/S0304-3894(97)00046-0.

(16) Reungoat, J.; Escher, B. I.; Macova, M.; Argaud, F. X.; Gernjak, W.; Keller, J. Ozonation and Biological Activated Carbon Filtration of Wastewater Treatment Plant Effluents. *Water Res.* **2012**, *46* (3), 863–872. https://doi.org/10.1016/j.watres.2011.11.064.

(17) Spahis, N.; Addoun, A.; Mahmoudi, H.; Ghaffour, N. Purification of Water by Activated Carbon Prepared from Olive Stones. *Desalination* **2008**, *222*, 519–527. https://doi.org/10.1016/j.desal.2007.02.065.

(18) Hopewell, J.; Dvorak, R.; Kosior, E. Plastics Recycling: Challenges and Opportunities. *Philos. Trans. R. Soc. B Biol. Sci.* **2009**, *364* (1526), 2115–2126. https://doi.org/10.1098/rstb.2008.0311.

(19) Rahimi, A. R.; Garciá, J. M. Chemical Recycling of Waste Plastics for New Materials Production. *Nat. Rev. Chem.* **2017**, *1*, 1–11. https://doi.org/10.1038/s41570-017-0046.

(20) Celik, G.; Kennedy, R. M.; Hackler, R. A.; Ferrandon, M.; Tennakoon, A.; Patnaik, S.; Lapointe, A. M.; Ammal, S. C.; Heyden, A.; Perras, F. A.; et al. Upcycling Single-Use Polyethylene into High-Quality Liquid Products. *ACS Cent. Sci.* **2019**, *5* (11), 1795–1803. https://doi.org/10.1021/acscentsci.9b00722.

(21) Ragaert, K.; Delva, L.; Van Geem, K. Mechanical and Chemical Recycling of Solid Plastic Waste. *Waste Manag.* **2017**, *69*, 24–58. https://doi.org/10.1016/j.wasman.2017.07.044.

(22) Zhang, B.; Zhong, Z.; Ding, K.; Song, Z. Production of Aromatic Hydrocarbons

from Catalytic Co-Pyrolysis of Biomass and High Density Polyethylene: Analytical Py-GC/MS Study. *Fuel* **2015**, *139*, 622–628. https://doi.org/10.1016/j.fuel.2014.09.052.

(23) Önal, E.; Uzun, B. B.; Pütün, A. E. Bio-Oil Production via Co-Pyrolysis of Almond Shell as Biomass and High Density Polyethylene. *Energy Convers. Manag.* **2014**, *78*, 704–710. https://doi.org/10.1016/j.enconman.2013.11.022.

(24) Abnisa, F.; Daud, W. M. . W.; Sahu, J. N. Pyrolysis of Mixtures of Palm Shell and Polystyrene: An Optional Method to Produce a High-Grade of Pyrolysis Oil. *Environ. Prog. Sustain. Energy* **2014**, *33* (3), 1026–1033. https://doi.org/10.1002/ep.11850.

Chapter 2 Physiochemical Properties of Biochar and Activated Carbon Produced from Corn Stover Carbonization

The text of this dissertation chapter, in full, is a reprint of the material as it appears in "Physiochemical Properties of Biochar and Activated Carbon from Biomass Residue: Influence of Process Conditions to Adsorbent Properties" 2021. The text has been modified to fit the dissertation guidelines. The co-author Dr. Kandis Leslie Gilliard-Abdul-Aziz listed in that publication directed and supervised the research which forms the basis for this dissertation chapter.

2.1 Abstract

This study evaluates the influence of hydrothermal carbonization (HTC) or slow pyrolysis (SP) process conditions on the physicochemical properties of precursor biochars and activated carbon (AC). The AC is achieved through a direct or two-step method with subsequent chemical activation using KOH. A theory is developed on the biochar propensity to be chemically activated based on the lignocellulosic structure composition. X-ray photoelectron spectroscopy (XPS) elemental analysis shows that the O/C ratio decreases after chemical activation for HTC biochar but remains the same for SP biochar. X-ray powder diffraction (XRD) indicates that SP biochar and all AC have broad amorphous carbon peaks, whereas the corn stover and HTC biochar have distinct cellulosic crystalline peaks. Vanillin absorbent experiments were performed on the various activated carbons with up to 98% reduction shown. The best absorbent for vanillin was the AC produced directly from corn stover, followed by AC HTC, and then AC SP.

2.2 Introduction

In a circular bioeconomy, maximizing the use of lignocellulosic biomass waste is paramount for the full utilization of energy, products, and chemical commodities with minimal environmental harm[1]. For example, corn stover is one of the most produced agricultural residues in the United States and is one of the primary feedstocks for cellulosic ethanol[2]. Corn stover, consisting of stalks, leaves, and cobs, was removed from approximately 6.3% of corn operations in the US, suggesting an ample supply with minimal demand[3]. In addition to bioethanol, corn stover can be used for other purposes, including fibers, hydrocarbons, and animal feed. The full utilization of lignocellulosic

11

biomass by turning corn stover into value-added products will help progress the circular bioeconomy, increase the agricultural sector's profitability, and decrease the dependence on non-renewable resources.

One beneficial and low-cost value-added product that can be produced from corn stover is activated carbon[4,5]. Activated carbon (AC) is a high surface area, porous structure made from various carbon sources using either a direct one-step or a two-step process requiring an initial carbon precursor before activation. AC has an abundance of uses[6–8] especially as adsorbents for wastewater treatment. Wastewater treatment plants utilize AC to remove pollutants, such as dyes, pharmaceuticals, heavy metals, and organic contaminants. The removal of industrial phenolic waste such as vanillin is especially important because they have adverse environmental effects[9–11]. The adsorbent capacity is often one of the key metrics used to evaluate the effectiveness of activated carbons. By converting agricultural residues into AC for wastewater treatment, it can lower costs and create a more sustainable pathway to clean drinking water.

Activated carbon properties, such as surface functional groups, pore size, and surface area, can be modified to fit the desired criterion or application. The AC properties can often be tailored by changing the reaction parameters for the preparation of biochar precursors and activation methods. One way to form biochar precursors is the use of hydrothermal carbonization (HTC). HTC is a green process that uses mild temperatures, water as a solvent, and an inert environment. HTC can produce three fractions: solid (char), liquid (bio-oil), and gas. The process is performed at a point where water is subcritical, which is useful in breaking down the polymeric backbone of the biomass. HTC uses

temperatures between 180 to 250 °C[12] and has several advantages compared to pyrolysis, including lower energy inputs, no need to dry the feedstock, reduced ash content, and higher solid yields[13]. Pyrolysis, an alternative to HTC, is a standard thermal method to convert biomass into biochar. It can use low or high temperatures with little to no oxygen. There are three major categories of pyrolysis based on the duration and associated temperature ramp: flash, slow, and fast pyrolysis[14]. For slow pyrolysis, the ramp rate is on the order of minutes or hours, ranging between 10 °C/min to 10 °C/h. The temperature range is lower than that of the flash pyrolysis, less than 500 °C[15]. To optimize biochar production, one should focus on utilizing low temperatures and moderate ramp rates like that of slow pyrolysis.

AC can be made from biochar precursors using either physical or chemical activation. Physical activation requires two separate steps: first with pyrolysis or thermal treatment, then exposure to an oxidizing gas such as steam or CO_2[16]. Chemical activation can be done either by a direct one-step process or a two-step process. The direct one-step process involves impregnating or mixing biomass with a chemical activating agent under thermal treatment[17]. The one-step method performs the carbonization and activation step simultaneously. The two-step process is done by an initial carbonization step to form biochar followed by thermal activation[18]. Several types of chemicals can be used as activating agents, including K_2CO_3, NaOH, $ZnCl_2$, and KOH[18–20]. In all cases, the activating agent is used with an ideal ratio to biomass to ensure complete activation and formation of pores and improved surface area. Several groups have studied the activation mechanism using KOH. Huang et al.[21] found KOH reacts with carbon around 530 °C to

13

produce K_2O and K_2CO_3, which react to create metallic K and a graphite-like microcrystalline structure. Otowa et al.[22] also found the formation of K_2O by dehydration and K_2CO_3 by a carbonate reaction. Metallic K is formed and intercalated in the carbon matrix at high temperatures, resulting in atomic layers of carbon being widened and forming pores.

The method used for the biochar precursor preparation can ultimately affect the AC's properties (surface area, porosity, and prevalent surface functional groups). This study performs an in-depth investigation on how biochar precursors derived from the direct method, HTC, and slow pyrolysis can affect the physiochemical properties of activated carbons. Vanillin adsorption experiments are used to probe the adsorption capabilities of AC. Vanillin was chosen to represent a phenolic pollutant in water. We utilized chemical activation with KOH due to its superior dehydrating abilities and propensity to achieve the highest surface areas in activated carbon. There are many studies on using HTC[23–25] or slow pyrolysis[15,26,27] of biomass residues to produce biochar; however, only a few compare the two methods for corn stover[28]. This article analyzes the biochar precursors, activated carbons, and probe the activated carbon's physiochemical and adsorptive properties.

2.3 Materials and Methods

2.3.1 Hydrothermal Carbonization (HTC)

A 300 mL Series 4561 Bench Parr Reactor was used for the HTC reactions. Corn stover was milled to 1 mm. DI water and corn stover were added 8:1 by mass, unless noted otherwise, to the reactor and purged with nitrogen for 10 minutes. The reactor was heated and held at the desired dwell temperature for 1, 2, or 4 hours. Once finished, the reactor

was submerged in ice water to stop the reaction. The liquid and solid phases were separated using vacuum filtration. The solid phase was rinsed with 300 mL of DI water to remove most of the bio-oils, leaving the solid biochar behind. While a portion of the liquid phase is not water-soluble and may still be left in the porous solid structure, we believe this is a negligible amount. The biochar was dried overnight in an oven at 105 °C before chemical activation with KOH.

2.3.2 Slow Pyrolysis (SP)

A Thermo Scientific Type 1315M Benchtop Muffle Furnace inside a nitrogen glovebox was used for slow pyrolysis. Corn stover, milled to 1 mm, was placed inside a crucible and purged in a nitrogen environment. The sample was then placed in the muffle furnace and heated to the desired temperature at a ramp rate of 10 °C/min. The sample was held for 1, 4, or 8 hours at the desired temperature, then allowed to cool to room temperature.

2.3.3 Chemical Activation of Biochar

The same muffle furnace setup for the slow pyrolysis experiments was used for the chemical and thermal activation of carbon. The biochar, either from HTC or SP, was combined with KOH in a 2:1 ratio of biochar to KOH by mass. DI water was added to the mixture and stirred for 1 hour to ensure it was homogeneous. The mixture was then dried in an oven at 105 °C. The sample was transferred into the nitrogen environment muffle furnace, heated to 300 °C for 2 hours at a ramp rate of 10 °C/min to remove moisture, then further heated to 800 °C for 3 hours with a ramp rate of 10 °C/min. Once cooled, the sample was washed with 0.1 M HCl solution to neutralize any remaining KOH. The sample was

vacuumed filtered and washed with DI water until the filtrate was pH neutral. The sample, now activated carbon, was dried in an oven overnight at 105 °C before characterization. For the direct chemical activation method, corn stover replaced the biochar in equal amounts and the rest of the procedure for chemical activation remained the same.

2.3.4 Surface Area Analysis

Surface analysis was conducted using the Micromeritics ASAP 2020 and ASAP 2020 Plus physisorption instruments to perform Brunauer-Emmett-Teller (BET) measurements. The sample was loaded and degassed for 4 to 11 hours until an outgassing rate of less than 5 μmHg/min was achieved to ensure moisture and volatile contaminants were removed before analysis. N_2 physisorption and 5-point BET analysis were used to measure surface area, pore-volume, and pore size. The BET was calibrated with a silica-alumina reference material with a standard error of 2.5%. Replicates of most of the biochar and AC were performed to determine the intrinsic errors in the surface areas and pore sizes with 95% confidence levels.

2.3.5 Scanning Electron Microscopy (SEM)

A TESCAN Vega3 SBH SEM was used to capture images of the various corn stover, biochar, and activated carbon samples. A ThermoFisher Scientific NNS450 was also used to capture images of activated carbon samples. Before imaging, the samples were placed under vacuum, purged with argon, then sputter-coated with Au for 10 seconds to improve the clarity of the images. The images were taken between 900-1,700-times magnification with a voltage of 5 kV.

2.3.6 X-ray Diffraction (XRD) and X-ray Photoelectron Spectroscopy (XPS)

A PANalytical Empyrean Series 2 XRD instrument was utilized to evaluate the carbon structures. The emission source was Cu-Kα (1.54056 A wavelength) with a Ni beta filter. A zero-diffraction plate was employed to minimize background peaks. X-ray photoelectron spectroscopy (XPS) characterization was carried out using a Kratos AXIS ULTRA XPS system equipped with an Al X-ray source and a 165-mm mean radius electron energy hemispherical analyzer. Neutralizing was applied during the measurements to compensate for sample charging.

2.3.7 Fourier – Transform Infrared Spectroscopy (FTIR)

Surface functional groups of char and the activated carbons were investigated using an FTIR Spectrometer (Nicolet iS10, Thermo Scientific) equipped with a Diffuse Reflectance Infrared Fourier Transform Spectroscopy accessory (Praying Mantis, Harrick) and a High Temperature Reaction Chamber (HVC, Harrick). Gathered spectra was an average of 64 scans with 8 cm^{-1} resolution between the range of 650 to 4,000 cm^{-1}. A general procedure would be diluting a small amount of the sample with KBr. The ratio of sample to KBr was about 1:100 by mass. The mixture was ground into a fine powder with a pestle and mortar and loaded into the chamber. The sample was held at 100 ºC under helium flow for 50 minutes before a spectrum was taken. A background spectrum consisting of only ground KBr was collected under the same heating conditions before FTIR experiments were done that day.

2.3.8 Batch Adsorption Study of Vanillin

The batch experiments of the vanillin adsorption studies using the activated carbon from slow pyrolysis, hydrothermal carbonization, and the direct method were conducted at room temperature in a 150 mL beaker. For each run, 20 to 50 mg of the adsorbent was placed in a beaker containing 50 mL of a vanillin solution, which had a range of concentration between 50 to 200 mg/L. The suspension was stirred for a desired time, between 30 to 120 min, using a magnetic agitator. After agitation, the suspensions were gravity filtered. The concentration of the filtrate was determined by using an Agilent Cary 60 UV-visible spectrophotometer. The absorbance wavelength was measured between 200 to 500 nm at a rate of 60 nm/min and a 0.50 nm interval.

Adsorbate capacity, normalized to the surface area, was calculated using the equation below,

$$Adsorbate\ capacity = \frac{\frac{C_0 - C_t}{m}V}{Surface\ area} \qquad (1),$$

where C_t is the concentration of adsorbate at time t in mg/L, C_0 is the initial concentration of adsorbate in mg/L, m is the mass of the activated carbon in mg, V is the volume of the adsorbate solution in L, and surface area is of the adsorbent and is in m^2.

2.4 Results and Discussion

2.4.1 Physiochemical Properties of Biochar

2.4.1.1 Hydrothermal Carbonization

We studied the influence of dwell temperature at 200 °C, 220 °C, and 240 °C on the formed biochar after hydrothermal treatment. Figure 2.1(a) shows the XRD pattern of

HTC-treated corn stover with a 2-hour dwell time at different temperatures. The patterns are compared with that of untreated corn stover. The XRD pattern of corn stover has prominent cellulosic peaks at ~16 2θ (101) and ~22 2θ (220). The cellulosic peaks of the formed biochars decrease in intensity and become broad as the temperature increases. This broadening coincides with the decrease in the crystallite sizes of the cellulose and hemicellulose. It indicates that the HTC process promotes the partial breakdown of the cellulosic and hemicellulosic components of the corn stover. Interestingly, the turbostratic carbon (t-carbon) peak at ~26 2θ increases as the temperature increases, showing the potential growth of graphene layers. T-carbon is a unique class of carbon having structural ordering in between that of amorphous carbon phase and crystalline graphite phase[29].

Figure 2.1(b) shows the change in the surface area as a function of the dwell temperature and time. The biochar formed at 200 °C for 1-hour produced the lowest surface area at 1.0 ± 0.12 m^2/g. As the temperature increased to 220 °C, the surface area increased to 3.5 ± 0.38 m^2/g. This change may coincide with cellulose chains hydrolyzing at temperatures >220 °C, as corroborated with our XRD data[30]. At 240 °C, the surface area decreased to 2.9 ± 0.34 m^2/g. The same trend was observed with the 4-hour dwell time at 200 °C, 220 °C, and 240 °C, with surface areas of 3.3 ± 0.36 m^2/g, 4.5 ± 0.50 m^2/g, and 2.8 ± 0.41 m^2/g, respectively. Based on our XRD and surface area analysis, we believe that the surface area increases as the biomass constituents are broken down, with the hemicellulose degrading first and the cellulose second. We would expect this degradation order as hemicellulose is much less resistant to hydrolysis than cellulose[31]. Any further thermal degradation of biomass may occur through hydrolysis, isomerization, dehydration, and

fragmentation[32,33]. The surface areas for the 2-hour dwell time at dwell temperatures 200 °C, 220 °C, and 240 °C were $3.0 \pm .17$ m^2/g, 2.6 ± 0.20 m^2/g, and 6.9 ± 1.3 m^2/g, respectively. We note that the highest achieved surface area for the HTC experiments was found using a 2-hour dwell time and 240 °C dwell temperature. Figure 2.2 (a) shows the average pore size as a function of temperature and dwell time. The average pore size increased when the temperature increased from 200 °C to 220 °C in all the cases. The increase in the pore size could coincide with the widening of pores caused by cellulose chains hydrolyzing. When the temperature was further increased to 240 °C, in the 1-hour run, there was a slight increase in average pore size but in the 2- and 4-hour runs, the average pore size decreased.

The color of the biochar varied with temperature and dwell time (Figure 2.3). The biochar color varied from light brown to a black fine powder consistency. The milled corn stover had the appearance of sawdust prior to the hydrothermal treatment. The color change of the biomass is most likely due to the Maillard reaction and the degradation of the sugars contained in the biomass[34]. The morphology changes of the corn stover for select biochar samples were studied using SEM. Figure 2.4(b-c) shows the evolution of the corn stover to HTC biochar as a function of temperature and duration. As the temperature and time increase, the surface becomes rougher indicating structural degradation from the hydrothermal process. Figure 2.4(a) shows the milled corn stover before HTC. The corn stover structure is rigid and fibrous. Figure 2.4(b) shows the biochar formed after the HTC process at 220 °C and 1-hour dwell time. The surface changes are apparent with the formation of pits that are possible starting locations for pore formation. As the temperature

and time are increased, as shown in Figure 2.4(c,d) to 240 °C for 4-hour dwell time shows the most dramatic changes with little to no resemblance to the original corn stover. The hydrothermal degradation process occurs due to a myriad of simultaneous reactions including hydrolysis[12,25], dehydration[31] and decarboxylation[35]. At higher temperatures, other reaction mechanisms are dominant such as condensation polymerization[35,36]. The temperatures of this study are sufficient for the promotion of these simultaneous reactions that become prevalent at 240 °C and promote the degradation of the corn stover. The effect of temperature on the properties and morphology of HTC biochar is complex and multifaceted. Despite a greater degree of degradation at higher temperatures, our findings indicate no clear trend in the surface area and pore size.

We varied the ratio of water to biomass from 8:1 to 5:1 or 10:1 at 220 °C to determine if the amount of water influenced the biochar characteristics. Table 2.1 shows the results for varying the ratio. The 5:1 ratio had the lowest surface area at 2.2 ± 0.24 m^2/g, the 8:1 had a higher surface area at 2.6 ± 0.41 m^2/g, and the 10:1 ratio had the highest surface area of 3.6 ± 0.40 m^2/g. Interestingly, the 8:1 experiment had the lowest solid biochar yield, while the highest biochar yield was achieved from the 5:1 ratio. Considering solid loss after the experiments, we surmise that the difference in solid retention is a higher production of liquid and gaseous products for the 8:1 compared to the other ratios. Nevertheless, the higher water to biomass ratio improves surface area and pore structure.

We wanted to determine if the reactor's volume influenced the biochar's properties as the amount to charge the reactor would be of interest for scaling up this process. We maintained the 8:1 ratio for water to biomass and studied HTC on 1 g, 5 g, and 10 g of

biomass. Table 2.1 shows the comparison of the three different runs as a function of added water volume. The run with 1 g of corn stover achieved the highest surface area at 5.6 ± 0.62 m^2/g. However, the biochar yield was very low due to some of the biochar residue adhering to the reactor's walls. The run for the 10 g sample indicated a higher biochar yield but a lower surface area, 4.1 ± 0.45 m^2/g. We surmise the different mass to reactor volume allowed for different heat transfer rates which in turn promoted different biochars. Thus, the reactor size has significance when optimizing the formation of biochar.

2.4.1.2 Slow Pyrolysis

Figure 2.5(a) shows the XRD patterns for biochar derived from slow pyrolysis at 300 ℃, 500 ℃, and 700 ℃. The XRD spectra for the biochar formed at 300 °C show cellulosic peaks comparable to the peaks from the corn stover. This indicates that at 300 °C, there was a minimal change in the structural characteristics of the biochar. The biochar formed at 500 °C and 700 °C are quite different, with the formation of broad peaks between 15 to 30 2θ, resembling amorphous carbon peaks. We surmise that temperatures above 500 °C were substantial enough to break down the lignocellulosic structure for the complete breakdown of cellulose and hemicellulose. Interestingly, all the HTC biochars have cellulosic peaks, while those of SP biochars at elevated temperatures above 500 °C were apparently amorphous. This is an indication of different reactions occurring in the different carbonization methods. The biochar from SP and HTC are both precursors to activated carbon, comparing biochar formed from the two different processes is essential. This breakdown in the structure corresponds to a higher surface area for SP biochar compared to that formed from HTC.

The change of the surface area as a function of the slow pyrolysis temperature is shown in Figure 2.5(b). The trend shows that as the temperature increases, the solid residue's surface area increases as well. From 300 °C to 500 °C, the surface area went from 1.5 ± 0.03 m^2/g to 5.0 ± 1.5 m^2/g, but once the temperature reaches 550 °C, the surface area increases to 111 ± 23 m^2/g. An SP 240 °C experiment was conducted to compare with HTC 240 °C biochar. Compared to HTC, SP biochar's surface area formed at 240 °C is 1.2 ± 0.2 m^2/g vs. HTC biochar of 6.9 ± 1.3 m^2/g. We surmise that HTC, using subcritical water, may be more effective with breaking down biomass structure than SP at low temperatures.

The decrease in the pore sizes and surface area after 550 °C could be due to the limited reactivity of the lignin-rich biochar. The decomposition of hemicellulose and cellulose usually occurs between 200 to 450 °C. Particularly, cellulose decomposition reactions dominate between 300 °C and 450 °C[37]. The thermal decomposition of corn stover is limited at low temperatures, and the large concentration of hemicellulose and cellulose limits the surface area and pore morphology. This can be seen when comparing HTC and SP at 240 °C, which highlights the impact of subcritical water in breaking down biomass. Fragmentation becomes a dominating reaction at higher temperatures and is at its maximum around 600 °C[37]. The lignin polymeric structure has a higher kinetic threshold for decomposition that dominates at temperatures above 500 °C[37]. It is possible that the increase in surface area at 550 °C is primarily due to the decomposition of cellulose and hemicellulose forming high surface area biochar. As the temperature increases, the solid degrades into aromatic species and other hydrocarbons that escape into the gas phase which a portion can be condensed into an oil phase. There is a small spike from 600 to 650 °C,

which could be some polymerization and some other products forming on the solid[37,38].

Generally, the surface area of the slow pyrolysis carbon samples decreases at higher temperatures, which may be attributed to the formation of large pores. Initially, the pore size of the samples is mesoporous, then decreases and increases again at elevated temperatures. Table 2.1 shows the morphological changes of the carbon as a function of a change of the duration at 550 °C. It appears the longer the dwell time, the higher the surface area. However, the increase in the surface area from 1 hour to 8 hours is less than 5%. The limited change after 1 hour confirms that the reaction reaches steady-state in 1 hour. The average pore size is plotted in Figure 2.2(b) as a function of temperature. Interestingly, the average pore size plot is an inverse of the surface area plot between 500 °C and 700 °C, Figure 2.2(b). As the average pore size decreases, the total surface area increases, which would suggest that there is an increased number of smaller pores that causes the increases in the available surface area. At higher temperatures, we observe a decrease in surface area. We speculate that the decrease can be attributed to either pore collapse or an increase in the size of the pores, as can be seen for temperatures above 650 °C.

The visual appearance of the biochar from the slow pyrolysis remained consistently black for all dwell times and temperatures tested. The slow pyrolysis did not show much color change over the range as the lowest temperature, 300 °C, would be past the Maillard reaction's upper limits. In Figure 2.6(a-d), the biochar SEM images for select samples from slow pyrolysis can be seen in which the structure changed as the temperature increased. Notably, SP biochar samples still had the rigid structure shown of the fibrous corn stover structure. Nevertheless, BET analysis confirms that the structure does become more porous

as the temperature increased. HTC and SP produced distinct biochar from each other which the degradation of cellulose and hemicellulose played an important role. HTC led to lower surface areas and larger average pore sizes while SP led to higher surface areas and smaller average pore sizes. The subcritical water of HTC and higher temperatures in SP leads to different reactions occurring and some were more prominent than others.

2.4.2 Activated carbon from Biochar derived from HTC and SP

The biochars from the HTC and SP methods were chemically activated to produce activated carbon for the adsorption of phenolic compounds. The properties of the activated carbons were characterized using XPS, XRD, FTIR, and SEM and compared to that of direct chemical activation of the corn stover. The results of XRD of select activated carbons show the formation of amorphous carbon (Figure 2.7). The activated carbon XRD patterns have two broad peaks from ~20 to 30 and ~40 to 50 2θ. These represent amorphous carbon peaks as one would generally find broad peaks ranging from 10 to 30 and 35 to 50 2θ for amorphous carbon composed of aromatic carbon sheets oriented in a considerably random fashion[39]. The XRD pattern for the direct activation of corn stover has a peak at 29.5°, which corresponds to silicate minerals in the sample[40]. XPS was conducted to perform an elemental analysis of the biochar materials prior to and after activation with KOH. We determined that the O/C content of the HTC biochars and AC direct materials decreased after activation. However, the O/C content of the SP biochar remained the same. This confirms that the SP biochar is not as amenable as HTC biochar for subsequent chemical activation by KOH.

Table 2.2 and Table 2.3 contains the surface areas of the activated carbon samples using biochar precursors from the direct, HTC, and SP methods. Surprisingly, the highest surface areas were achieved with the direct and HTC biochar precursors. For example, the highest surface area from the activation of the HTC biochar sample prepared at 240 °C for 2-hour was $1,167 \pm 164$ m^2/g. We activated milled corn stover with no prior treatment as a control and observed a surface area of 956 ± 39 m^2/g. This surface area is around what can be found on many commercial activated carbons. The highest surface area from the AC SP series of experiments was from the biochar formed from the 300 °C 1-hour run at $1,008 \pm 94$ m^2/g. The lowest achieved surface area was from 550 °C slow pyrolysis biochar at 376 ± 107 m^2/g. Despite having higher starting surface areas compared to HTC biochars, the activated carbons formed from SP biochars have lower surface areas than those created from HTC biochars. Thus, the increased biochar surface area is inversely proportional to activated carbon surface area, this trend can be seen in Table 2.3. Figure 2.8 shows the N$_2$ adsorption/desorption isotherms of the produced activated carbons. The AC Direct (Figure 2.8(a)) and AC HTC (Figure 2.8(b)) had the highest porosity suggesting saturation of micropores and mesopores in the structure. The isotherm for AC SP (Figure 2.8(c)) indicates a lower adsorptive capacity with a microporous structure. The average pore size of all the activated carbons as seen in Table 2.3 was between 4 and 9 nm, indicating there are mesopores in each sample. There were minimal differences in the AC direct, AC HTC, and AC SP average pore size. The most noticeable difference between the samples was surface area primarily contributed by the micropore region. AC direct and AC HTC had surface areas with a higher micropore area.

Figures 2.9(a-d) show the SEM images of the activated carbon samples for select

samples. The HTC activated carbon images in Figures 2.9(a-b) have a stark difference in

appearance and morphology than the SP biochar activated carbon images in Figures 2.9(c-

d). The HTC biochar activated carbon samples have significant surface changes with a

clear breakdown of the rigid structure and courser appearance. This is especially apparent

when compared to the original corn stover shown in Figure 2.4a. The slow pyrolysis

activated carbon images from the slow pyrolysis biochar still have a rigid structure with

less visible change compared to HTC activated carbons. The differences observed from

SEM in the activated carbon derived from either the HTC or SP biochar could indicate the

differences in the surface area and pore sizes.

We surmise that the difference in the maximum surface area achieved and porosity

for HTC biochar or SP biochar-derived activated carbon is due to cellulose and lignin

concentration. For instance, a study by Tiryaki et al. created activated carbon from tomato

leaves that had 10.9% cellulose and 24.8% lignin that produced a surface area of 305

m^2/g[41]. In comparison, carbon with a higher cellulose content with a ratio of 26.2%

cellulose and 36.5% lignin had a surface area of 839 m^2/g. A study performed by Zhang et

al. determined that as the lignin concentration increased, the surface area decreased[42]. It

was theorized that the polysaccharide structure of cellulose allowed the formation of a

mesoporous structure. The complex polymeric aromatic structure of lignin though

contributed to the layered and microporous structure. We conclude that the SP biochars at

high temperatures above 500 °C lack an appreciable amount of cellulose, corroborated by

XRD, and thus are less prone to mesoporous structure formation. The hydroxyl groups in

the cellulose and hemicellulose structure are reactive to the KOH chemical activation, reducing micropores. In contrast, lignin's aromatic backbone is more predisposed to produce macropores and carbon sheets. Thus, the HTC samples rich in cellulose are more prone to micropore formation.

2.4.3 Adsorbent Properties of Activated carbons for vanillin

2.4.3.1 Characterization of Functional Groups

The adsorption characteristics of the AC HTC, AC SP, and AC direct materials depends on the surface functional groups. FTIR analysis was used to analyze the surface functional groups of the formed biochars and the associated activated carbons. Figure 2. 10(a) shows the comparative structures of biochar formed from HTC and SP. Both spectra show a broad band between $3,150 - 3,400$ cm^{-1} attributed to the O – H stretching of the hydroxyl groups. The area between $3,000 - 2,800$ cm-^{1} is attributed to the C – H stretching. The peak intensity for the HTC 240 °C is greater, showing that there are more of these functional groups formed after hydrotreatment. The peaks between $1,700 - 1,650$ cm^{-1} and at $1,050$ cm^{-1} can be assigned to the C – O stretching of the carboxyl groups. The peaks between $1,100 - 1,000$ cm^{-1} refer to the C – OH and C – O stretch. These results indicate that the surface of the biochars is mostly oxygen containing groups, including hydroxyl (– OH) and carboxylic (–COOH) functional groups. The activated carbons from all biochars formed from the direct, HTC, and SP had peaks indicative of C – O, C – H, and C – OH bonds as seen in Figure 2.10(b). The lower intensities infer that the surface of the carbon has predominant hydroxyl and C – O groups, however, at a lower concentration than the biochar precursors. This is also corroborated by the O/C ratio measured by XPS in Table

2.2 showing a lower O/C ratio than the biochars. The additional peaks and stronger intensity for the HTC corn stover over the other samples show that it has more oxygen-containing groups, which could be attributed to the higher concentration of cellulose and hemicellulose.

2.4.3.2 Adsorption performance

Physical adsorption of vanillin molecules depends on the functional groups on the surface of the activated carbon. We compared the vanillin adsorption performance of the activated carbon with respect to their biochar precursor characteristics and synthesis. Batch adsorption experiments of the activated carbons were carried out, and the results are presented in Figure 2.11 and Figure 2.12. The results show that the samples perform about the same for concentrations between 50 – 200 mg/L (Figure 2.11,2.12(a)). For example, 98% of vanillin can be removed within 60 min by using the activated carbon prepared from the corn stover direct method and the HTC biochar. Comparatively, it takes the activated carbon prepared from the SP biochar greater than 120 mins to adsorb 98% of vanillin.

The surface functional groups, pore volume, and pore size of activated carbon positively influence the adsorption rate, and amount of vanillin adsorbed onto the activated carbon surface. Therefore, the effect of the mass of the activated carbon to the reaction medium was used to determine the effects of the removal of vanillin. The solution volume and concentration were kept constant at 50 mL of 50 mg/L and were used at room temperature with a 60-minute contact time. As shown in Figure 2.11,2.12(b), at 20 mg loading, AC direct had the best removal of vanillin at ~14% more removed than AC HTC and even greater for AC SP. While AC direct had slightly less surface area, it adsorbed

more than AC HTC by a noticeable amount, which may have implications that surface area is not the only parameter that affects the adsorption of vanillin. Parameters like surface functional groups and pore structure may affect the adsorption of vanillin. Each sample adsorbed more vanillin when the loading increased from 20 to 35 mg, with AC direct and AC HTC having removed similar amounts. With further increased amounts, AC HTC and AC direct remained the same, and AC SP continued to increase in adsorption capabilities. At the 50 mg loading, over 98% is removed for AC direct and AC HTC, while only 58% is removed for AC SP. The surface and morphology of the AC SP are drastically different than the other two ACs. This can be seen in the normalized adsorption capacity, where even per m^2 the adsorption of vanillin onto AC SP is less than that of the others. This is an indication that more than the surface area is involved in the removal of vanillin, which we speculate could be due to the number of adsorption sites, the pore structure, and/or the surface functional groups.

Surface functional groups can affect the adsorptive properties of activated carbon. The presence of dissolved oxygen on activated carbon can increase the adsorptive capacity of phenolic compounds through oxidative coupling reactions[43]. From the FTIR data, the HTC biochar had more oxygen-containing surface functional groups than SP biochar. However, when activated, distinguishing which has the most oxygen-containing surface functional groups becomes difficult. The results from the AC Direct and AC HTC are very similar, indicating similar surface functional groups, which we speculate is a reason for the higher adsorption of vanillin compared to AC SP.

The contact time between the activated carbon and vanillin is a critical parameter for the adsorption process, thus contact time optimization was investigated. The effect of contact time on the adsorption of vanillin by the prepared activated carbons was examined at room temperature by using 50 mg of activated carbon and 50 ml of 50 mg/L vanillin solution. The adsorption experiment was carried out for up to 2 hours to determine the adequate adsorption time, and the result is presented in Figure 2.11(c). The amount of the absorbed vanillin for AC HTC and AC direct increased from 0 minutes to 30 minutes and plateaued afterward. The adsorption on SP, however, increased rapidly from 60 minutes to 120 minutes. For AC HTC and AC direct the results show that the adsorption sites were saturated after 30 minutes. The AC SP continued to adsorb as the time increased, indicating that the maximum adsorption had not been achieved. This shows a possibility that the adsorption rate for SP is slower when compared to that of the AC HTC and AC direct.

2.5 Conclusion

This paper compared the properties of biochar precursors and activated carbons that were chemically activated either from corn stover using the direct method, HTC, or SP. XRD and BET analysis showed that HTC and SP biochar differed in their lignocellulosic composition after the reaction at elevated temperatures. The role of water in HTC plays an integral part in the decomposition of corn stover as it allows hydrolysis and other reactions to break down the biomass more efficiently than SP. SEM analysis showed that the HTC and SP biochars formed more pores as the temperature increased. FTIR spectroscopy analysis showed that HTC biochars had a higher density of oxygen-based surface

functional groups than SP biochars. Additionally, the formed AC from corn stover and HTC biochar precursors was apparently more oxygen-rich.

The activated carbon formed from the studied biochar precursors was then probed for the adsorption of vanillin. The lignocellulosic composition of the biochar is influential on the surface area, pore size, pore structure, and available surface functional groups for the formed activated carbons. In terms of their adsorptive abilities, the AC direct and AC HTC had significantly better adsorption of vanillin than the AC SP. When normalized to the surface area, AC direct and AC HTC had improved performance compared to AC SP as a function of duration and total AC amount used, which implies that other properties such as pore structure and surface functional groups are important. The AC direct and AC HTC performed better than AC SP, indicating the importance of the biochar pretreatment method to activated carbon properties. Overall, activated carbon was produced from a highly relevant agricultural residue, corn stover. The results suggest that AC generated directly from corn stover had properties comparable to the absorbents made from HTC and SP biochars. The production of activated carbon as adsorbents for phenolic compounds may not warrant the extra thermochemical step of biochar precursor synthesis from HTC and SP.

2.6 Conflict of Interest

The authors declare no competing interest including but not limited to financial or personal interests relating the work reported in this paper.

2.7 Acknowledgements

2.8 Figures and Tables
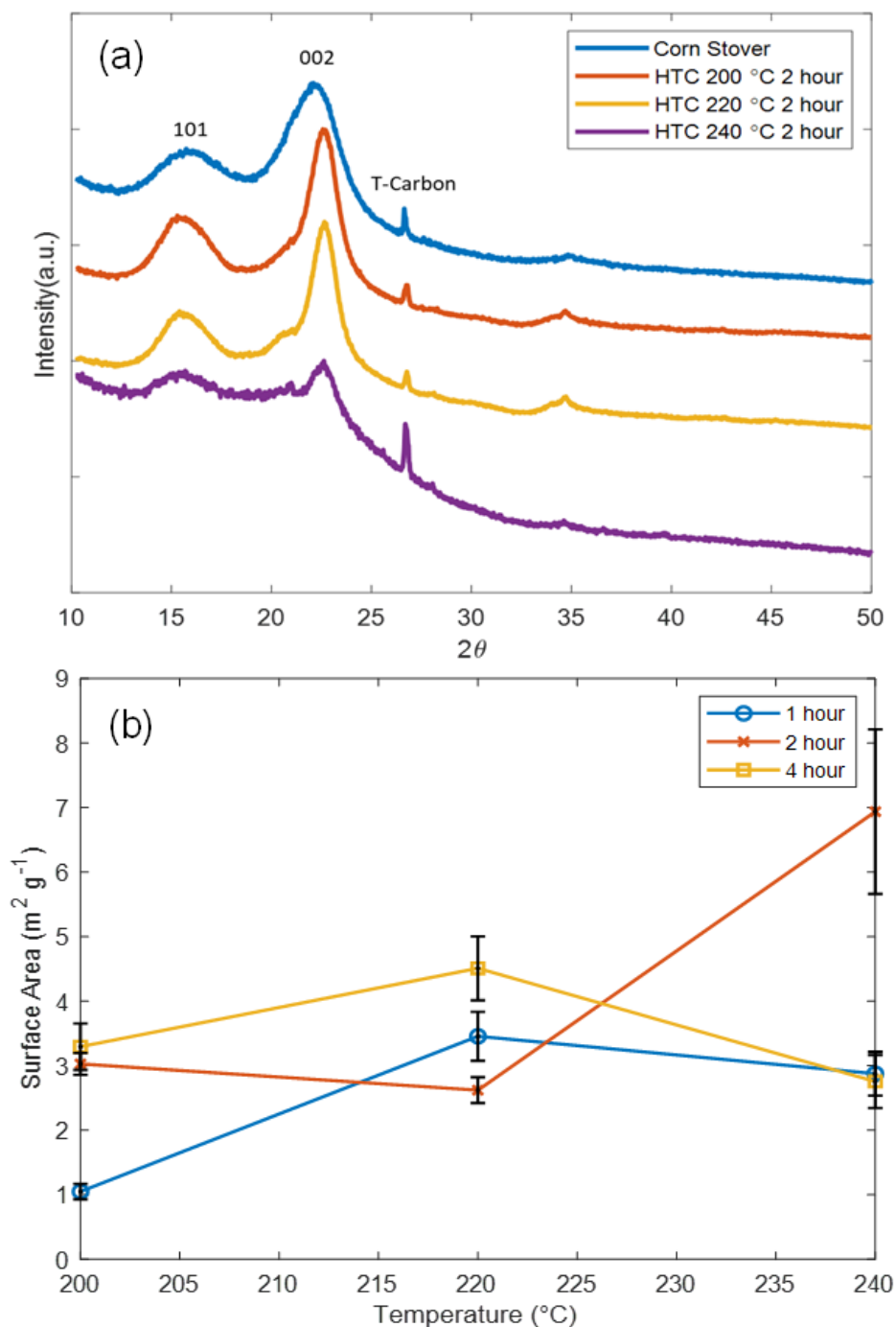
Figure 2.1 (a) XRD spectra of HTC biochar prepared at different temperatures and a dwell time of 2 hours. (b) Surface areas of HTC formed biochar plotted as a function of temperature.
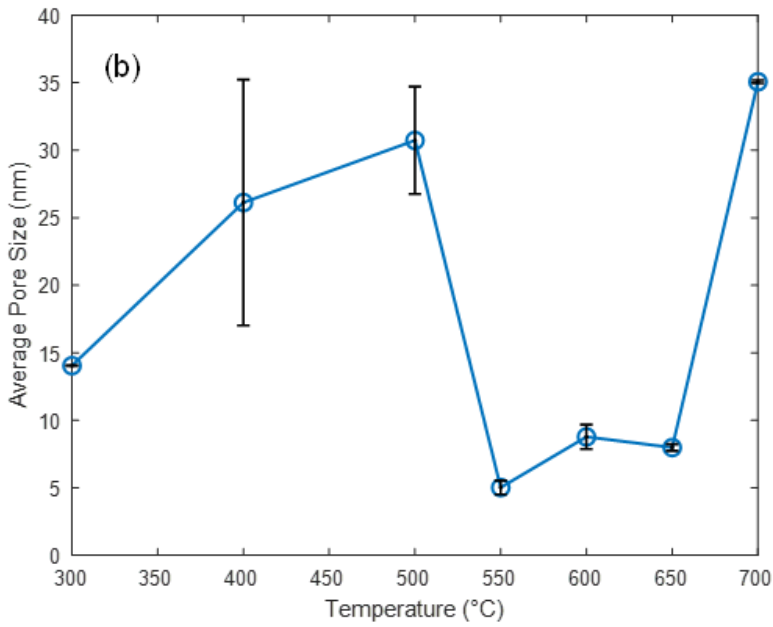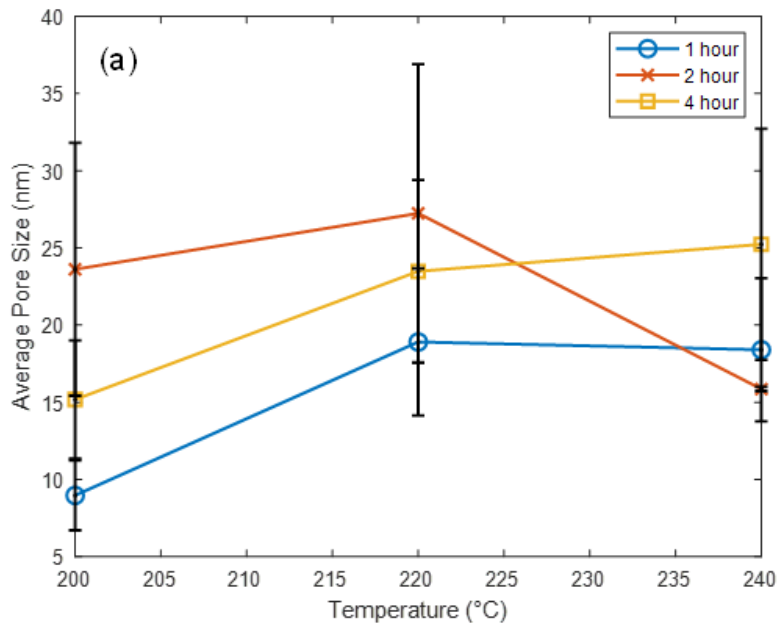
Figure 2.2 (a) Average pore size for HTC biochar. (b) Average pore size of SP biochar for various temperatures after 1-hour duration
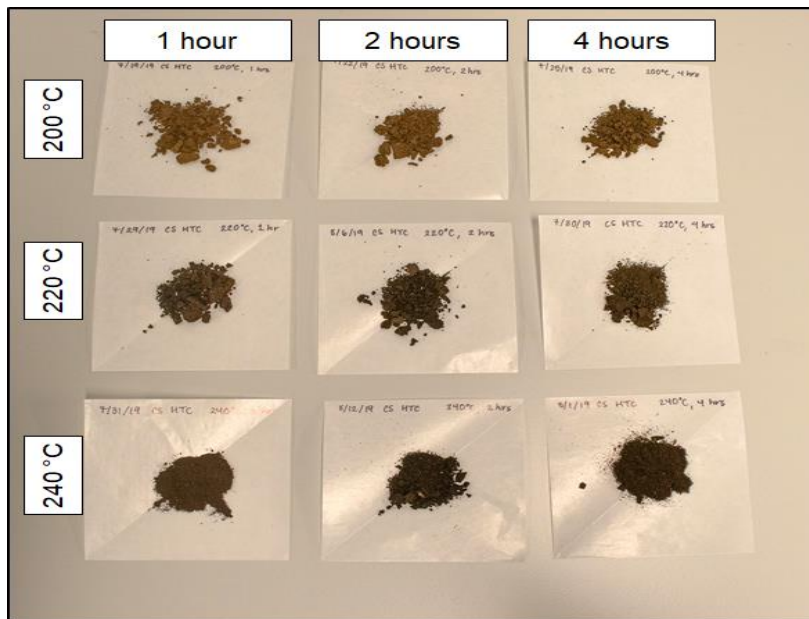
Figure 2.3 Images of hydrothermal carbonization biochar as a function of temperature and duration.
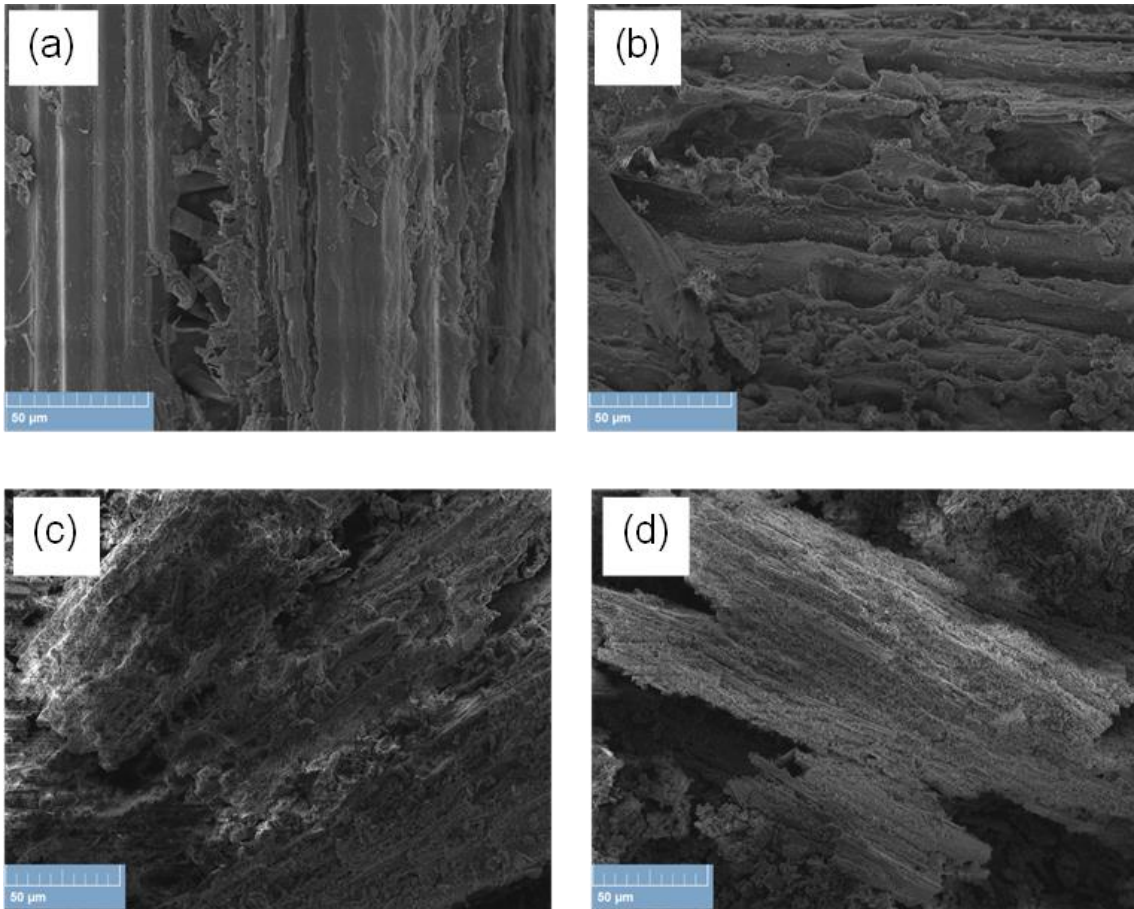
Figure 2.4 SEM images of the HTC biochar at different temperatures and dwell time. (a) Corn stover milled 1mm (Mag:1.43 kx). (b) HTC 220 °C 1 hour (Mag: 1.43 kx). (c) HTC 220 °C 2 hours (Mag: 1.15 kx). (d) HTC 240 °C 4 hours (Mag: 1.17 kx).
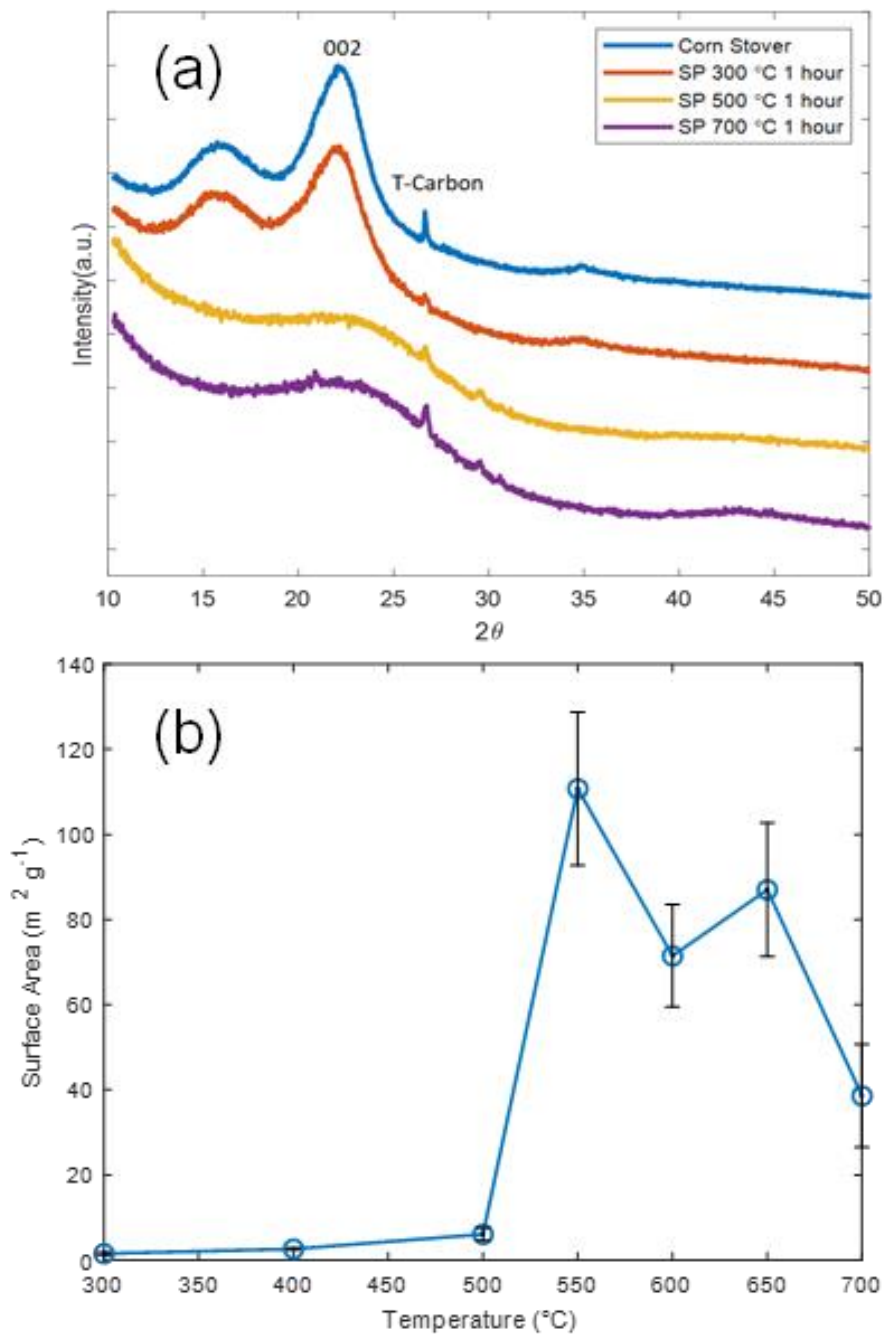
Figure 2.5 (a) XRD spectra for slow pyrolysis of corn stover at different temperatures. (b) Surface area of slow pyrolysis of corn stover for 1 hour over a range of 300 - 700 °C.
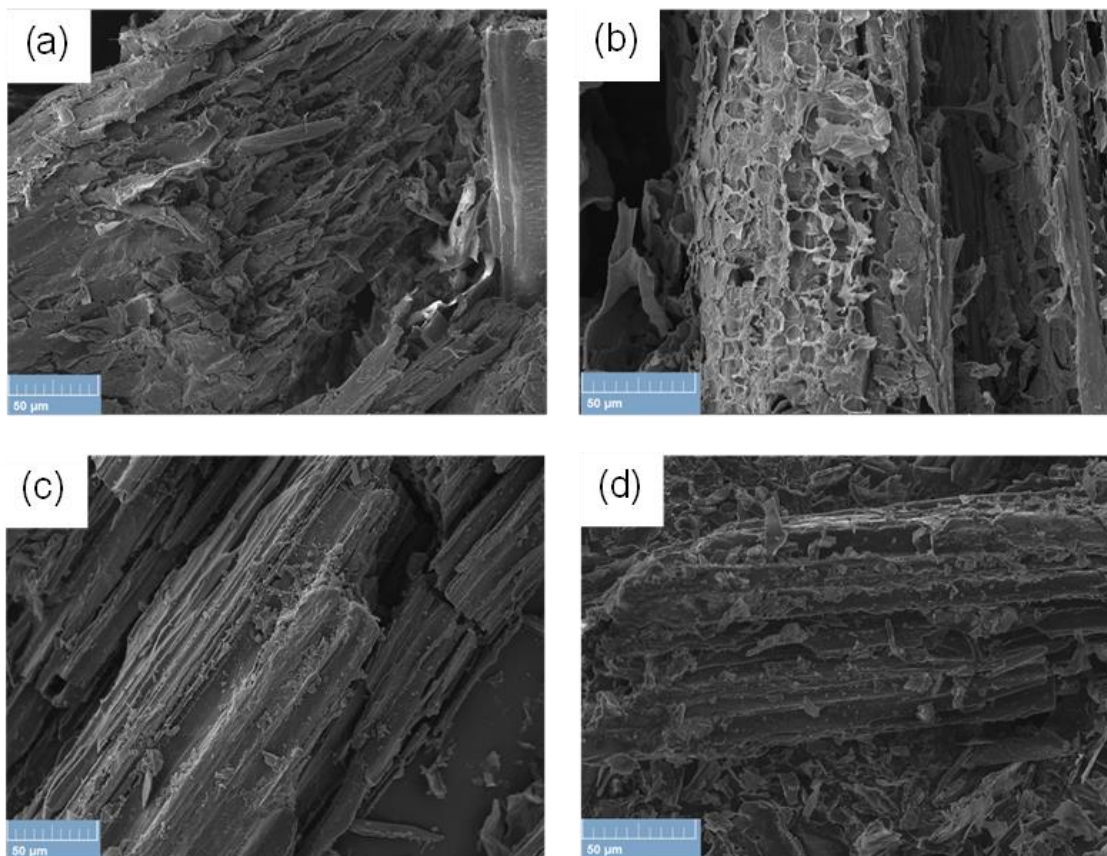
Figure 2.6 SEM images of SP biochar at different temperatures. (a) SP 400 °C 1 hour (Mag: 931 x). (b) SP 500 °C 1 hour (Mag: 1.23 kx). (c) SP 600 °C 1 hour (Mag: 934 kx). (d) SP 600 °C 1 hour (Mag: 1.28 kx).
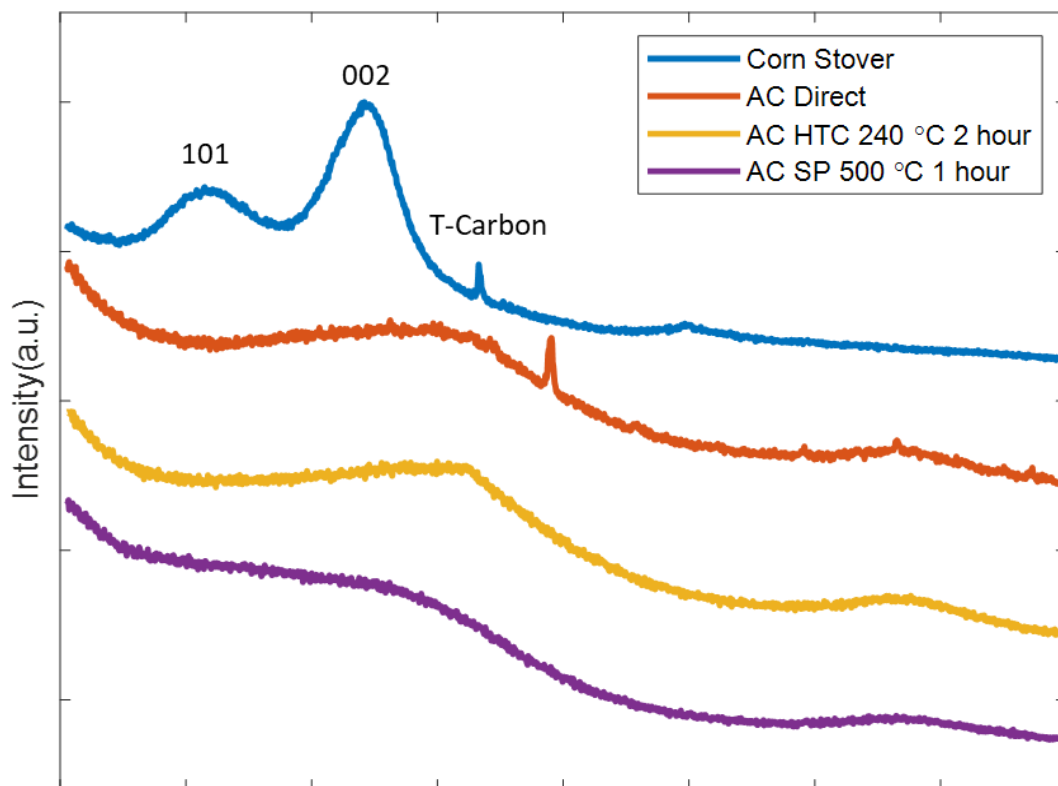
Figure 2.7 XRD spectra of activated carbon prepared from corn stover directly and SP & HTC biochars.
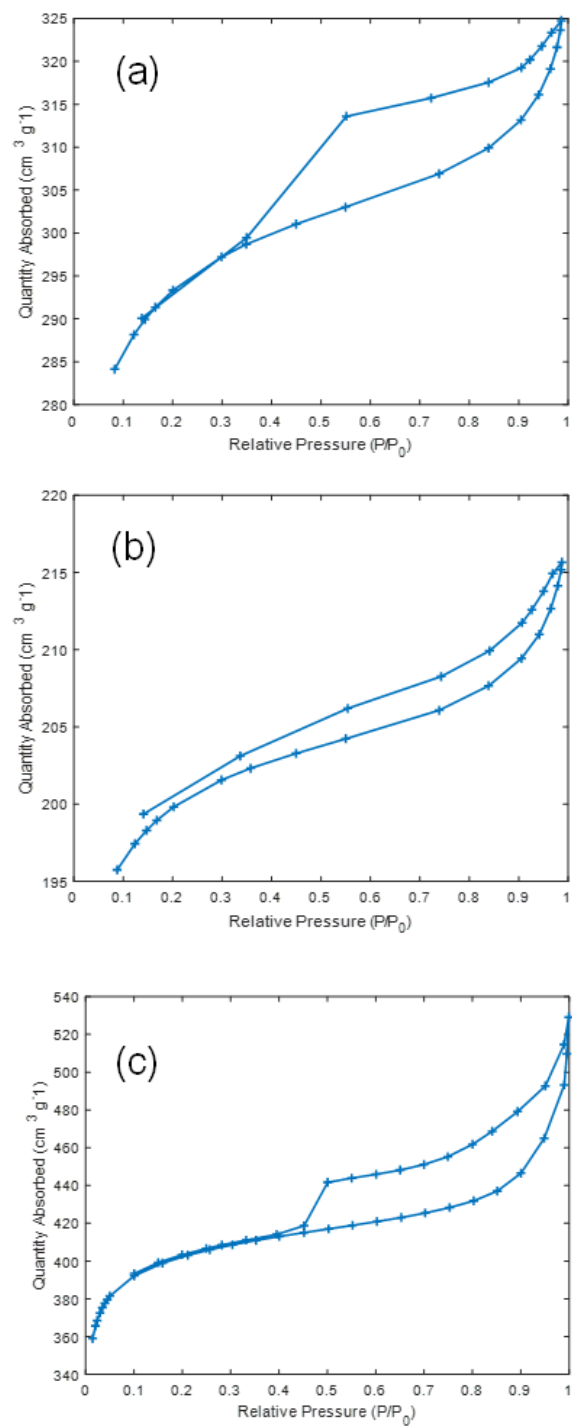
Figure 2.8 BET Isotherm of (a) AC Direct, (b) AC SP
and (c) AC HTC 240.
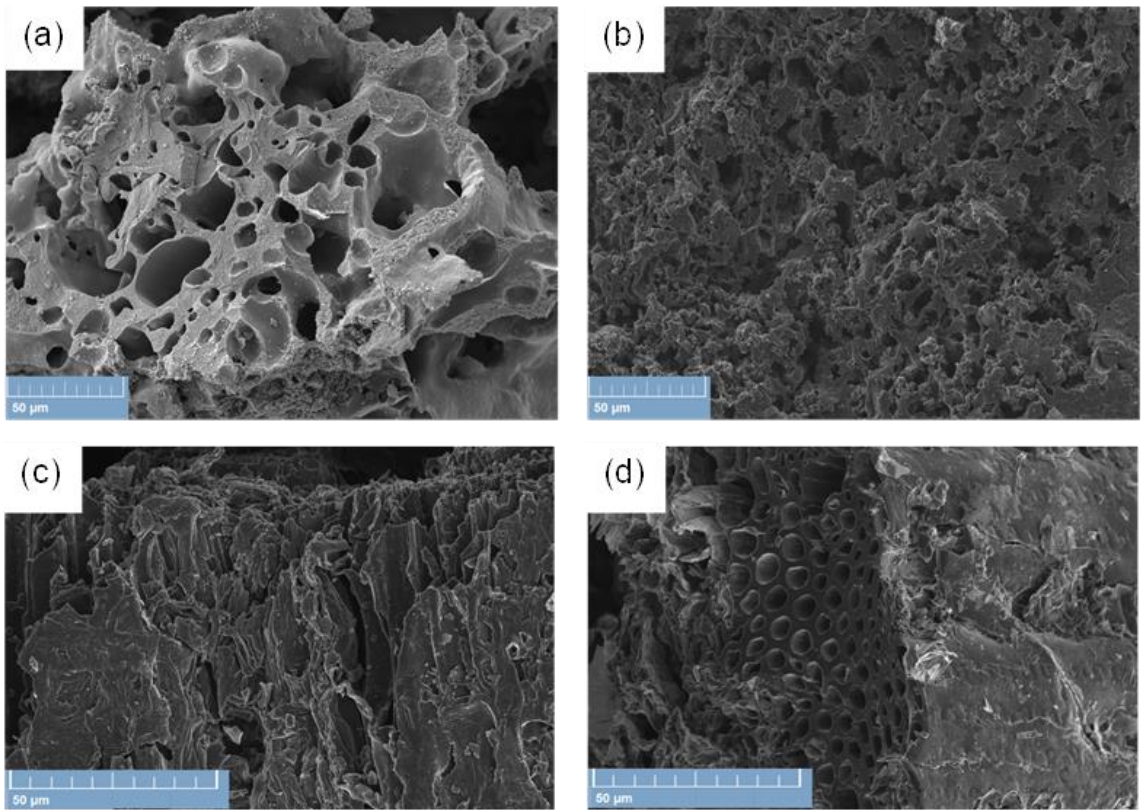
Figure 2.9 SEM images of Activated Carbon. (a) AC HTC 200 °C 1 hour (Mag: 1.14 kx). (b) AC HTC 240 °C 2 hours (Mag: 1.14 kx). (c) AC SP 400 °C 1 hour (Mag: 1.0 kx). (d) AC SP 550 °C 1 hour (Mag: 1.0 kx).
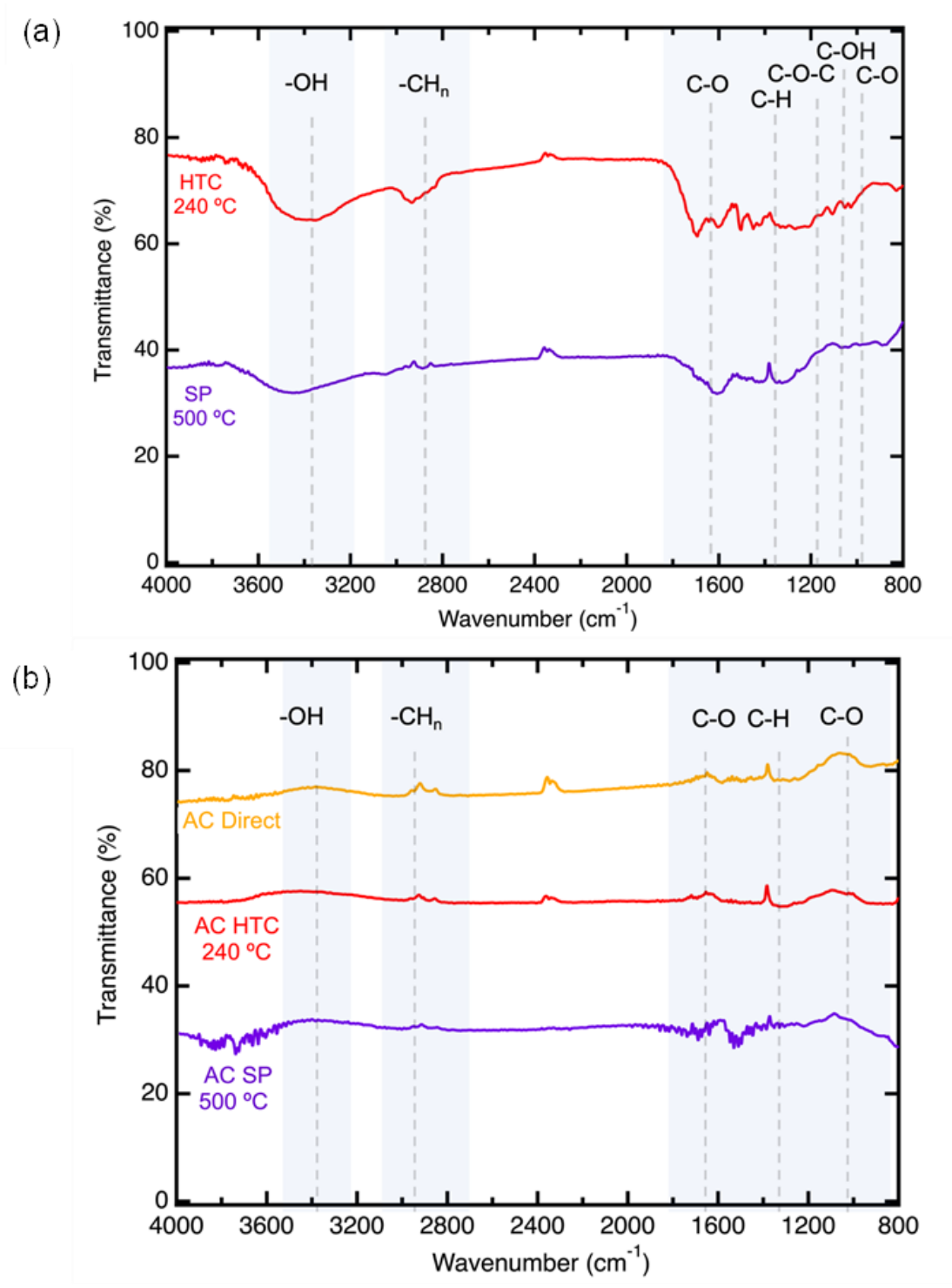
Figure 2.10 FTIR analysis of the (a) biochar from either the HTC or SP and (b) Activated carbon
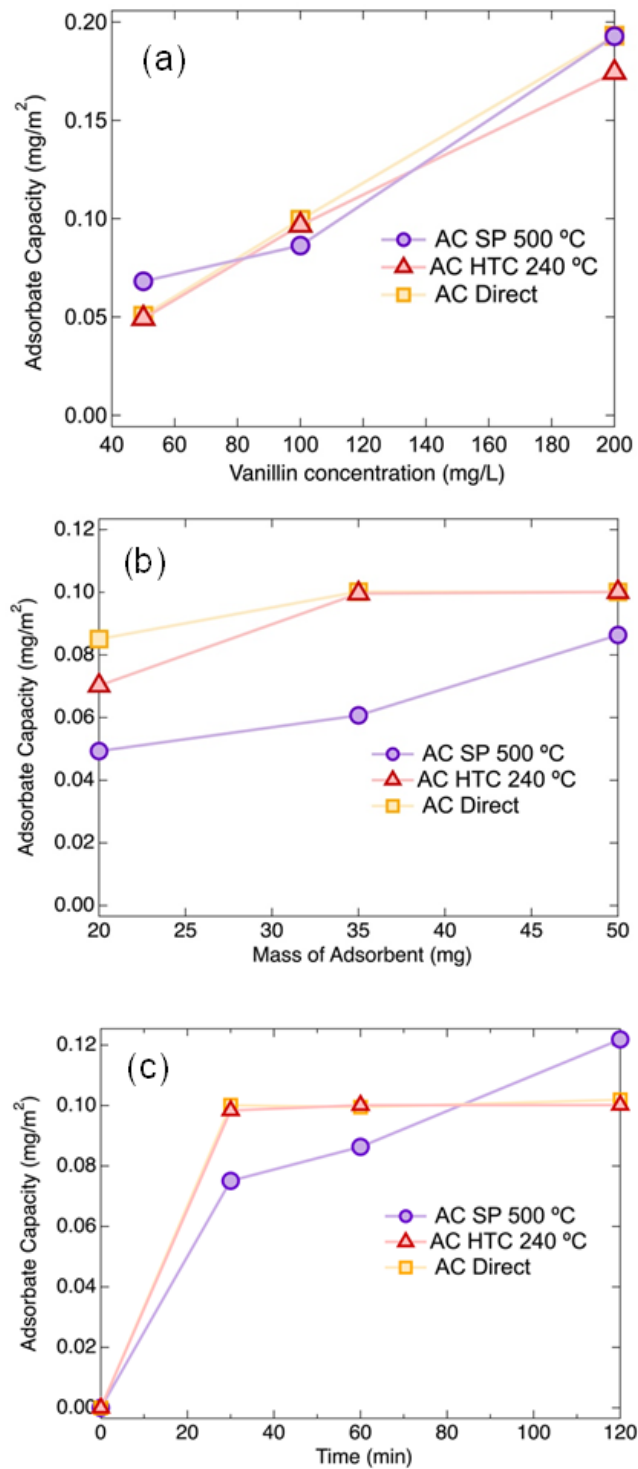
Figure 2.11 Vanillin adsorbate capacity normalized to surface area of the activated carbons as a function of (a) vanillin concentration, (b) dosage, and (c) time.
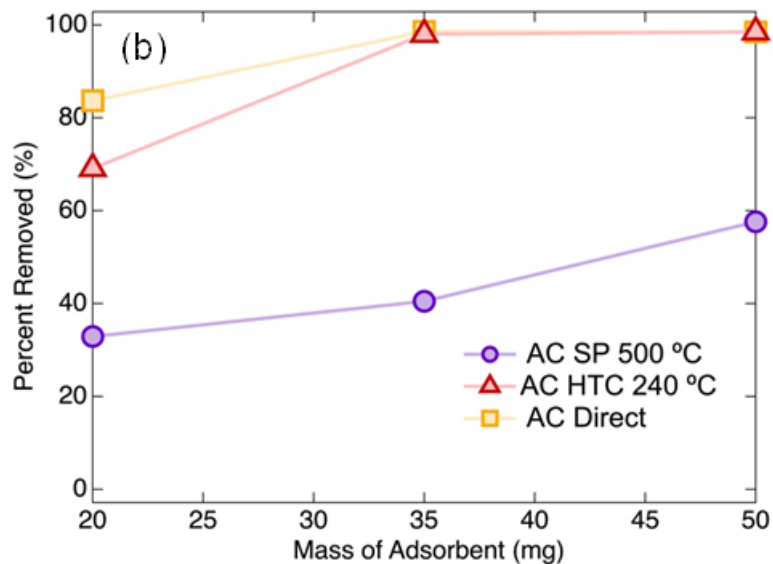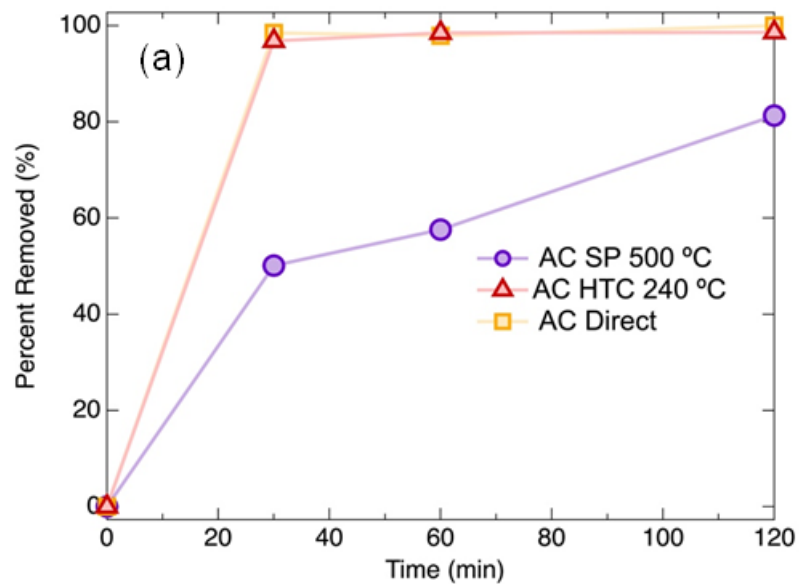
Figure 2.12 Vanillin removal as a percentage of Activated Carbons as a function of (a) Time and (b) Mass

Table 2.1 HTC biochar surface area when varying the ratio of water to biomass and total amount of biomass Slow pyrolysis biochar surface area with changing duration

Sample	Surface Area $m^2 g^{-1}$	Average Pore Size nm	% Recovered
HTC 5:1 Ratio[α]	$2.2 \pm 0.24^{\varepsilon}$	$30 \pm 7.6^{\varepsilon}$	50.8%
HTC 8:1 Ratio[α]	2.6 ± 0.41	18 ± 4.6	46.5%
HTC 10:1 Ratio[α]	$3.6 \pm 0.40^{\varepsilon}$	$35 \pm 8.9^{\varepsilon}$	49.0%
HTC 1 g[β]	$5.6 \pm 0.62^{\varepsilon}$	$23 \pm 5.8^{\varepsilon}$	39.3%
HTC 5 g[β]	2.6 ± 0.41	18 ± 4.6	46.5%
HTC 10 g[β]	$4.1 \pm 0.45^{\varepsilon}$	$20 \pm 5.1^{\varepsilon}$	52.7%
SP 550 °C 0 hour	$9.9 \pm 1.6^{\varepsilon}$	$33 \pm 3.4^{\varepsilon}$	29.3%
SP 550 °C 1 hour	111 ± 23	5.0 ± 0.51	27.8%
SP 550 °C 4 hours	$107 \pm 18^{\varepsilon}$	$5.7 \pm 0.58^{\varepsilon}$	27.0%
SP 550 °C 8 hours	$105 \pm 17^{\varepsilon}$	$7.0 \pm 0.71^{\varepsilon}$	27.4%

[α]HTC experiments ran at 220 °C for 2 hours with 5g of biomass.
[β]HTC experiments ran at 220 °C for 2 hours with a ratio of 8:1 water to biomass.
[ε]Approximate error calculated from previous data replicates in similar pretreatment conditions

Table 2.2 The surface area and X-ray photoelectron spectroscopic elemental analysis of the biochar and associated activated carbons.

Sample	Surface Area (m²/g)	Relative Atomic Concentration (%)				
		O	N	C	S	O/C
CS	1.2 ± 0.13	24	1	75	0	0.32
SP500	5.0 ± 1.5	18	1	81	0	0.22
HTC240	6.9 ± 1.3	22	1	77	0	0.29
AC Direct	956 ± 39	17	0	82	0	0.21
AC SP500	646 ± 19	18	1	81	0	0.22
AC HTC240	1,167 ± 164	13	1	86	0	0.15

Table 2.3 Activated carbon surface area of direct activation, HTC, and SP precursors.

Sample	Surface Area $m^2\ g^{-1}$	Average Pore Size nm	Micropore Area $m^2\ g^{-1}$
AC Corn Stover Direct	956 ± 39	6.9 ± 0.09	814 ± 9.5
AC HTC 200 °C 1 hour	$759 \pm 71^{\varepsilon}$	$5.7 \pm 0.40^{\varepsilon}$	$664 \pm 58^{\varepsilon}$
AC HTC 200 °C 2 hour	940 ± 28	5.9 ± 0.56	821 ± 24
AC HTC 220 °C 4 hour	$989 \pm 92^{\varepsilon}$	$8.5 \pm 0.60^{\varepsilon}$	$849 \pm 74^{\varepsilon}$
AC HTC 240 °C 1 hour	$984 \pm 92^{\varepsilon}$	$3.9 \pm 0.27^{\varepsilon}$	$812 \pm 70^{\varepsilon}$
AC HTC 240 °C 2 hour	$1,167 \pm 164$	6.0 ± 1.0	994 ± 121
AC SP 300 °C 1 hour	$1,008 \pm 94^{\varepsilon}$	$6.9 \pm 0.49^{\varepsilon}$	$840 \pm 73^{\varepsilon}$
AC SP 400 °C 1 hour	$821 \pm 77^{\varepsilon}$	$4.6 \pm 0.32^{\varepsilon}$	$710 \pm 62^{\varepsilon}$
AC SP 500 °C 1 hour	646 ± 19	4.1 ± 0.17	563 ± 20
AC SP 550 °C 1 hour	376 ± 107	4.4 ± 0.31	326 ± 102
AC SP 600 °C 1 hour	$521 \pm 49^{\varepsilon}$	$4.0 \pm 0.28^{\varepsilon}$	$448 \pm 39^{\varepsilon}$
AC SP 650 °C 1 hour	579 ± 24	4.4 ± 0.16	488 ± 4.4

$^{\varepsilon}$Approximate error calculated from previous data replicates

2.9 References

(1)   Sherwood, J. The Significance of Biomass in a Circular Economy. *Bioresour. Technol.* **2020**, *300*, 122755. https://doi.org/10.1016/j.biortech.2020.122755.

(2)   Oak Ridge National Laboratory. US Billion Ton Update: Biomass Supply for a Bioenergy and Bioproducts Industry. *US DOE Energy Effic. Renew. Energy* **2011**, 1–195. https://doi.org/10.1089/ind.2011.7.375.

(3)   Obrycki, J. F.; Karlen, D. L. Is Corn Stover Harvest Predictable Using Farm Operation, Technology, and Management Variables? *Agron. J.* **2018**, *110* (2), 749–757. https://doi.org/10.2134/agronj2017.08.0504.

(4)   Ioannidou, O.; Zabaniotou, A. Agricultural Residues as Precursors for Activated Carbon Production-A Review. *Renew. Sustain. Energy Rev.* **2007**, *11* (9), 1966–2005. https://doi.org/10.1016/j.rser.2006.03.013.

(5)   Zhang, T.; Walawender, W. P.; Fan, L. T.; Fan, M.; Daugaard, D.; Brown, R. C. Preparation of Activated Carbon from Forest and Agricultural Residues through CO_2 Activation. *Chem. Eng. J.* **2004**, *105* (1–2), 53–59. https://doi.org/10.1016/j.cej.2004.06.011.

(6)   Zhai, Y.; Xu, G.; Zhang, Y.; Liu, X.; Ma, Y.; Li, C. Depolymerization of Lignin via a Non-Precious Ni–Fe Alloy Catalyst Supported on Activated Carbon. *Green Chem.* **2017**, *19* (8), 1895–1903. https://doi.org/10.1039/c7gc00149e.

(7)   Abumaizar, R. J.; Kocher, W. M.; Smith, E. H. Biofiltration of Benzene Contaminated Air Streams Using Compost-Activated Carbon Filter Media. *J. Hazard. Mater.* **1998**, *60* (2), 111–126. https://doi.org/https://doi.org/10.1016/S0304-3894(97)00046-0.

(8)   Reungoat, J.; Escher, B. I.; Macova, M.; Argaud, F. X.; Gernjak, W.; Keller, J. Ozonation and Biological Activated Carbon Filtration of Wastewater Treatment Plant Effluents. *Water Res.* **2012**, *46* (3), 863–872. https://doi.org/10.1016/j.watres.2011.11.064.

(9)   El-Naas, M. H.; Al-Zuhair, S.; Alhaija, M. A. Removal of Phenol from Petroleum Refinery Wastewater through Adsorption on Date-Pit Activated Carbon. *Chem. Eng. J.* **2010**, *162* (3), 997–1005. https://doi.org/10.1016/j.cej.2010.07.007.

(10)   Rodrigues, L. A.; da Silva, M. L. C. P.; Alvarez-Mendes, M. O.; Coutinho, A. dos R.; Thim, G. P. Phenol Removal from Aqueous Solution by Activated Carbon Produced from Avocado Kernel Seeds. *Chem. Eng. J.* **2011**, *174* (1), 49–57. https://doi.org/10.1016/j.cej.2011.08.027.

(11) Shinde, S. D.; Meng, X.; Kumar, R.; Ragauskas, A. J. Recent Advances in Understanding the Pseudo-Lignin Formation in a Lignocellulosic Biorefinery. *Green Chem.* **2018**, *20* (10), 2192–2205. https://doi.org/10.1039/c8gc00353j.

(12) Funke, A.; Ziegler, F. Hydrothermal Carbonization of Biomass: A Summary and Discussion of Chemical Mecha- Nisms for Process Engineering. *Biofuels, Bioprod. Biorefining* **2010**, *4* (2), 160–177. https://doi.org/10.1002/bbb.198.

(13) Fang, J.; Zhan, L.; Ok, Y. S.; Gao, B. Minireview of Potential Applications of Hydrochar Derived from Hydrothermal Carbonization of Biomass. *J. Ind. Eng. Chem.* **2018**, *57*, 15–21. https://doi.org/10.1016/j.jiec.2017.08.026.

(14) Goyal, H. B.; Seal, D.; Saxena, R. C. Bio-Fuels from Thermochemical Conversion of Renewable Resources: A Review. *Renew. Sustain. Energy Rev.* **2008**, *12* (2), 504–517. https://doi.org/10.1016/j.rser.2006.07.014.

(15) Park, J.; Lee, Y.; Ryu, C.; Park, Y. K. Slow Pyrolysis of Rice Straw: Analysis of Products Properties, Carbon and Energy Yields. *Bioresour. Technol.* **2014**, *155*, 63–70. https://doi.org/10.1016/j.biortech.2013.12.084.

(16) Bouchelta, C.; Medjram, M. S.; Bertrand, O.; Bellat, J. P. Preparation and Characterization of Activated Carbon from Date Stones by Physical Activation with Steam. *J. Anal. Appl. Pyrolysis* **2008**, *82* (1), 70–77. https://doi.org/10.1016/j.jaap.2007.12.009.

(17) Hayashi, J.; Horikawa, T.; Takeda, I.; Muroyama, K.; Nasir Ani, F. Preparing Activated Carbon from Various Nutshells by Chemical Activation with K2CO3. *Carbon N. Y.* **2002**, *40* (13), 2381–2386. https://doi.org/10.1016/S0008-6223(02)00118-5.

(18) Hayashi, J.; Kazehaya, A.; Muroyama, K.; Watkinson, A. P. Preparation of Activated Carbon from Lignin by Chemical Activation. *Carbon N. Y.* **2000**, *38* (13), 1873–1878. https://doi.org/10.1016/S0008-6223(00)00027-0.

(19) Jin, H.; Wang, X.; Shen, Y.; Gu, Z. A High-Performance Carbon Derived from Corn Stover via Microwave and Slow Pyrolysis for Supercapacitors. *J. Anal. Appl. Pyrolysis* **2014**, *110* (1), 18–23. https://doi.org/10.1016/j.jaap.2014.07.010.

(20) Yang, T.; Lua, A. C. Characteristics of Activated Carbons Prepared from Pistachio-Nut Shells by Potassium Hydroxide Activation. *Microporous Mesoporous Mater.* **2003**, *63* (1–3), 113–124. https://doi.org/10.1016/S1387-1811(03)00456-6.

(21) Huang, Y.; Ma, E.; Zhao, G. Thermal and Structure Analysis on Reaction Mechanisms during the Preparation of Activated Carbon Fibers by KOH

Activation from Liquefied Wood-Based Fibers. *Ind. Crops Prod.* **2015**, *69*, 447–455. https://doi.org/10.1016/j.indcrop.2015.03.002.

(22)   Otowa, T.; Tanibata, R.; Itoh, M. Production and Adsorption Characteristics of MAXSORB: High-Surface-Area Active Carbon. *Gas Sep. Purif.* **1993**, *7* (4), 241–245. https://doi.org/10.1016/0950-4214(93)80024-Q.

(23)   Xiao, L. P.; Shi, Z. J.; Xu, F.; Sun, R. C. Hydrothermal Carbonization of Lignocellulosic Biomass. *Bioresour. Technol.* **2012**, *118*, 619–623. https://doi.org/10.1016/j.biortech.2012.05.060.

(24)   Demir, M.; Kahveci, Z.; Aksoy, B.; Palapati, N. K. R.; Subramanian, A.; Cullinan, H. T.; El-Kaderi, H. M.; Harris, C. T.; Gupta, R. B. Graphitic Biocarbon from Metal-Catalyzed Hydrothermal Carbonization of Lignin. *Ind. Eng. Chem. Res.* **2015**, *54* (43), 10731–10739. https://doi.org/10.1021/acs.iecr.5b02614.

(25)   Libra, J. A.; Ro, K. S.; Kammann, C.; Funke, A.; Berge, N. D.; Neubauer, Y.; Titirici, M. M.; Fühner, C.; Bens, O.; Kern, J.; et al. Hydrothermal Carbonization of Biomass Residuals: A Comparative Review of the Chemistry, Processes and Applications of Wet and Dry Pyrolysis. *Biofuels* **2011**, *2* (1), 71–106. https://doi.org/10.4155/bfs.10.81.

(26)   Lee, Y.; Park, J.; Ryu, C.; Gang, K. S.; Yang, W.; Park, Y. K.; Jung, J.; Hyun, S. Comparison of Biochar Properties from Biomass Residues Produced by Slow Pyrolysis at 500°C. *Bioresour. Technol.* **2013**, *148*, 196–201. https://doi.org/10.1016/j.biortech.2013.08.135.

(27)   Ben, H.; Ragauskas, A. J. Comparison for the Compositions of Fast and Slow Pyrolysis Oils by NMR Characterization. *Bioresour. Technol.* **2013**, *147*, 577–584. https://doi.org/10.1016/j.biortech.2013.07.151.

(28)   Wilk, M.; Magdziarz, A. Hydrothermal Carbonization, Torrefaction and Slow Pyrolysis of Miscanthus Giganteus. *Energy* **2017**, *140*, 1292–1304. https://doi.org/10.1016/j.energy.2017.03.031.

(29)   Ruz, P.; Banerjee, S.; Pandey, M.; Sudarsan, V.; Sastry, P. U.; Kshirsagar, R. J. Structural Evolution of Turbostratic Carbon: Implications in H2 Storage. *Solid State Sci.* **2016**, *62*, 105–111. https://doi.org/10.1016/j.solidstatesciences.2016.10.017.

(30)   Sevilla, M.; Fuertes, A. B. The Production of Carbon Materials by Hydrothermal Carbonization of Cellulose. *Carbon N. Y.* **2009**, *47* (9), 2281–2289. https://doi.org/10.1016/j.carbon.2009.04.026.

(31)   Bobleter, O. Hydrothermal Degradation of Polymers Derived from Plants. *Prog.*

Polym. Sci. **1994**, *19* (5), 797–841. https://doi.org/10.1016/0079-6700(94)90033-7.

(32)   Huber, G. W.; Iborra, S.; Corma, A. Synthesis of Transportation Fuels from Biomass: Chemistry, Catalysts, and Engineering. *Chem. Rev.* **2006**, *106* (9), 4044–4098. https://doi.org/10.1021/cr068360d.

(33)   Chheda, J. N.; Huber, G. W.; Dumesic, J. A. Liquid-Phase Catalytic Processing of Biomass-Derived Oxygenated Hydrocarbons to Fuels and Chemicals. *Angew. Chemie - Int. Ed.* **2007**, *46* (38), 7164–7183. https://doi.org/10.1002/anie.200604274.

(34)   Lam, P. S.; Sokhansanj, S.; Bi, X. T.; Lim, C. J. Colorimetry Applied To Steam-Treated Biomass And Pellets Made From Western Douglas Fir (Pseudotsuga Menziesii L.). *Trans. ASABE* **2012**, *55* (2), 673–678.

(35)   Bevan, E.; Fu, J.; Zheng, Y. Challenges and Opportunities of Hydrothermal Carbonisation in the UK; Case Study in Chirnside. *RSC Adv.* **2020**, *10*, 31586–31610.

(36)   Shu Lai Mok, W.; Antal, M. Uncatalyzed Solvolysis of Whole Biomass Hemicellulose by Hot Compressed Liquid Water. *Ind. Eng. Chem. Res.* **1992**, *31* (4), 1157–1161.

(37)   Van de Velden, M.; Baeyens, J.; Brems, A.; Janssens, B.; Dewil, R. Fundamentals, Kinetics and Endothermicity of the Biomass Pyrolysis Reaction. *Renew. Energy* **2010**, *35* (1), 232–242. https://doi.org/10.1016/j.renene.2009.04.019.

(38)   Boukis, I. P. Fast Pyrolysis of Biomass in a Circulaing Fluidised Bed Reactor, Aston University, 1997.

(39)   Hara, M.; Yoshida, T.; Takagaki, A.; Takata, T.; Kondo, J. N.; Hayashi, S.; Domen, K. A Carbon Material as a Strong Protonic Acid. *Angew. Chemie - Int. Ed.* **2004**, *43* (22), 2955–2958. https://doi.org/10.1002/anie.200453947.

(40)   Bakti, A. I.; Gareso, P. L. Characterization of Active Carbon Prepared from Coconuts Shells Using FTIR, XRD and SEM Techniques. *J. Ilm. Pendidik. Fis. Al-Biruni* **2018**, *7* (1), 33. https://doi.org/10.24042/jipfalbiruni.v7i1.2459.

(41)   Tiryaki, B.; Yagmur, E.; Banford, A.; Aktas, Z. Comparison of Activated Carbon Produced from Natural Biomass and Equivalent Chemical Compositions. *J. Anal. Appl. Pyrolysis* **2014**, *105*, 276–283. https://doi.org/10.1016/j.jaap.2013.11.014.

(42)   Xue, Y.; Du, C.; Wu, Z.; Zhang, L. Relationship of Cellulose and Lignin Contents in Biomass to the Structure and RB-19 Adsorption Behavior of Activated Carbon. *New J. Chem.* **2018**, *42* (20), 16493–16502. https://doi.org/10.1039/c8nj03007c.

(43)   Tessmer, C. H.; Vidic, R. D.; Uranowski, L. I. Impact of Oxygen-Containing Surface Functional Groups on Activated Carbon Adsorption of Phenols. *Environ. Sci. Technol.* **1997**, *31* (7), 1872–1878. https://doi.org/10.1021/es960474r.

Chapter 3 Physiochemical Properties of Biochar and Activated Carbon from Co-Pyrolysis of Corn Stover and Plastics

3.1 Abstract

The physiochemical properties of biochar and activated carbon produced from co-pyrolysis (CoSP) of corn stover (CS) and plastics, polystyrene (PS) and polyethylene terephthalate (PET). The hydrogen donor effect of PS on CS is evaluated for the solid fraction and proved to create a lower quality biochar and activated for surface area and adsorption. CS-PET biochar produced high surface area biochar, 423.8 ± 24.8 m^2/g for 500 °C 2h 1:1 biochar, but contained microplastics on the surface. Chemically activated with KOH, the microplastics and acids produced from PET degradation inhibited activation and thus created lower surface area for the samples containing high amounts of PET, 1:1 and 4:1 samples. X-ray diffraction, scanning electron microscopy, x-ray photoelectron spectroscopy, and Fourier-transform infrared spectroscopy highlighted the differences between the biochars and activated carbon. Vanillin adsorption testing showed AC CS performed the best at removing 95% of the vanillin after 2 hours, whereas the AC CS-PS and AC CS-PET removed 45% and 46%, respectively.

3.2 Introduction

Plastic upcycling is an alternative to recycling where plastic is converted to value-added products like activated carbon, fuels, waxes, and lubricants[1–3]. Plastic waste is a growing problem in the world with some forms of plastic can take up to 1,000 years to decompose in landfills[4]. In 2015, an estimated 4,900 million tons of plastic have been discarded, and the number is projected to increase to 12,000 million tons by 2050[5]. A common belief is that recycling is a viable solution for the plastic waste; however, several factors prevent recycling on all forms of plastics[1,6–8]. These include the lower value

products formed from mechanical recycling and select forms of plastic are very inexpensive materials to make, which means there is little profit margin for adopting recycling strategies. Recycling plastic is a challenging and energy-intensive process due to contamination and additives. For these reasons, there is little to no economic incentive to recycle plastic. Plastic is an overarching term to describe a synthetic material comprising of polymers. Around 40% of plastic produced falls into the single use products composed of polyethylene, polypropylene, and polyethylene terephthalate (PET)[9]. PET is a polymer containing repeating ethylene glycol and terephthalic acid monomers. Polyesters like PET that contain high ratio of aromatic components are very resistant to microbial degradation which can pose issues with limiting accumulation[10,11]. In 2016, 14 million tons of polystyrene (PS) were produced and PS is an aromatic polymer comprised of styrene monomers[12]. The high molecular weight of PS contributes to the difficulty in degradation of the material[13]. The attributes of PET and PS that make it widely used such as stability and low resistance to outside forces are also what make it difficult to degrade. Finding ways to transform these plastics will be necessary to combat the growing accumulation problem.

One technique to transform plastics into a value-added product is by using pyrolysis to breakdown the polymeric structure into three fractions: solid, liquid and gas that can be valorized to chemical commodities and material sorbents. A strategy that incorporates the existing biorefinery framework seeks to combine processing of natural and synthetic polymers in a process called co-pyrolysis (CoSP). Co-pyrolysis involves thermoconversion of the biomass and plastic feeds in an inert environment and temperatures between 300-

700 °C. The liquid fraction is known as pyrolysis (or bio) oil and is one of the most valuable streams that can be used a s a feed for fuels and chemical commodities[14–16]. During co-pyrolysis, many studies have indicated a synergistic relationship between the plastic and biomass to improve the oil qualities higher calorific value and alkenes[17,18]. It is theorized that certain plastics act as a hydrogen donor in co-pyrolysis[19,20]. The solid fraction, biochar, has not been studied in depth and is often regarded for use as a sorbent; however, it is not clear whether co-pyrolysis also improves the qualities of the biochar. While the co-pyrolysis of corn stover and polystyrene have been studied together, the focus was on the pyrolysis oil yield and quality[21]. Generally, biochar is largely ignored; however, additional research is needed on biochar to optimize the use of all fractions from pyrolysis. The goal of this study is to evaluate the physiochemical properties of biochar produced from co-pyrolysis of corn stover and PS/PET and assess whether there are synergistic qualities that can improve their use for sorbents or activated carbon.

Biochar in of itself is nutrient rich and can be utilized for soil remediation, among other applications. Typically, biochar can be further chemically or physically treated to form activated carbon. Activated carbon is utilized in industries such as water treatment[22,23], air purification[24,25], and catalysis[26,27] often as a support or used for pollution remediation. Chemical activation is a method in which an activating agent such as KOH reacts with the biochar to form large pores and are exfoliated. In a two-step process where biochar is first formed then activated, the reaction temperature and dwell time can influence the final activated carbon pore structure, surface area and pore size. This study will evaluate the different physiochemical properties of the activated carbon produced from co-pyrolysis

utilizing CS-PS biochar, CS-PET biochar, and CS biochar. The physiochemical and morphological properties of biochar and AC were analyzed using BET surface area, XRD, SEM, FTIR, and XPS. Vanillin adsorption experiments were conducted to investigate the adsorptive properties of the AC to mimic phenolic removal of chemical compounds in industrial wastewater streams.

3.3 Materials and Methods

3.3.1 Slow Pyrolysis and Co-pyrolysis.

A Carbolite Gero Tube Furnace with a constant flow of nitrogen gas at a rate of 600 mL/minute was used for the pyrolysis experiments. The feedstock was comprised of either corn stover, milled to 1 mm, and a plastic, either Sigma Aldrich Polystyrene MW 192,000 or hand cut 0.5 cm squares of PET plastic from plastic water bottles. The feedstock was placed in a ceramic boat and purged with nitrogen for 5 volumes of the reactor to ensure an oxygen free environment. The sample was then placed in the tube furnace and heated to the desired temperature at a ramp rate of 10 °C/min and held for the desired duration and then allowed to cool to room temperature. The oil was collected using a single pass cold trap attached to the end of the exhaust of the tube furnace.

3.3.2. Chemical Activation of Biochar.

A Thermo Scientific Type 1315M Benchtop Muffle Furnace inside a nitrogen glovebox setup was used for the chemical and thermal activation of carbon. The biochar was combined with KOH in a 2:1 ratio of biochar to KOH by mass. DI water was added to the mixture and stirred for 1 h to ensure it was homogeneous. The mixture was then dried in an oven at 105 °C overnight. The sample was transferred into the nitrogen environment

muffle furnace, heated to 300 °C for 2 h at a ramp rate of 10 °C/min to remove moisture, and then further heated to 800 °C for 3 h with a ramp rate of 10 °C/min. Once cooled, the sample was washed with a 0.1 M HCl solution to neutralize any remaining KOH. The sample was vacuumed-filtered and washed with DI water until the filtrate was pH neutral. The formed activated caron (AC) was dried in an oven overnight at 105 °C before characterization. For the direct chemical activation method, corn stover replaced the biochar in equal amounts and the rest of the procedure for chemical activation remained the same.

3.3.3. Surface Area Analysis.

Surface analysis was conducted using the Micromeritics ASAP 2020 physisorption instrument to perform BET measurements. The sample was loaded and degassed for 8 h until an outgassing rate of less than 5 μm Hg/min was achieved to ensure moisture and volatile contaminants were removed before analysis. N_2 physisorption and five-point BET analysis were used to measure the surface area, pore volume, and pore size. The BET was calibrated with a silica−alumina reference material with a standard error of 2.5%. Replicates of most of the biochar and AC were performed to determine the intrinsic errors in the surface areas and pore sizes with 95% confidence levels.

3.3.4. Scanning Electron Microscopy.

A TESCAN Vega3 SBH SEM was used to measure images of the various corn stover, biochar, and AC samples. Before imaging, the samples were placed under vacuum, purged with argon, and then sputter-coated with Au for 10 s to improve the clarity of the

images. The images were taken at 1,000 times magnification with a voltage of 5 kV unless stated otherwise.

3.3.5. XRD and XPS

A PANalytical Empyrean Series 2 XRD instrument was utilized to evaluate the carbon structures. The emission source was Cu Kα (1.54056 A wavelength) with a Ni beta filter. A zero-diffraction plate was employed to minimize the background peaks. XPS characterization was carried out using a Kratos AXIS ULTRA XPS system equipped with an Al X-ray source and a 165 mm mean radius electron energy hemispherical analyzer. Neutralizing was applied during the measurements to compensate for sample charging.

3.3.6. Fourier Transform Infrared Spectroscopy (FTIR).

Surface functional groups of char and the ACs were investigated using an FTIR Spectrometer (Nicolet 6700, Thermo Electron Corporation). The FTIR used a KBr beam splitter with a deuterated triglycine sulfate (DTGS) detector. Gathered spectra was an average of 16 scans with 4 cm^{-1} resolution between the range of 525−4000 cm^{-1}.

3.3.7. Batch Adsorption Study of Vanillin.

The batch experiments of the vanillin adsorption studies using the AC and biochar were conducted at room temperature in a 150 mL beaker. For each run, 50 mg of the adsorbent was placed in a beaker containing 50 mL of a vanillin solution, which had a concentration of 100 mg/L. The suspension was stirred for a desired time, between 30 and 120 min, using a magnetic agitator. After agitation, the suspensions were gravity-filtered. The concentration of the filtrate was determined by using an Agilent Cary 60 UV−visible

spectrophotometer. The absorbance wavelength was measured between 200 and 500 nm at a rate of 60 nm/min and a 0.50 nm interval.

3.4 Results and Discussion

3.4.1 Biochar Properties from Co-Pyrolysis of Corn Stover and Plastics

3.4.1.1 Physiochemical Properties of Biochar from CS and PS

The physiochemical properties of the biochar from co-pyrolysis of corn stover and polystyrene (CS-PS) were investigated. The effect of temperature on surface area was studied using the following temperatures: 400 °C, 500 °C, and 600 °C, shown in Table 3.1. Surface area is a key indicator of biochar as it plays a critical role in many applications. The surface area of the 500 °C and 600 °C biochars are higher than 400 °C biochar. At 400 °C, the degradation of corn stover is low and likely the cause of the lowest surface area. When corn stover is carbonized using slow pyrolysis, an optimal point for surface area was found around 550 °C, which was due to multiple reactions, primarily fragmentation[28]. At 550 °C the decomposition of cellulose and hemicellulose play an important role in surface area. The 500 °C and 600 °C having an increase in surface area compared to the 400 °C is due to the degradation reaction in corn stover. The addition of polystyrene seems to have not had significant impact on this trend. A low surface area is observed overall for these biochars.

A study of pyrolysis of PS showed no degradation at 300 °C, but between 350°C the sample had completely degraded to a liquid. Between 350-500 °C char was formed with the maximum at 500 °C which is an indication of condensation if the ring structure if the aromatic compounds at higher temperatures[29]. The experiments in the study were

conducted in a closed batch reactor where the co-pyrolysis experiments were conducted in a tube furnace with a constant flow of N_2 sweep gas. The sweep gas will likely cause no condensation reactions to occur with the biochar due to limited exposure to the biomass biochar. For PS pyrolysis temperatures greater than 500 °C are recommended if the desired product is gas or char[30]. The CS-PS biochar produced did not show significant benefit in surface area and showed a decrease in biochar production from increased temperatures. The constant flow of N_2 could be the cause for PS not having a significant impact on the biochar. Another study of pyrolysis of polystyrene that had the vapor removed from the solid fraction showed results that agreed with ours, as temperature increased solid char decreased[31]. Around 500 °C, there is primarily random scission and depolymerization forming styrene reactions occurring and at slightly higher temperatures, intramolecular hydrogen transfer occur[32].

The impact of duration on co-pyrolysis was studied, and the results are shown in Table 3.2. The 1-hour duration run produced a biochar of 11.1 ± 1.5 m^2/g and when the duration increased, a slight increase of surface area was observed with the 2-hours and 4-hours producing 11.7 ± 2.8 m^2/g and 14.3 ± 5.3 m^2/g, respectively. In slow pyrolysis of corn stover an optimal temperature was found to be around 550 °C[28]. Paired with the temperature effect results, there is justification to assume that 500 °C is under the optimal temperature for surface area generation reactions. Longer duration allows for more surface rich compounds to be formed. If the duration effect was tested at a higher temperature, the reverse may be observed due to reactions like cracking and further fragmentation

completely converting the solid mass into the gas and liquid phases. The impact of duration may vary depending on the vessel due to the kinetics and heat transfer differences.

The ratio of CS to PS was varied from 1:1, 4:1, 9:1, and 1:0 to further investigate the impact of PS in CoSP. Table 3.3 provides the surface area results. The highest surface area of the biochars containing PS was the 4:1 ratio at 11.7 ± 2.8 m^2/g. The pure biomass has a higher surface area of 12.4 ± 3.7 m^2/g than any of the CS-PS biochars. Overall, the biochars had low surface areas. The optimal point at 4:1 ratio shows there is an impact on the properties of biochar from PS. The hydrogen donor effect may be a cause the differences between ratios.

The amount of biochar recovered as a ratio of initial corn stover changed very little with the ratio change of polystyrene. This is an indication that the solid residue is comprised mainly of corn stover, and PS residue mass is playing little to no part in the char. While the polymer may not be playing a role in the mass of the biochar, the PS can still be affecting how the final biochar ends up. The temperature and duration effects showed as each parameter increased, more of the char is converted into the liquid and gas fractions. This is expected as pyrolysis of biomass is well documented, that increases in temperature and duration will cause less solid residue.

PS has been shown to be a hydrogen donor in co-pyrolysis of cellulose and PS and produces monocyclic aromatic hydrocarbons[33]. However, the hydrogen donor effect on the biochar did not benefit the biochar in surface area or production. When the CS-PS biochar is compared with the CS biochar, the surface area is lower.

Figure 3.1 shows the XRD spectra of the biochars produced from slow pyrolysis of corn stover and co-pyrolysis of corn stover and plastic. The XRD shows the transformation of corn stover into biochar. At 500 °C, the cellulose peaks have disappeared and broad amorphous carbon peaks, 15-30° 2θ, are visible. Turbostratic carbon (t-carbon) peak has also become more intense indicating a higher ratio of t-carbon. On the CS-PS biochar, there is a lack of a peak at 18-19° 2θ, which is a peak for polystyrene[34,35]. There are no detectable levels of polystyrene on the surface of the biochar which furthers the idea polystyrene is not playing a significant role in biochar mass. The 1:1 ratio of CS-PS biochar has less intense peaks of t-carbon and quartz than the 4:1 ratio or the CS biochar.

Scanning electron microscopy (SEM) images were taken of the CS-PS biochars and are shown in Figure 3.2. As temperature increases, the observable degradation on the surface increases as well. The CS-PS biochar shows a resemblance to biochar produced from CS. The wood like structure of corn stover is still visible. This promotes the idea that the impact of PS on biochar is minimal.

FTIR of the CS-PS biochar can be seen in Figure 3.3A. The biochars of CS and CS-PS show some triple bond stretching around 2100 cm^{-1} (C≡C). There is stretching in the double bond region around 1530-1610 cm^{-1} which is attributed to C=O and C=C. The 4:1 CS-PS biochar has as deeper peak in the double bond region whereas the biochar CS and CS-PS 1:1 have shallower peaks. C-O and C=O from alcohols, carbonyl groups, and potentially silicone stretching can be observed from 860-1200 cm^{-1}.

3.4.1.2 Physiochemical Properties of Biochar from CS and PET

The physiochemical properties of the biochar from co-pyrolysis of corn stover and polyethylene terephthalate (PET) were investigated. The effect of temperature was studied using the same temperatures as the polystyrene experiment: 400 °C, 500 °C, and 600 °C, shown in Table 3.4. The 400 °C biochar had the lowest surface area by a significant margin at 12.9 ± 11.9 m^2/g. Thermal degradation of PET starts after 400 °C with a the maximum weight loss at 442 °C[36]. The surface area produced at 400 C is likely due to the carbonization of corn stover and PET is playing little part. However, once thermal degradation of PET occurs, the surface area drastically increases. At 500 °C, the biochar had the highest surface areas of the tested temperature range at 91.2 ± 20.4 m^2/g. PET pyrolysis creates benzoic acid, terephthalic acid, and cyclic oligomers from random scission at ester links and potentially transesterification involving end groups[37,38]. Co-pyrolysis of cellulose and PET has been studied, where the benzoic acid and terephthalic acid are likely consumed during the char formation[33]. The surface area is suspected to be due to the interactions of the acids and the cyclic oligomers with the corn stover. The oligomers may be depositing on the surface and creating additional surface area structures.

To ascertain a better understanding of PET influencing corn stover, varying the ratio can between CS and PET can be used. The ratio effect was studied with ratios (corn stover to PET) of 1:1, 4:1, 9:1 and 1:0 shown in Table 3.5. The ratio that gave the highest surface area with PET was 1:1 with a surface area of 423.8 ± 24.2 m^2/g. This is a very high surface area for a biochar and rivals some activated carbon surface areas. As the ratio of CS to PET increases, the surface area falls with the 4:1 and 9:1 biochars having surface

areas of 91.2 ± 20.4 m^2/g and 74.5 ± 26.8 m^2/g, respectively. This advances the importance of thermal degradation of PET on co-pyrolysis. The biochar from corn stover produced significant lower surface area biochar, 12.4 ± 3.7 m^2/g, when compared to the CS-PET biochar. The PET is helping to form high surface area compounds on the biochar. To confirm this, the amount of biochar produced as a function of initial corn stover showed that the PET did impact the mass of the biochar.

SEM can be used to look at the surface changes with the addition of PET. Figure 3.4 shows the SEM imaging of the PET biochar ratio effect. When comparing Figure 3.4A and 3.4C, 1:1 and 9:1 ratio, respectively, a noticeable surface difference is observed. The 1:1 biochar has a flakier looking structure which is a result of a more intense decomposition. The biochar does not resemble the original corn stover. However, in the 9:1 biochar, the corn stover stalks within the structure are visible. This can be seen in the rectangular and wood-like structures on the SEM image. When looking at the difference of ratios, the 9:1 has 80% more corn stover than the 1:1 ratio, which partially accounts for the drastic difference. The other portion is the PET; PET is in the formation of the biochar and thus will contribute to the morphology differences. The SEM images help explain how PET has changed the surface which led to increased surface area.

When the images are zoomed in more an interesting structure is observed on the surface. Figure 3.5 shows the 1:1 and 9:1 biochar zoomed in to 4,200 times and 8,000 times, respectively. "Rice grain" structures that appear on the surfaces of our samples. Figure 3.5B has sharp "rice grains" on the surface which looks to have created additional ridges. Ridges can increase surface area, as it is similar to adding fins to a heat exchanger.

Figure 3.5D, 9:1 CS-PET biochar, shows small rice grains all over the surface without creating as merged of a look. The results indicate that these structures are microplastics, the oligomers formed during PET degradation. The microplastics may present contamination issues and there are potential harmful effects being studied[39]. The PET biochars may not be suitable for applications where human consumption is involved such as water filtration.

XRD is used to observe changes in the surface of the biochars, shown in Figure 3.1. As corn stover is converted to biochar through CoSP with PET, the disappearance of the cellulose peaks is apparent. Both the 4:1 and 1:1 ratio show increased t-carbon peaks at 26.6° 2θ. When comparing the biochar from CS and biochars from CS-PET, there are more pronounced peaks of crystalline quartz and carbon. At 24.3° 2θ, there is a peak for PET plastic[40]. The peak at 20.6-21.2° 2θ coincides with quartz as well as PET plastic[40–42]. This indicates that there is residual PET on the surface in detectable levels which furthers the theory that microplastics are on the surface of the CS-PET biochars. A peak at 27.7° 2θ is likely to be crystalline carbon in the biochar[43]. Broad amorphous carbon peaks are show in all the biochars.

FTIR of CS-PET biochar can be observed in Figure 3.3A. The CS-PET biochars show deep stretching in the double bond region which is attributed to C=O and C=C. An additional peak is observed around 1400 cm^{-1} which indicated C-C, C-O-C, and C-O bonds. This peak is not observed in the biochars of CS and CS-PS. This peak may be attributed to the PET polymer residue left on the biochar. C=O and C-O stretching are observed on all the biochar around 880-1200 cm^{-1}.

The CS-PET and CS-PS biochars can also be compared to evaluate the different effects of each plastic. CS-PS biochar had lower surface areas at the same conditions for each temperature and ratio when compared with CS-PET biochar. The difference in plastic degradation is the major difference. PET degradation produces acids and oligomers that PS degradation does not. PS is a hydrogen donor, and the extra hydrogen is causing reactions like dehydration. The PET degradation compounds are likely creating the surface area difference. SEM imaging showed the microplastics on the surface of CS- PET biochars; however, when CS-PS biochars were probed no such structures were found. Following that the XRD showed a polymer peak for CS-PET and none for CS-PS biochars. The FTIR also showed a potential residue polymer peak around 1400 cm^{-1} that the CS and CS-PS did not show.

3.4.2 Activated Carbon Properties from Co-Pyrolysis of Corn Stover and Plastics

3.4.2.1 Physiochemical Properties of AC from CS and PS

The biochar from CoSP CS-PS was chemically activated with KOH to form activated carbon (AC). The surface area of the AC was examined to observe how the different parameter changes of biochar production affect the final product. Table 3.6 shows the temperature effect parameter for AC. The lowest temperature, 400 °C, had the highest surface area at 572.6 ± 21.5 m^2/g. The 500 °C and 600 °C ACs produced lower surface areas, 477.0 ± 40.8 m^2/g and 440.1± 59.3 m^2/g, respectively. AC CS from SP showed the same trend that a lower pyrolysis temperature created higher surface area AC[28]. For biochar, the addition of PS to CS showed little difference to trends observed with only CS.

Also, PS showed little low interaction with the biochar mass, indicating that the biochar is mainly CS. Previous work showed activation and pyrolysis used similar compounds in the biomass thus higher pyrolysis temperature will decompose more of the necessary compounds to produce high surface area[28].

Table 3.7 shows the duration effect of CoSP on the AC surface area. The shortest duration, 1-hour of CoSP, produced the highest surface area AC at 482.6 ± 22.9 m^2/g. Surface area has an inverse relationship with duration at 500 °C and 4:1 ratio, as the duration increased the surface area decreased. The change in surface area between the 1-, 2-, and 4-hour runs is small but a distinct difference. The higher surface area biochars tended to produce lower surface area ACs, which was a general trend observed with SP of CS[28]. The longer duration is degrading the CS-PS mixture which is causing the KOH to react with other species that do not produce as high of surface area compounds.

Table 3.8 shows the ratio effect on the AC. The AC 4:1 ratio had the highest surface area of CS-PS ACs with 477.0 ± 40.8 m^2/g. The 1:1 and 9:1 activated carbons had surface areas of 445.9 and 404.7 ± 5.7 m^2/g, respectively. This indicates there is an optimal point for the CS-PS ratio. However, the pure biomass AC had a surface area of 614.4 ± 0.2 m^2/g, which is the highest surface area AC. When evaluating the ratio effect, the 4:1 ratio had the highest surface are for both the biochar and AC which contradicts the theory that a higher surface area biochar will produce a lower surface area AC. This signifies an impact of PS on the solid fraction. The activation mechanisms may provide insight on the impact.

The activation method of KOH reacts with the carbon and oxygen species in biomass and plastics. KOH chemical activation of carbon rich species can be summarized

by K-species etching the carbon matrix through redox reactions, H_2O, formed during the reaction, increasing porosity through gasification, and metallic K expanding the carbon lattices[44,45]. These interactions with carbon rich species lead to high surface area and high porosity structures. Another important interaction in chemical activation is KOH with oxygen containing species, C-O, C-O-H, and C-O-C[46]. KOH reacts with O-containing species in biomass to remove O-containing groups thereby creating free radicals and vacancies. OH^-, from KOH, will fill the vacancies to form new O-containing groups which will increase oxygen and porosity in the sample[47].

XRD can provide additional information on the crystalline structure shown in AC. In Figure 3.6, the XRD spectra for the various AC. The 4:1 ratio CS-PS biochar activation shows little change in XRD spectra, the quartz peak is more intense in the AC- Figure 3.1 is compared with Figure 3.6. Both show t-carbon peak at 26.6° 2θ, broad amorphous carbon peaks, 15-30° and 40-50° 2θ, and crystalline carbon. The 1:1 ratio CS-PS does show more changes. The quartz peak, 20.9° 2θ, and crystalline carbon peaks disappear with a graphite oxide peak appearing, 23.3° 2θ[48], and a more intense t-carbon peak.

SEM imaging of the activation of CS-PS biochar can be seen in Figure 3.7. In Figure 3.7B, the AC surface morphology and appearance has changed drastically from the biochar, Figure 3.7A. KOH has reacted with the biochar and formed a significant porosity in the structure. From the images, more macropores and mesopores can be observed in the AC, and micropores can be inferred to have formed as well.

Fourier transform infrared (FTIR) spectrometry was conducted on the biochar samples and activated carbon to examine the surface functional groups. FTIR spectra for

the AC of CS-PS can be observed in Figure 3.3B. The major stretching is attributed to the triple bond region of C≡C around 2100 cm⁻¹. The AC produced from CS and CS-PS are nearly identical. The AC CS-PS has a slightly shallower triple bond peak which would be attributed to the hydrogen donor effect from PS degradation. The FTIR spectras show that the activation tends to create similar surface function groups. The activation can be observed by comparing Figure 3.3A and 3.3B. The biochar stretching in the double bond and fingerprint regions disappear when activated. There is no more observed C=O, C=C, and C-O bonds in the FTIR in Figure 3.3B.

Table 3.9 shows the elemental analysis, XPS, of biochar and AC. The impact on the plastics during CoSP can be highlighted here. The CS-PS biochar produced a lower oxygen content by percentage than CS biochar. PS is a hydrogen donor in CoSP and the extra hydrogen is likely causing deoxygenation reactions thus creating a lower O-containing biochar. When the CS-PS biochar is activated the oxygen content jumps from 18% to 26%, the highest of any of the samples. The KOH is adding oxygen to the vacancies created during activation. The importance of having O-containing groups in the feedstock of activation was discussed by Chen et al[47]. The decrease in oxygen containing groups in CoSP of CS-PS is likely playing the significant role in lower surface area of activated carbon.

3.4.2.2 Physiochemical Properties of AC from CS and PET

The CS-PET biochar was chemical activated and studied for its physiochemical properties. Once activated, the temperature effect shows some unexpected results. Table 3.10 shows the surface area results for changes in the temperature parameter. At the high

71

temperature of 600 °C, the surface area is the highest at 510.7 ± 4.7 m^2/g. The lowest surface area was recorded from the 500 °C sample of 87.8 ± 3.2 m^2/g. The 400 °C was in the middle with a surface area of 359.9 ±1.0 m^2/g. The impact of temperature on AC CS-PET tend to challenge many of the results gained from AC pyrolysis. The results highlight the need for further investigation of PET plastic influence in CoSP. The 500 C AC had a reduction in surface area when compared with the biochar. The CoSP biochar inhibited the activation method. The ratio effect and analysis of the KOH activation may help explain the results.

To investigate more into the relationship between PET and CS, the ratio effect was evaluated for AC. The ratio effect was studied with biochar produced at 500 °C 2 hours and varying the ratio from 1:1, 4:1, and 9:1 of CS-PET, respectively. The surface areas from the ACs are shown in Table 3.11. The 1:1 ratio AC produced the highest surface area at 409.2 ± 1.2 m^2/g, and 9:1 ratio was just under the 1:1 with a surface area of 390.1 ± 10.7 m^2/g The 4:1 ratio produced the lowest surface area at 87.8 ± 3.2 m^2/g. The surface area of the CS-PET biochar from the 1:1 ratio decreased slightly from 423.8 ± 24.2 m^2/g to 409.2 ± 1.2 m^2/g as well as the 4:1 AC saw a decrease from biochar to AC. The 9:1 ratio CS-PET increased in surface area post activation. PET is the cause of the decrease as the samples with the higher concentrations of PET showed decreases in surface area. The 9:1 sample is predominantly CS which is the probable cause why it did not show the same trend as the 4:1 and 1:1 samples.

Alkali assisted pyrolysis of PET allowed for lower temperature thermal decomposition[38]. The alkali strongly affected the thermal degradation of PET polymer. The

chemical activation of biochar uses an Akali reactant, KOH, to form the AC. This helps explain the decrease in surface area as likely the KOH is being reacted with the oligomers and leftover PET polymers at low temperatures. Thus, the biomass section of the biochar may not be as influenced due to the KOH reacting with polymers first. The polymers in the previous section were hypothesized to be a key contribution to surface area and if they are consumed during activation a loss in surface area would be expected. Another theory is the acids that are produced from pyrolysis of PET are reacting with the KOH prior to the temperature. The acid site may be on the surface of the biochar as well as trapped inside the pores as bio-oil.

SEM imaging was taken to observe the changes on the surface. In Figure 3.8, the ratio effect can be observed on the surface. As the amount of corn stover increases, the surface morphology changes as well, becoming a more porous. The microplastics on the surface of the biochar are no longer visible. The disappearance is attributed to the high temperatures thermally degrading the polymers completely and KOH reacting with the polymers first. The surface on the 1:1 AC looks similar to the 1:1 biochar, which may be an indication that the KOH did not have as dramatic impact as it does with corn stover. The 9:1 ratio AC looks like the pure corn stover AC. The 4:1 AC looks like some portions have reacted while others still look like the biochar. These observations further indicate the KOH is reacting with the PET plastic first prior to reacting with the corn stover biochar, which is a reason for the lower surface area upon activation for the 1:1 and 4:1 AC.

The AC from corn stover has higher surface area, 614.4 ± 0.2 m^2/g, than any of the CS-PET ACs. While the CS-PET biochars had higher surface areas, once activated the AC

CS produced a higher surface area. If one's goal is to create a high surface area AC, the addition of PET should not be valued highly.

Figure 3.6 has the XRD results for the AC CS-PET. In the AC 1:1 CS-PET XRD spectrum, there are only amorphous carbon peaks. No other peaks are visible. The AC 4:1 CS-PET spectrum contains the amorphous carbon, quartz, and t-carbon peaks. The activation removed the PET peak shown in the biochar, Figure 3.1. The XRD helps further the idea that KOH is reacting with the polymers on the surface first and removing them.

Figure 3.3B shows the FTIR results of the CS-PET activated carbon. The biochar, Figure 3.3A, once activated, no longer contains the stretching of C-O, C=O, C-O-C and C=C. There is also no peak around 1400 cm^{-1} which may be credited to the microplastics which furthers the idea that PET is no longer on the surface. The activated carbon spectrum from CS-PET looks like the AC from other samples like CS-PS and CS. In fact, all the activated carbons have similar shapes and slightly different peaks for CO_2 and triple bonds.

Elemental analysis for CS and PET is shown in Table 3.9. CoSP of CS-PET created the lowest oxygen containing biochar at 15%. While it created a lower oxygen content, the biochar had the highest surface area. After activation the oxygen content increased to 23%, the lowest of the ACs. KOH is known to fill in vacancies during activation and increase oxygen content. When activated though the surface area of the CS-PET sample was reduced. O-containing groups in biomass are significant during activation, and the reduction during CoSP of CS-PET is a potential cause for the reduction in surface area. Activation of CS had a minor jump in oxygen content, 21% to 24%, and CS-PS had a more significant jump, 18% to 26%. AC CS-PS and AC CS-PET had low surface areas, and both

shared a lower oxygen biochar as a starting point which supports the importance of O-containing groups in biomass prior to activation.

3.4.3 Adsorption Properties of AC

Vanillin adsorption experiments were conducted on the activated carbon to test the application of the products, Table 3.12. AC CS was able to remove 95% of the vanillin (100 mg/L) after 2 hours. AC CS-PS and ACPET were able to remove 45% and 46%, respectively, after 2 hours. The AC from CS-PS and CS-PET performed almost identical for all the trials with a slight advantage at removal to AC CS-PET. AC CS outperformed the other ACs by a significant margin across all tested durations. Surface area is a metric to help determine adsorption capacity. The higher surface area of AC CS played a role in the better adsorption; however, surface area does not tell the entire story. While AC CS-PS has a marginally higher surface area than AC CS-PET, the performance was slight worse. If surface area was the only metric that matter, then the biochar of CS-PET would outperform the AC. When the CS-PET biochar was tested for vanillin adsorption, the sample removed too little for the UV Vis to detect. The surface functional group can play a significant role in the ability to adsorb the vanillin. The FTIR for the activated carbon data showed similar spectra for all and the surface functional groups could not be distinguished from it. However, the activation mechanisms of the CS, CS-PS, and CS-PET are all different which lead to different adsorption capabilities.

3.5 Conclusion

The physiochemical properties of biochar and activated carbon produced from co-pyrolysis of corn stover and a plastic (PS or PET) were evaluated. The biochar and

activated carbon produced from CS-PS showed lower surface areas than that made from corn stover. The hydrogen donor effect of PS did not create better biochar or AC for surface area or adsorption properties. The biochars from CS-PET have high surface areas in particularly the 500 °C 2h 1:1 ratio, 423.8 ± 24.8 m^2/g. However, polymers were found on the surface of the biochar. Once activated, the polymers were no longer present, but the surface area decreased. The 1:1 and 4:1 CS-PET samples both had lower surface areas when activated which is attributed to the PET thermal degradation. PET thermal degradation produces oligomers and acids which interact with the KOH thus inhibiting high surface area formations. Overall, co-pyrolysis of corn stover and plastic produced lower surface area activated carbons that performed worse at vanillin adsorption when compared to pyrolysis of corn stover. Co-pyrolysis may have many applications such as upgrading bio-oil, however, this may come at the expense of the solid fraction.

3.6 Conflict of Interest
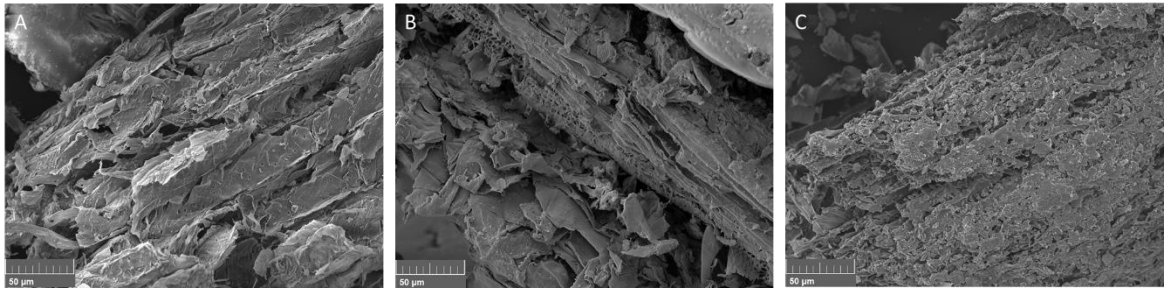
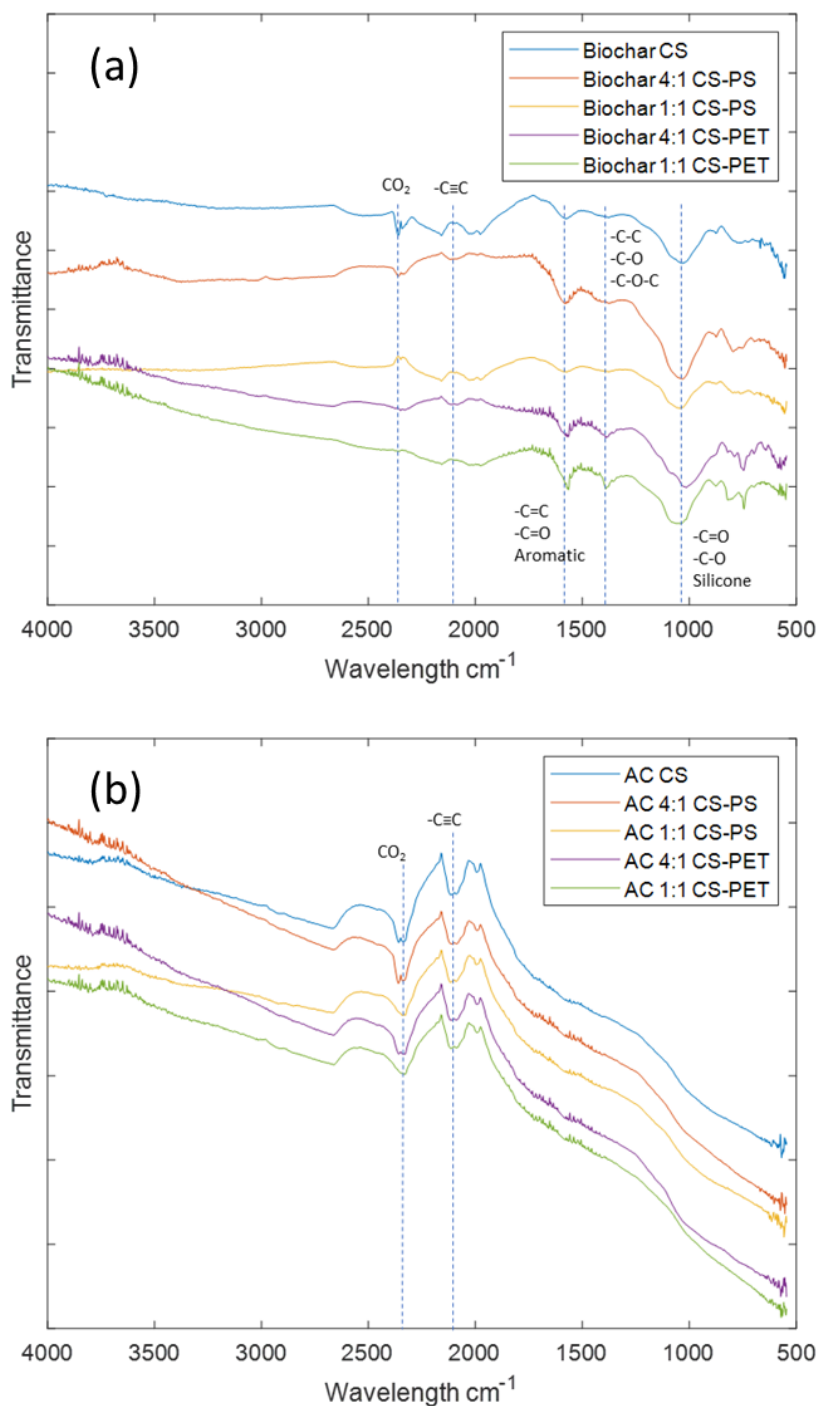The authors declare no conflict of interest.

3.7 Acknowledgements
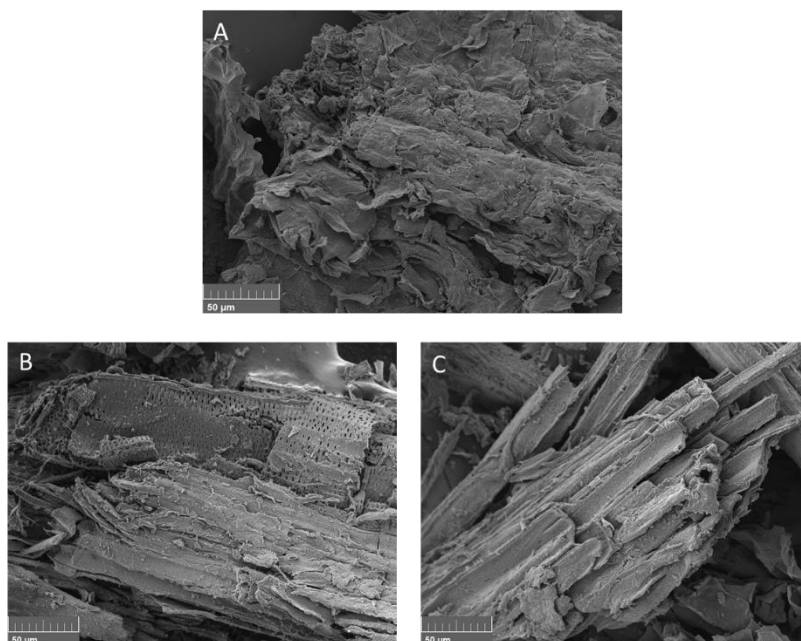
3.8 Figures and Tables
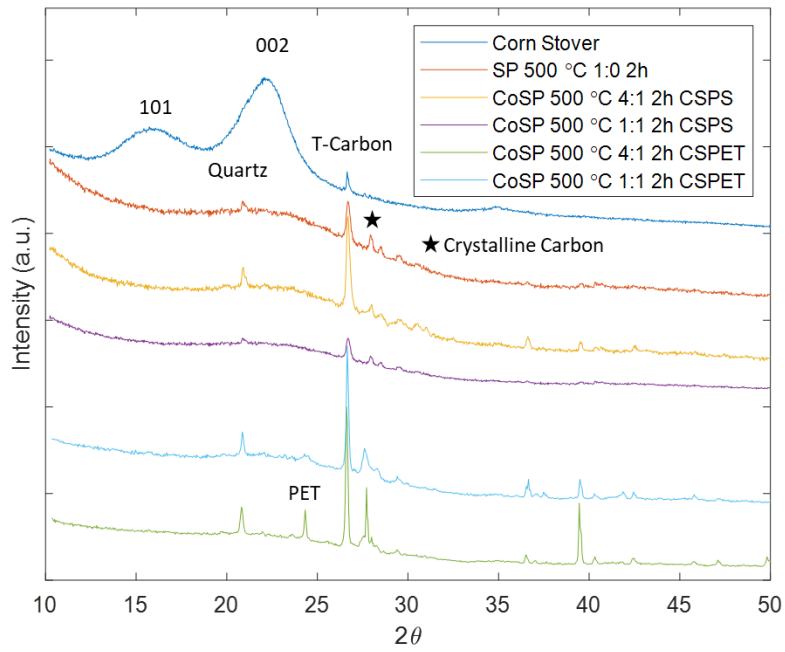
Figure 3.1 X-ray diffraction of biochars and corn stover

Figure 3.2 SEM images of CoSP biochar 2h 4:1 CS-PS A) 400 °C. B) 500 °C C) 600 °C
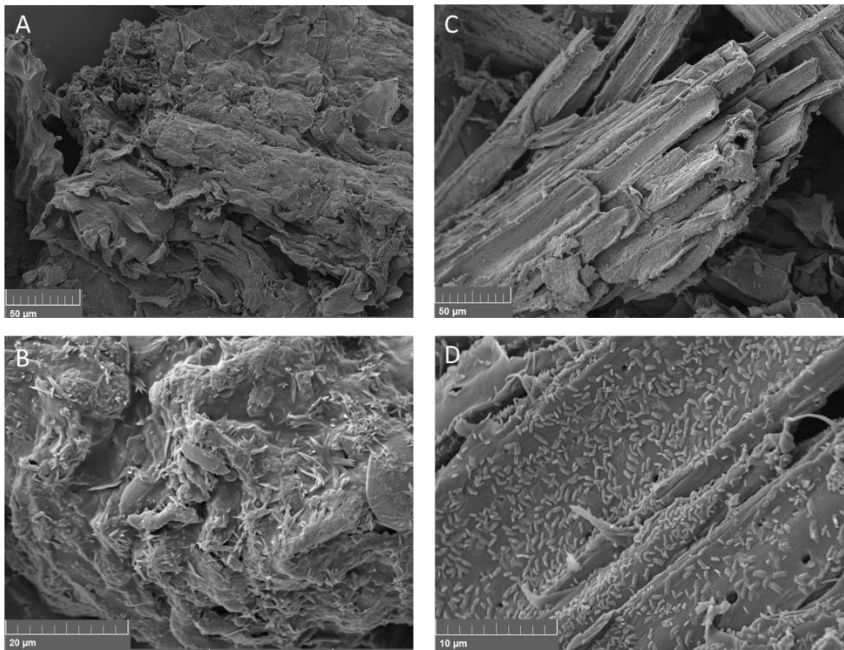
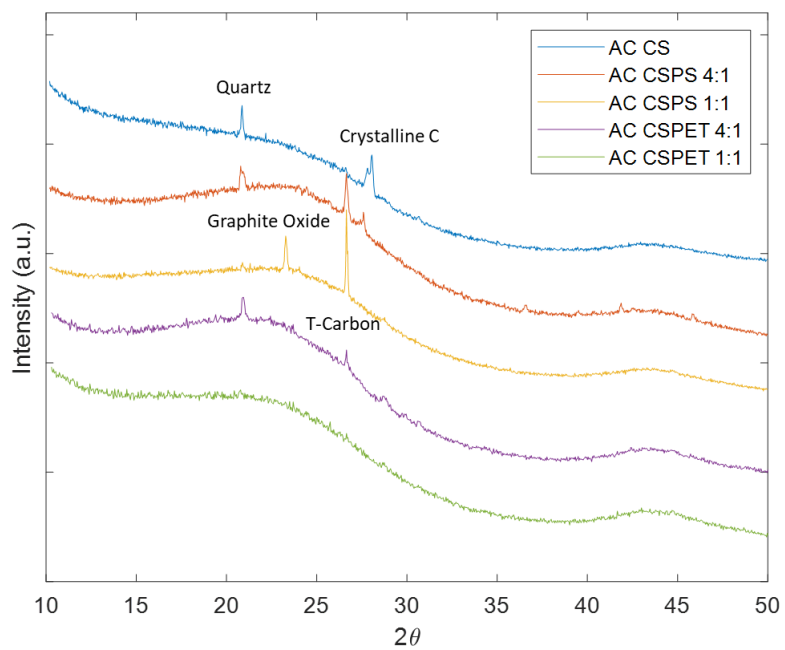**Figure 3.3** FTIR spectra a) Biochar b) AC 500 2h for CoSP conditions

Figure 3.4 SEM images for biochar of CS-PET. Conditions 500 °C 2h CS-PET A) 1:1 ratio. B) 4:1 ratio. C) 9:1 Ratio
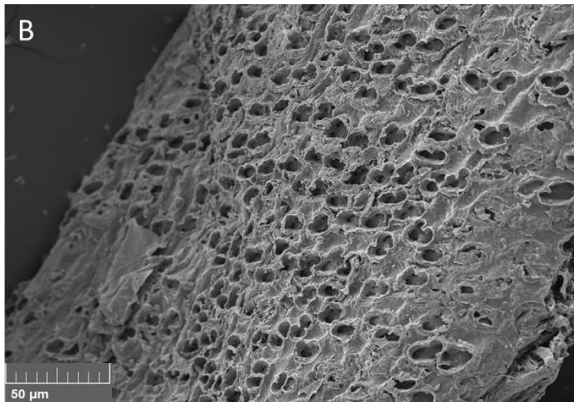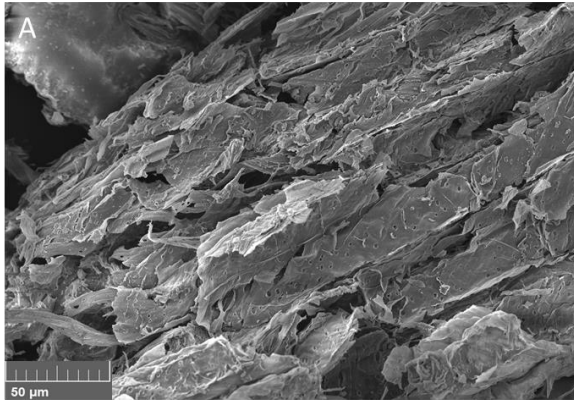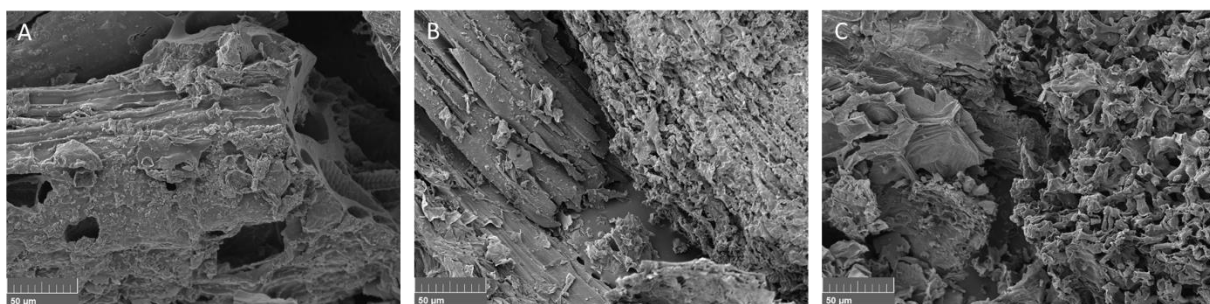
Figure 3.5 Biochar SEM CS-PET 500 C 2h A) 1:1 1 kx B) 1:1 4.2kx C) 9:1 1kx D) 9:1 8kx

Figure 3.6 X-ray diffraction of activated carbons

Figure 3.7 SEM Images. 1,000x magnification A) Biochar 400 C 2h 4:1 CS-PS B) AC of Biochar from A

Figure 3.8 SEM images of AC CS-PET 500 C 2h 1,000x magnification A) 1:1 ratio B) 4:1 ratio C) 9to1 ratio.

Table 3.1 Temperature effect biochar CS-PS

Sample 2 h 4:1 ratio CS-PS	Surface Area (m²/g)	% Recovered as a function of corn stover
400 °C	2.5 ± 0.3	38.1%
500 °C	11.7 ± 2.8	32.2%
600 °C	10.8 ± 8.5	31.3%

Table 3.2 Duration effect of Biochar CS-PS

Sample 500 °C 4:1 ratio CS-PS	Surface Area (m²/g)	% Recovered as a function of corn stover
1 h	11.1 ± 1.5	32.4%
2 h	11.7 ± 2.8	32.2%
4 h	14.3 ± 5.3	31.3%

Table 3.3 Ratio effect of Biochar CS-PS

Sample 500 °C 2 h CS-PS	Surface Area (m^2/g)	% Recovered as a function of corn stover
1:1 ratio	6.5 ± 0.8	31.3%
4:1 ratio	11.7 ± 2.8	32.2%
9:1 ratio	7.0 ± 3.2	31.7%
1:0 ratio	12.4 ± 3.7	32.4%

Table 3.4 Temperature Effect Biochar CS-PET

Sample 2 h 4:1 ratio CS-PET	Surface Area (m^2/g)	% Recovered as a function of corn stover
400 °C	12.9 ± 11.9	45.2%
500 °C	91.2 ± 20.4	39.3%
600 °C	81.3 ± 4.1	36.0%

Table 3.5 Ratio Effect of Biochar CS-PET

Sample 500 °C 2 h CS-PET	Surface Area (m^2/g)	% Recovered as a function of corn stover
1:1 ratio	423.8 ± 24.2	53.2%
4:1 ratio	91.2 ± 20.4	39.3%
9:1 ratio	74.5 ± 26.8	36.1%
1:0 ratio	12.4 ± 3.7	32.4%

Table 3.6 AC Surface Area Temperature Effect CS-PS

Sample AC 2 h 4:1 ratio CS-PS	Surface Area (m^2/g)
400 °C	572.6 ± 21.5
500 °C	477.0 ± 40.8
600 °C	440.1 ± 59.3

Table 3.7 AC Surface Area Duration effect CS-PS

Sample AC 500 °C 4:1 ratio CS-PS	Surface Area (m²/g)
1 h	482.6 ± 22.9
2 h	477.0 ± 40.8
4 h	436.5 ± 13.3

Table 3.8 AC Surface area ratio effect CS-PS

Sample AC 500 °C 2 h CS-PS	Surface Area (m^2/g)
1:1 ratio	430.3 ± 15.6
4:1 ratio	477.0 ± 40.8
9:1 ratio	404.7 ± 5.7
1:0 ratio	614.4 ± 0.2

Table 3.9 XPS Atomic Surface Composition. Biochars are all 500 C 2h. CS-PS and CS-PET are 1:1 ratio. AC is made from the respective biochar.

Sample	Surface Area m^2/g	C	O	N
Biochar CS	12.4 ± 3.7	78	21	1
Biochar CS-PS	6.5 ± 0.8	81	18	1
Biochar CS-PET	423.8 ± 24.8	84	15	1
AC CS	614.4 ± 0.2	75	24	1
AC CS-PS	430.3 ± 15.6	73	26	1
AC CS-PET	409.2 ± 1.2	76	23	1

Table 3.10 AC Surface Area Temperature effect CS-PET

Sample AC 2 h 4:1 CS-PET	Surface Area (m^2/g)
400 °C	359.9 ± 1.0
500 °C	87.8 ± 3.2
600 °C	510.7 ± 4.7

Table 3.11 AC surface area for ratio effect

Sample AC 500 °C 2 h CS-PET	Surface Area (m^2/g)
1:1 ratio	409.2 ± 1.2
4:1 ratio	87.8 ± 3.2
9:1 ratio	390.1 ± 10.7
1:0 ratio	614.4 ± 0.2

Table 3.12 Vanillin Adsorption

Sample	Percent Removed%		
500 °C 2h	30 min	1h	2h
AC 1:1 CS-PS	33	42	45
AC 1:1 CS-PET	31	44	46
AC CS	78	84	95

3.9 References

(1)   Celik, G.; Kennedy, R. M.; Hackler, R. A.; Ferrandon, M.; Tennakoon, A.;
       Patnaik, S.; Lapointe, A. M.; Ammal, S. C.; Heyden, A.; Perras, F. A.; et al.
       Upcycling Single-Use Polyethylene into High-Quality Liquid Products. *ACS Cent.
       Sci.* **2019**, *5* (11), 1795–1803. https://doi.org/10.1021/acscentsci.9b00722.

(2)   Zhuo, C.; Levendis, Y. A. Upcycling Waste Plastics into Carbon Nanomaterials: A
       Review. *J. Appl. Polym. Sci.* **2014**, *131* (4), 1–14.
       https://doi.org/10.1002/app.39931.

(3)   Allred, R. E.; Busselle, L. D. Tertiary Recycling of Automative Plastics and
       Composites. *J. Thermoplast. Compos. Mater.* **2000**, *13* (March 2000), 92–101.

(4)   Harussani, M. M.; Sapuan, S. M.; Khalina, A.; Ilyas, R. A.; Hazrol, M. D. Review
       on Green Technology Pyrolysis for Plastic Wastes. *7th Postgrad. Semin. Nat.
       Fibre Reinf. Polym. Compos. 2020* **2020**, No. December, 50–53.

(5)   Geyer, R.; Jambeck, J. R.; Law, K. L. Production, Use, and Fate of All Plastics
       Ever Made. *Sci. Adv.* **2017**, *3* (7), 25–29. https://doi.org/10.1126/sciadv.1700782.

(6)   Hopewell, J.; Dvorak, R.; Kosior, E. Plastics Recycling: Challenges and
       Opportunities. *Philos. Trans. R. Soc. B Biol. Sci.* **2009**, *364* (1526), 2115–2126.
       https://doi.org/10.1098/rstb.2008.0311.

(7)   Rahimi, A. R.; Garciá, J. M. Chemical Recycling of Waste Plastics for New
       Materials Production. *Nat. Rev. Chem.* **2017**, *1*, 1–11.
       https://doi.org/10.1038/s41570-017-0046.

(8)   Ragaert, K.; Delva, L.; Van Geem, K. Mechanical and Chemical Recycling of
       Solid Plastic Waste. *Waste Manag.* **2017**, *69*, 24–58.
       https://doi.org/10.1016/j.wasman.2017.07.044.

(9)   Gibb, B. C. Plastics Are Forever. *Nat. Chem.* **2019**, *11* (5), 394–395.
       https://doi.org/10.1038/s41557-019-0260-7.

(10)   Yoshida, S.; Hiraga, K.; Takehana, T.; Taniguchi, I.; Yamaji, H.; Maeda, Y.;
       Toyohara, K.; Miyamoto, K.; Kimura, Y.; Oda, K. A Bacterium That Degrades
       and Assimilates Poly(Ethylene Terephthalate). *Science (80-.).* **2016**, *351* (6278),
       1196–1199. https://doi.org/10.1126/science.aaf8305.

(11)   Müller, R. J.; Kleeberg, I.; Deckwer, W. D. Biodegradation of Polyesters
       Containing Aromatic Constituents. *J. Biotechnol.* **2001**, *86* (2), 87–95.
       https://doi.org/10.1016/S0168-1656(00)00407-7.

(12)   Danso, D.; Chow, J.; Streita, W. R. Plastics: Environmental and Biotechnological Perspectives on Microbial Degradation. *Appl. Environ. Microbiol.* **2019**, *85* (19). https://doi.org/10.1128/AEM.01095-19.

(13)   Ho, B. T.; Roberts, T. K.; Lucas, S. An Overview on Biodegradation of Polystyrene and Modified Polystyrene: The Microbial Approach. *Crit. Rev. Biotechnol.* **2018**, *38* (2), 308–320. https://doi.org/10.1080/07388551.2017.1355293.

(14)   Rutkowski, P. Influence of Zinc Chloride Addition on the Chemical Structure of Bio-Oil Obtained during Co-Pyrolysis of Wood/Synthetic Polymer Blends. *Waste Manag.* **2009**, *29* (12), 2983–2993. https://doi.org/10.1016/j.wasman.2009.07.013.

(15)   Rutkowski, P.; Kubacki, A. Influence of Polystyrene Addition to Cellulose on Chemical Structure and Properties of Bio-Oil Obtained during Pyrolysis. *Energy Convers. Manag.* **2006**, *47* (6), 716–731. https://doi.org/10.1016/j.enconman.2005.05.017.

(16)   Abnisa, F.; Daud, W. M. . W.; Sahu, J. N. Pyrolysis of Mixtures of Palm Shell and Polystyrene: An Optional Method to Produce a High-Grade of Pyrolysis Oil. *Environ. Prog. Sustain. Energy* **2014**, *33* (3), 1026–1033. https://doi.org/10.1002/ep.11850.

(17)   Önal, E.; Uzun, B. B.; Pütün, A. E. Bio-Oil Production via Co-Pyrolysis of Almond Shell as Biomass and High Density Polyethylene. *Energy Convers. Manag.* **2014**, *78*, 704–710. https://doi.org/10.1016/j.enconman.2013.11.022.

(18)   Abnisa, F.; Wan Daud, W. M. A. A Review on Co-Pyrolysis of Biomass: An Optional Technique to Obtain a High-Grade Pyrolysis Oil. *Energy Convers. Manag.* **2014**, *87*, 71–85. https://doi.org/10.1016/j.enconman.2014.07.007.

(19)   Sharypov, V. I.; Beregovtsova, N. G.; Kuznetsov, B. N.; Cebolla, V. L.; Collura, S.; Finqueneisel, G.; Zimny, T.; Weber, J. V. Influence of Reaction Parameters on Brown Coal-Polyolefinic Plastic Co-Pyrolysis Behavior. *J. Anal. Appl. Pyrolysis* **2007**, *78* (2), 257–264. https://doi.org/10.1016/j.jaap.2006.08.004.

(20)   Wang, J.; Jiang, J.; Wang, X.; Wang, R.; Wang, K.; Pang, S.; Zhong, Z.; Sun, Y.; Ruan, R.; Ragauskas, A. J. Converting Polycarbonate and Polystyrene Plastic Wastes Intoaromatic Hydrocarbons via Catalytic Fast Co-Pyrolysis. *J. Hazard. Mater.* **2020**, *386* (16), 121970. https://doi.org/10.1016/j.jhazmat.2019.121970.

(21)   Muneer, B.; Zeeshan, M.; Qaisar, S.; Razzaq, M.; Iftikhar, H. Influence of In-Situ and Ex-Situ HZSM-5 Catalyst on Co-Pyrolysis of Corn Stalk and Polystyrene with a Focus on Liquid Yield and Quality. *J. Clean. Prod.* **2019**, *237*, 117762. https://doi.org/10.1016/j.jclepro.2019.117762.

(22)   Velten, S.; Boller, M.; Ko, O.; Helbing, J.; Weilenmann, H.; Hammes, F. Development of Biomass in a Drinking Water Granular Active Carbon (GAC) Filter. *Water Res.* **2011**, *45*, 6347–6354. https://doi.org/10.1016/j.watres.2011.09.017.

(23)   Spahis, N.; Addoun, A.; Mahmoudi, H.; Ghaffour, N. Purification of Water by Activated Carbon Prepared from Olive Stones. *Desalination* **2008**, *222*, 519–527. https://doi.org/10.1016/j.desal.2007.02.065.

(24)   Abumaizar, R. J.; Kocher, W. M.; Smith, E. H. Biofiltration of Benzene Contaminated Air Streams Using Compost-Activated Carbon Filter Media. *J. Hazard. Mater.* **1998**, *60* (2), 111–126. https://doi.org/https://doi.org/10.1016/S0304-3894(97)00046-0.

(25)   Yang, S.; Zhu, Z.; Wei, F.; Yang, X. Carbon Nanotubes / Activated Carbon Fiber Based Air Filter Media for Simultaneous Removal of Particulate Matter and Ozone. *Build. Environ.* **2017**, *125*, 60–66. https://doi.org/10.1016/j.buildenv.2017.08.040.

(26)   Dimitratos, N.; Villa, A.; Prati, L. Liquid Phase Oxidation of Glycerol Using a Single Phase (Au-Pd) Alloy Supported on Activated Carbon: Effect of Reaction Conditions. *Catal. Letters* **2009**, *133* (3–4), 334–340. https://doi.org/10.1007/s10562-009-0192-8.

(27)   Jung, K. Bin; Lee, J.; Ha, J. M.; Lee, H.; Suh, D. J.; Jun, C. H.; Jae, J. Effective Hydrodeoxygenation of Lignin-Derived Phenols Using Bimetallic RuRe Catalysts: Effect of Carbon Supports. *Catal. Today* **2018**, *303*, 191–199. https://doi.org/10.1016/j.cattod.2017.07.027.

(28)   Gale, M.; Nguyen, T.; Moreno, M.; Gilliard-AbdulAziz, K. L. Physiochemical Properties of Biochar and Activated Carbon from Biomass Residue: Influence of Process Conditions to Adsorbent Properties. *ACS Omega* **2021**, *6* (15), 10224–10233. https://doi.org/10.1021/acsomega.1c00530.

(29)   Onwudili, J. A.; Insura, N.; Williams, P. T. Composition of Products from the Pyrolysis of Polyethylene and Polystyrene in a Closed Batch Reactor: Effects of Temperature and Residence Time. *J. Anal. Appl. Pyrolysis* **2009**, *86* (2), 293–303. https://doi.org/10.1016/j.jaap.2009.07.008.

(30)   Maafa, I. M. Pyrolysis of Polystyrene Waste: A Review. *Polymers (Basel).* **2021**, *13* (2), 1–30. https://doi.org/10.3390/polym13020225.

(31)   Miandad, R.; Nizami, A. S.; Rehan, M.; Barakat, M. A.; Khan, M. I.; Mustafa, A.; Ismail, I. M. I.; Murphy, J. D. Influence of Temperature and Reaction Time on the Conversion of Polystyrene Waste to Pyrolysis Liquid Oil. *Waste Manag.* **2016**, *58*,

250–259. https://doi.org/10.1016/j.wasman.2016.09.023.

(32)   Mo, Y.; Zhao, L.; Wang, Z.; Chen, C. L.; Tan, G. Y. A.; Wang, J. Y. Enhanced Styrene Recovery from Waste Polystyrene Pyrolysis Using Response Surface Methodology Coupled with Box-Behnken Design. *Waste Manag.* **2014**, *34* (4), 763–769. https://doi.org/10.1016/j.wasman.2014.01.005.

(33)   Kumagai, S.; Yamamoto, M.; Takahashi, Y.; Kameda, T.; Saito, Y.; Yoshioka, T. Impact of Common Plastics on Cellulose Pyrolysis. *Energy Fuels* **2019**, *33*, 6837–6841. https://doi.org/10.1021/acs.energyfuels.9b01376.

(34)   Uhl, F. M.; Wilkie, C. A. Polystyrene / Graphite Nanocomposites : Effect on Thermal Stability. *Polym. Degrad. Stab.* **2002**, *76*, 111–122.

(35)   Tian, K.; Liu, C.; Yang, H.; Ren, X. In Situ Synthesis of Copper Nanoparticles / Polystyrene Composite. *Colloids Surfaces A Physicochem. Eng. Asp.* **2012**, *397*, 12–15. https://doi.org/10.1016/j.colsurfa.2012.01.019.

(36)   Çit, I.; Sinağ, A.; Yumak, T.; Uçar, S.; Misirlioğlu, Z.; Canel, M. Comparative Pyrolysis of Polyolefins (PP and LDPE)and PET. *Polym. Bull.* **2010**, *64* (8), 817–834. https://doi.org/10.1007/s00289-009-0225-x.

(37)   Buxbaum, B. Y. L. H. The Degradation of Poly(Ethylene Terephthalate). *Angew. Chem. internat. Ed.* **1968**, *7* (3), 182–190.

(38)   Dimitrov, N.; Kratofil Krehula, L.; Ptiček Siročić, A.; Hrnjak-Murgić, Z. Analysis of Recycled PET Bottles Products by Pyrolysis-Gas Chromatography. *Polym. Degrad. Stab.* **2013**, *98* (5), 972–979. https://doi.org/10.1016/j.polymdegradstab.2013.02.013.

(39)   Rezania, S.; Park, J.; Md Din, M. F.; Mat Taib, S.; Talaiekhozani, A.; Kumar Yadav, K.; Kamyab, H. Microplastics Pollution in Different Aquatic Environments and Biota: A Review of Recent Studies. *Mar. Pollut. Bull.* **2018**, *133* (March), 191–208. https://doi.org/10.1016/j.marpolbul.2018.05.022.

(40)   Kevin Eiogu, I.; Ibeneme, U.; Aiyejagbara, O. M. Identification of Polyethylene Terephthalate (PET) Polymer Using X-Ray Diffractogarm Method: Part 1. *Am. J. Nano Res. Appl.* **2020**, *8* (4), 58. https://doi.org/10.11648/j.nano.20200804.11.

(41)   Melo, D. M. A.; Ruiz, J. A. C.; Melo, M. A. F.; Sobrinho, E. V.; Schmall, M. Preparation and Characterization of Terbium Palygorskite Clay as Acid Catalyst. *Microporous Mesoporous Mater.* **2000**, *38* (2–3), 345–349. https://doi.org/10.1016/S1387-1811(00)00155-4.

(42)   Xiao, W.; Han, L.; Zhao, Y. Comparative Study of Conventional and Microwave-

Assisted Liquefaction of Corn Stover in Ethylene Glycol. *Ind. Crops Prod.* **2011**, *34* (3), 1602–1606. https://doi.org/10.1016/j.indcrop.2011.05.024.

(43)   Chen, T.; Liu, R.; Scott, N. R. Characterization of Energy Carriers Obtained from the Pyrolysis of White Ash, Switchgrass and Corn Stover - Biochar, Syngas and Bio-Oil. *Fuel Process. Technol.* **2016**, *142*, 124–134. https://doi.org/10.1016/j.fuproc.2015.09.034.

(44)   Wang, J.; Kaskel, S. KOH Activation of Carbon-Based Materials for Energy Storage. *J. Mater. Chem.* **2012**, *22* (45), 23710–23725. https://doi.org/10.1039/c2jm34066f.

(45)   Wang, J.; Nie, P.; Ding, B.; Dong, S.; Hao, X.; Dou, H.; Zhang, X. Biomass Derived Carbon for Energy Storage Devices. *J. Mater. Chem. A* **2017**, *5* (6), 2411–2428. https://doi.org/10.1039/c6ta08742f.

(46)   Chunlan, L.; Shaoping, X.; Yixiong, G.; Shuqin, L.; Changhou, L. Effect of Pre-Carbonization of Petroleum Cokes on Chemical Activation Process with KOH. *Carbon N. Y.* **2005**, *43* (11), 2295–2301. https://doi.org/10.1016/j.carbon.2005.04.009.

(47)   Chen, W.; Gong, M.; Li, K.; Xia, M.; Chen, Z.; Xiao, H.; Fang, Y.; Chen, Y.; Yang, H.; Chen, H. Insight into KOH Activation Mechanism during Biomass Pyrolysis: Chemical Reactions between O-Containing Groups and KOH. *Appl. Energy* **2020**, *278* (August), 115730. https://doi.org/10.1016/j.apenergy.2020.115730.

(48)   Jeong, H. K.; Jin, M. H.; So, K. P.; Lim, S. C.; Lee, Y. H. Tailoring the Characteristics of Graphite Oxides by Different Oxidation Times. *J. Phys. D. Appl. Phys.* **2009**, *42* (6). https://doi.org/10.1088/0022-3727/42/6/065418.

.

Chapter 4 Heterogeneous Catalyst Design Principles for the Conversion of Lignin into High-Value Commodity Fuels and Chemicals

The text of this dissertation chapter, in full, is a reprint of the material as it appears in "Heterogeneous Catalyst Design Principles for the Conversion of Lignin into High-Value Commodity Fuels and Chemicals" 2020. The text has been modified to fit the dissertation guidelines. The co-author Dr. Kandis Leslie Gilliard-Abdul-Aziz listed in that publication directed and supervised the research which forms the basis for this dissertation chapter.

4.1 Abstract

Lignin valorization has risen as a promising pathway to supplant the use of petrochemicals for chemical commodities and fuels. However, the challenges of separating and breaking down lignin from lignocellulosic biomass are the primary barriers to success. Integrated biorefinery systems that incorporate both homo- and heterogeneous catalysis for the upgrading of lignin intermediates have emerged as a viable solution. Homogeneous catalysis can perform selected chemistries, such as the hydrolysis and dehydration of ester or ether bonds, that are more suitable for the pretreatment and fractionation of biomass. Heterogeneous catalysis, however, offers a tunable platform for the conversion of extracted lignin into chemicals, fuels, and materials. Tremendous effort has been invested in elucidating the necessary factors for the valorization of lignin by using heterogeneous catalysts, with efforts to explore more robust methods to drive down costs. Current progress in lignin conversion has fostered numerous advances but understanding the key catalyst design principles is important for advancing the field. This Minireview aims to provide a summary on the fundamental design principles for the selective conversion of lignin by using heterogeneous catalysts, including the pairing of catalyst metals, supports, and solvents. The review puts a particular focus on the use of bimetallic catalysts on porous supports as a strategy for the selective conversion of lignin. Finally, future research on the valorization of lignin is proposed on the basis of recent progress.

4.2 Introduction

The world currently relies heavily on natural resources such as coal, gas, and petroleum as a source for fuel and chemicals. In fact, 87% of the energy produced in the

United States comes from non-renewable sources[1]. Much of the petrochemical resources are finite and the development of an alternative infrastructure that relies on renewable resources will be key to the economic and environmental wellbeing of the world. Plant biomass may relieve the dependence on petroleum by utilizing the abundant source of carbon to create sustainable feedstocks. There are many challenges with achieving this goal but utilizing all parts of biomass to their full economic potential may make this a reality. One potential solution is to continue improving current biorefinery strategies towards integrated catalytic approaches that seek to improve total utilization of biomass waste towards fungible fuels and biochemicals. Lignin in particular, has rightfully garnered significant attention due to its substantial contribution in biomass, in terms of mass and carbon content. However, its valorization to commercially relevant fuels and chemicals has been relatively challenging compared to carbohydrates due to lignin's high degree of polymerization, diverse spectrum of chemical moieties, and complex structure.

The most promising route for the catalytic conversion of biomass is the development of catalyst systems that can be streamlined into biorefineries to economically achieve high selectivity, conversion, and robustness. At a high level, catalytic processing can be categorized as either homogeneous or heterogeneous that can be differentiated by the use of catalysts that are either soluble or insoluble in the liquid medium during the intended reaction, respectively. Both types are useful for processing biomass and biomass-derived intermediates and a combinatory strategy is often proposed to take advantage of the merits of both[2–9]. Homogeneous catalysis for biomass upgrading primarily addresses the challenges of direct processing raw biomass feedstocks to drive sufficient biomass

deconstruction by solubilization, hydrolysis, and dehydration to liquid chemical intermediates such as sugars, furfurals, oxo acids, polyols, and depolymerized technical lignins[10–12]. However, homogeneous biomass reactions often produce a limited scope of water-soluble intermediates that necessitate subsequent separation steps to recover valuable reactive chemical intermediates while separating them from the catalytic component and contaminates such as mineral ash, chlorine, and acids. A recent combinatory integrated approach of homogeneous reaction in tandem with heterogeneous process has achieved an impressive 60% total carbon utilization of biomass to fungible fuels and technical grade lignin[2]. Heterogeneous catalysts can be manipulated to extend the chemistries not seen in homogeneous catalysis. Albeit, heterogeneous catalysts have issues of their own when it comes to the surface-active sites of the catalyst interacting with the lignin polymeric structure. In an effort to enhance the use of heterogeneous catalysts for lignin valorization strategies, the material design principles for the choice of the catalyst(s), supports, and even the solvents must be understood to improve both the selectivity and conversion. This review will detail pertinent material principles to improve for the selective conversion of model lignin intermediates or extracted lignin into chemicals and fuels. While some reviews have just focused on homogeneous[13,14] and heterogeneous[3,15,16] catalysts, our review has a wholistic view of the optimization of material and solvent properties needed for biomass upgrading.

4.3 Lignin Structure

Biomass can be used to produce energy, food, chemicals, and many other products. Cellulose, hemicellulose, and lignin, in varying amounts, comprise biomass[17]. Cellulose is

composed of glucose monomers that make up the largest fraction[17]. The next predominant form is hemicellulose which is comprised of glucose and other sugars such as xylose and five-carbon monosaccharides[17]. Cellulose and hemicellulose are the most frequently used biomass feedstock to produce biofuels[18–22] and chemicals[23–27]. Lignin is the structural component that adds a hydrophobic protective layer in the cell walls of plants[28]. Depending on the plant species, the fraction of lignin can vary between 15% in tobacco leaf to over 40% in wood bark and hazelnut shells[29]. The structural robustness and complicated network of lignin, consisting of polymeric aromatic groups, renders it an ample resource for value-added chemicals and materials. Thus, current research thrusts serve to utilize lignin as a viable feedstock opposing the common belief that "you can make anything out of lignin except money."

The structure of lignin is complicated and can differ depending on the species[30,31], temperature[32,33], and environmental history of biomass resources[34,35]. Some common features of the lignin structure include ether and diethyl bonds such as $\beta - O - 4$, $\alpha - O - 4$, $5 - 5$, $\beta - 5$, $4 - O - 5$, and $\beta - \beta$ linkages[36–38]. Figure 4.1 shows a representation of the lignin structure including the common linkages mentioned above. Most research on the valorization of lignin uses model compounds to optimize the reaction conditions and materials properties of the catalysts. Afterwards, the optimized catalysts are applied to raw or extracted lignin where further optimization of both the process, scaling and separation is needed to improve the activity, selectivity and stability which can differ from model studies significantly[39].

4.4 Pretreatment Methods

The pretreatment method or isolation of lignin from lignocellulosic biomass is a significant factor that can influence the final product distribution and yield. Biomass can either be pretreated using mechanical or chemical-based methods. The factors that determine the effectiveness of the pretreatment method include the complicated network of lignin around the structure, the crystallinity of cellulose, environmental historical effects and the integrity of the biomass source. Select mechanical methods include ball milling or grinding which acts to disrupt the crystallinity and polymeric structure of lignin and the other cellulosic components. Ball milling of biomass undergoes ultrafine grinding to create submicron particles and powders breaking up the lignocellulosic structure allowing for the extraction. There are many factors that influence the effectiveness of ball milling including the ball-to-biomass ratio, milling time, and the condition of the biomass (e.g. dry or wet conditions). Despites its use as a possible environmentally friendly alternative to chemical-based methods, the quality of lignin obtained is far inferior to that needed for further upgrading. Ball milling and other mechanical grinding methods are often not used as a stand-alone pretreatment method and is often followed by chemical-based methods for solubilization or separation of the lignin from the milled lignocellulosic biomass framework [40–42].

The chemical-based pretreatment methods play an important for preserving the quality of lignin needed for valorization. Chemical methods provide a less destructive alternative to ball milling where enzymes, solvents, acid or base chemistry can separate the cellulose, hemicellulose and lignin fractions. The chemical methods can be divided into

biological, acid/base or solvation chemistry. In biological chemical separation, enzymes or fungi are used to breakdown the polymer by selective scission of ether or ester bonds[43,44]. Biological pretreatments have high selectivity with relatively low process conditions and little to no need for harsh chemicals making them an environmentally friendly and energy efficient process. The enzymes and fungi can be genetically engineered to produce desired products. However, the genetic tools are still under development and need to surpass several milestones before being effective for pretreatment[42,44–46]. Despite these advantages, biological pretreatments can take long periods of incubation time, large amounts of space for reactors, and can have prohibitive costs for large scale applications.

Acidic pretreatment methods including sulfuric acid and hydrochloric acid are used to promote the delignification of biomass. The acidic conditions help to degrade lignin through fragmentation of the β-O-4 aryl ether bonds leading to its depolymerization; however, if the acid environment is sufficiently severe, additional cross-condensation reactions may occur between lignin and sugars that lead to repolymerization and the formation of unwanted pseudo-lignins[42,46–49]. At elevated temperatures, the use of acid chemistry accelerates the hydrolysis of cellulose and hemicellulose producing sugar monomers primarily consisting of glucose and xylose, respectively[45,50]. The Klason method uses sulfuric acid to solubilize the cellulose and hemicellulose while lignin is extracted as the insoluble component[51]. The lignin that comes out of the Klason process has undergone changes due to the acidic media and oxygen-containing groups at the benzylic positions.

Alkaline pretreatment uses high pH reagents like sodium hydroxide and ammonia to delignify biomass. The alkaline conditions promote the solubilization of lignin through saponification of the ester bonds. Alkaline pretreatment is effective at removing lignin, but the relatively higher concentrations of bases used compared to dilute acid reactions can lead to significant recovery and treatment costs (as observed by the paper pulp industry). The saponification reactions involved may adversely affect the lignin structure for subsequent catalytic upgrading[42,46,52].

The combination of solvents with dilute concentrations of acid or bases is used to promote the glycolysis or scission of bonds for facile separation of lignin from cellulose and hemicellulose. There are many different chemical methods that utilize solvents such as the Klason[51,53], Kraft[36,54], Organosolv[55,56] and Co-Solvent Enhanced Lignocellulosic Fractionation (CELF) [57,58]. Each of these isolation techniques utilize solvents with either acids or bases giving unique isolated lignin feedstocks. There are several types of solvents employed to isolate and dissolve lignin ranging from harsh solvents, such as tetrahydrofuran, ethanol, benzene to more green and sustainable alternatives such as water and ionic liquids[59–61]. Ionic liquids consist of liquid salts with anion and cation components that can selectively extract and recover lignin with an anti-solvent[62]. The use of ionic liquids can separate lignin with little or no structural degradation.

Co-solvent pretreatments, such as Organosolv, are effective modifications to dilute acid or base homogeneous processes that employs a combination of organic solvents and water to promote the dissolution and fractionation of biomass into separate lignin, hemicellulose, and cellulose streams[50]. Many co-solvent pretreatment methods are also

capable of producing high quality lignin. The extracted lignin contains a minimal amount of ashes and sugars for more effective catalytic upgrading, serving as the primary lignin feedstock to many of the catalytic systems mentioned in this review. Co-solvent systems such as ethanol-water[55,63], methanol-water[64,65], acetone-water[66,67], formic acid-water[68,69], tetrahydrofuran (THF)-water[2,58], and gamma-Valerolactone (GVL)-water[8,70] have been shown to produce high quality lignin feedstocks. The lignin is precipitated out and has a higher purity and less structural changes than acid and base pretreated lignin[56]. . The CELF method uses tetrahydrofuran (THF) with dilute acid to remove lignin and solubilize biomass from hardwoods and corn stover[57,58]. This method is able to recover over 90% of lignin from maple wood and keep the lignin in a relatively unaltered and pristine form. Once the pristine lignin is separated it will then dissolve in THF to react with the homogeneous or heterogeneous catalysts. The use of co-solvent pretreatments in tandem with subsequent heterogeneous processes are pertinent for a bioeconomic conversion system that fully utilizes the pristine structure of lignin.

Aside from pretreatment methods, there are industrial chemical processes that produce lignin as waste: one of the most prolific being the Kraft pulping process. In the paper industry, lignin is a byproduct of the Kraft pulping process. Lignin is found in the black liquor of the process, which also contains impurities such as sulfur and sodium[54]. Due to the low quality of Kraft lignin, it is often used as an energy source through high-temperature burning[71]. Lignin is also a common byproduct of refineries that produce ethanol from the catalytic conversion of cellulose and hemicellulose[72]. Valorization strategies discussed in the next section can ensure increasing the profitability of

biorefineries by utilizing rationally-designed heterogeneous catalysts to convert the lignin byproducts into fungible chemical commodities and fuels.

4.5 Lignin Valorization

The selective depolymerization of lignin using heterogeneous catalysts can create aromatic monomers or products such as benzene, toluene, and xylenes (BTX)[73]. BTX is commonly derived from petroleum and represents a 100 billion-dollar market[74]. Additional value-added products from lignin feedstocks include jet fuel[75,76], food additives[77,78], carbon fiber[79,80], hydrogels[73,81], industrial and household cleaners[82,83], and resins[84,85]. There are even efforts to design and polymerize extracted lignin monomers and dimers into polymers[74,86–88]. For example, thermoplastics can be formed from lignin polymerization[89]. Lignin-derived guaiacols and aldehydes were synthesized into triphenylmethane-type polyphenols which can be used to create epoxy thermostats[89].

The majority of lignin valorization research usually starts with studying the effectiveness of developed catalysts for the conversion of model lignin monomers, dimers and oligomers into high-value fuels, chemicals or materials. After optimization of the process conditions, the catalysts are applied to raw or extracted lignin where the heterogeneity of the lignin structure and cross-condensation reactions increases the process complexity and significantly influence yields. One of the most viable strategies to overcome some of these challenges is improving the properties of the catalyst and solvent where the metal nanoparticle, pore structure and active site distribution must be rationally designed to obtain the desired products.

While this paper will primarily focus on catalytic strategies for the conversion of lignin into chemicals and fuels, it is worth mentioning the non-catalytic pathways for lignin valorization. Such as the thermal decomposition of lignin through pyrolysis[90]. Pyrolysis is conducted at high temperatures in inert conditions, devoid of O_2 or air, to breakdown biomass into bio-oil and other byproducts such as natural gas. Bio-oil contains many different types of organic compounds including sugars, aromatics, amines, and alkanes. Due to its complex composition, bio-oil can be used for many different applications such as transportation fuel, heating oil, electricity generation, and chemicals[91–93]. Another thermal decomposition method is hydrothermal carbonization where water is used as a solvent to produce biochar. The carbonization process can be done at either elevated temperatures, $> 300\ °C$, or lower temperatures, $< 300\ °C$[94]. High temperature hydrothermal carbonization usually produces high carbon content materials like carbon nanotubes[94], graphene, and graphite[95]. Low temperature carbonization produces lower carbon content including sugars and hydrochar. The hydrochar can be further utilized as a precursor for biodiesel and chemical production[96].

4.6 Depolymerization of Lignin

Noble metals are the most commonly used heterogeneous catalysts for the depolymerization of lignin. Very active catalysts include Pd[97,98], Ru[99,100], and Rh[100,101], while transition-metals, such as Ni[102,103], Fe[104,105], and Cu[106,107], are most frequently used as well. The combination of alloys of metals can promote activity through electronic, interfacial and synergistic effects. This combination in bimetallic catalysts can have several advantages such as increased activity and/or selectivity with conversion rivaling that of

precious metals. Some catalyst metal combinations have synergistic natures that may improve activity, selectivity and/or stability for enhanced depolymerization and valorization through selective scission of carbon-carbon or carbon-heteroatoms[108]. When using more than one metal, the bimetallic catalyst can add complexity since the results can be notably different from the monometallic catalyst counterparts.

4.6.1 Hydrogenolysis and Hydrogenation

Hydrogenolysis uses H_2 to cleave $C - C$ or $C - O$ bonds[109]. Figure 4.2 shows a model of how hydrogenolysis can occur in a model lignin compound, diphenyl ether, one of the common building blocks for the structure of lignin. The selective use of H_2 to cleave ether bonds has become one of the most used methods for the depolymerization of lignin. This reaction can occur without the use of catalysts; however, the catalyst acts to selectively use H_2 to scission certain bonds. A specified form of hydrogenolysis is hydrodeoxygenation (HDO), where HDO cleaves $C - O$ bonds and the oxygen is removed as H_2O. HDO is often employed to remove excess oxygen from the lignin fraction. The presence of high concentrations of oxygen limits the use of lignin in fuel and chemicals because of its low energy density. Excess oxygen can also prohibit the storage of biomass because of the high acidity and reactivity.

The selectivity of hydrogenolysis can be enhanced with the use of bimetallic catalysts to increase activity and yield for the desired product. Zhang et al. employed Ni based bimetallic catalysts, with Ru, Rh and Pd, respectively, stabilized by Polyvinylpyrrolidone(PVP) in order to depolymerize extracted wood lignin and 2-phenoxy-1-phenethanol in water[100]. Their goal was to perform hydrogenolysis at mild

conditions, 130 °C and 10 bar of H_2, using NiRu, NiRh and NiPd to determine if the combinations of the metals changes the catalyst performance. A comparison of the monomer or dimer product yields and conversion was made between the monometallic metals, Ni, Rh, Ru and Pd, to the bimetallic catalysts. After one hour of reaction time, the monometallic monomer product yields were: Ni 0 wt%, Ru 0.16 wt%, Rh 0.27 wt%, and Pd 0.46 wt%; compared to bimetallic catalyst product yields: $Ni_{85}Ru_{15}$ 0.8 wt%, $Ni_{85}Rh_{15}$ 2.6 wt%, and $Ni_{85}Pd_{15}$ 2.4 wt%. After 12 hours the monomer product yield increased to $Ni_{85}Ru_{15}$ 6.4 wt%, $Ni_{85}Rh_{15}$ 3.6 wt%, and $Ni_{85}Pd_{15}$ 4.6 wt%. Zhang explored the change of the H_2 pressure effects in model lignin compounds using $Ni_{85}Ru_{15}$ at 130 °C for 0.5 hours. The conversion remained constant at higher pressures however the product yield changed. Monomer yield was higher at low pressures and dimer yield was dominant at high pressures[100]. It is surmised that the improved synergistic effects between Ni and Ru occurred due to the greater concentration of Ni surface atoms and the orientation of the reactants on the surface prohibiting hydrogenation of the aromatic rings.

Optimization of the bimetallic metal ratios must be done to find the best composition for the desired reaction and lignin phenotype. A sort of "goldilocks" zone must be obtained for bimetallic catalysts. Zhai et al. studied the change in the selectivity and activity for hydrogenolysis of Organosolv extracted birch lignin using different ratios of Ni and Fe over activated carbon[104]. The lignin was depolymerized using Ni:Fe ratios of 2:1, 1:1, and 1:2. The 1:1 ratio gave the highest conversion with 20.3% compared to 2:1 of 17.7% and 1:2 of 14.6%. The 1:1 had the highest selectivity to propylguaiacol (PG) and propylsyringol (PS) out of the three. The 1:1 metal ratio enhanced the ability to remove the

hydroxyl group whereas the 1:2 and 2:1 ratios formed byproducts including 4-(3-hydroxypropyl)-2-methoxyphenol (PG-OH) and 4-(3-hydroxy-propyl)-2,6-dimethoxyphenol (PS-OH).

Pd/C will react with benzyl phenyl ether to create toluene and cyclohexanol through hydrogenolysis and hydrogenation. When the Pd catalyst is alloyed with W, PdW/C, the hydrogenation is significantly limited. The Pd/C catalyst had a 36.5% product yield of cyclohexanol while PdW/C had a 0.4% product yield. And, Pd had a 0% product yield of phenol while PdW had a 29% product yield. The bimetallic synergy of Pd and W show increased conversion to the desired toluene product while limiting hydrogenation[99]. Pt-WO$_3$/C showed very similar trends to PdW/C when reacting with m-cresol. Pt/C converted 8.3% of m-cresol and had selectivity of 23% 3-methylcyclohexanone, 7.4% 3-methylcyclohexanol, 5.5% methylcyclohexane, and 62% toluene. When combined with WO$_3$, Pt-WO$_3$ was able to increase conversion to 61% with 98% selectivity to toluene[110]. When tungsten was mixed with the precious metals, Pd and Pt, the catalyst became more selective to aromatic products and had significantly less hydrogenation.

Alloying Pd with transition metals have also been effective in modulating the hydrogenation behavior of the developed catalyst. Ni/C and NiPd/C catalysts were compared at varying temperatures from 180 to 240 °C. At 240 °C, the Ni/C catalyst had the highest conversion of 79% with a selectivity of 46% to cyclohexanol. NiPd/C increased the conversion from 78% to 96% conversion with the same selectivity towards cyclohexanol. At the lower temperature ranges, NiPd/C had a lower occurrence of

115

hydrogenating the aromatic rings when compared to Ni/C with a selectivity towards cyclohexanol being 14% versus 21%, respectively.[98]

The hydrogenolysis of raw or extracted lignin can change based on the heterogeneity and irrevocable cross condensation of the raw lignin. As stated earlier, lignin comes in differing structures and qualities which can drastically change the depolymerization products. Furthermore, condensation reactions of the aromatic products also prevent efficacy of the reaction. NiFe/C was used to depolymerize Organosolv extracted birch lignin vs a lignin-first approach with birch sawdust biomass [111–113]. The lignin-first approach performs depolymerization and conversion in a one pot manner where lignin is extracted and disassembled preserving the aromaticity of products. Under the same conditions (Table 4.1), the Organosolv extracted birch had lower conversion at 20.3% compared to the lignin-first sawdust at 39.5%. However, the Organosolv extracted had higher selectivity towards PG and PS than the lignin-first sawdust[104].

The catalysts commonly used in HDO are Ni[114], Ru[115], Pd[99], Fe[105], Co[116] and W[99]. Monometallic and bimetallic catalysts of transition and noble metals were used in the cleavage of the C – O bond on benzyl phenyl ether (BPE)[99]. The use of tungsten-based catalysts seems to promote the aromaticity of the products formed, limiting hydrogenation. The combination of a noble metal with tungsten is surmised to promote the scission of β–O–4 and α–O–4 bonds, while preserving the aromaticity of the products. Ru/C depolymerized BPE into toluene and phenol with a conversion of 94.2% and product yields of 81.4% and 48.6%, respectively. W/C, in comparison, converts 79.5% of BPE with product yields of 40.3% of toluene and 33.8% of phenol. The combination of Ru and W

bimetallic catalyst synergistically increased the conversion to 99.7% and product yields at 92.6% and 61.5% which are higher than either monometallic catalyst[99]. Each of these reactions were held at the same conditions as seen in Table 4.2. Higher conversion and greater selectivity are some of the major advantages of bimetallic catalysts over monometallic catalysts. Other examples are shown with Pd/C and PdW/C as well. Pd/C has a conversion of 99.7% of BPE and has product yields of 89% toluene, 0% phenol, and 36.5% cyclohexanol. When Pd is alloyed with W, the conversion increases to 100% and the product yields change to 100% of toluene, 29% of phenol, and 0.4% cyclohexanol. The Pd/W bimetallic promoted higher conversion of the ether, promoting hydrogenolysis and increasing the selectivity towards toluene and phenol. The use of W metal typically has preference to cleave the lower energy aryl ether bonds instead of the higher energy C = C[117] of the aromatic rings. Coupling W with other metals promotes a synergistic effect showing that for selective bond cleavage for aromatic products the Metal-W bimetallic catalyst is more advantageous than using the monometallic catalysts.

Hydrogenation is the saturation of bonds with using H_2 to convert C = C or C = O to C – C or C – OH, respectively. Figure 4.3 shows an example of hydrogenation where benzene is converted to cyclohexane. Hydrogenation often occurs as an unwanted side reaction during hydrogenolysis to create different products. The depolymerization of lignin using either hydrogenation or hydrogenolysis requires a delicate balance which often changes with the process conditions, solvent, and catalyst used. Nevertheless, the hydrogenation of bonds is often utilized to create starting materials for polymers, chemicals, and resins[118]. Finding highly selective catalysts can be difficult as many noble

metals are excellent at hydrogenation, however, they produce many byproducts that can be difficult to separate[119].

Hydrogenation of the aromatic ring products usually proliferate at higher temperatures. For example, elevated temperatures above 300 °C promoted hydrogenated yields from the depolymerization of P1000 soda lignin. Transition metal catalysts were used in supercritical ethanol at 300 °C and 340 °C, and in each case, the increase in temperature resulted in increased conversion to hydrogenated products. TiN catalyst made by the urea glass method, increased the monomer yield from 12 wt% to 19 wt%, however, the hydrogenated products increased as well. While the hydrogenated yields are less than 5% in both cases, there is an increase in yield with an increase in temperature.[108] The TiN catalyst was tested against 3 other types of Organosolv extracted lignin from wheat straw, poplar, and spruce. The monomer product distribution of each lignin source was very similar to each other. The spruce depolymerization gave the highest yield at 21 wt% and on the lower end of hydrogenated products.

In addition to temperature, the variation in pressure can also be used to promote or inhibit the hydrogenation of aromatic products. Pressure can have effects on hydrogenation of the aromatic ring. For model compounds such as 2-phenoxy-1-phenylethanol (1-20 bar)[100] and p-Cresol (25-89 bar)[120], higher hydrogen pressure leads to higher ring hydrogenation. However, when tested with extracted poplar lignin, a higher hydrogen pressure lead to more aromatic yield (0-30 bar) and limited hydrogenation[121]. In model lignin, hydrogenation and HDO could be competing reactions whereas in the more complex lignin systems other reactions can occur with additional bonds and functional groups which

can consume hydrogen. The complexities and heterogeneity of the lignin structure make it difficult to quantify the effect of pressure on hydrogenation as there could be a multitude of reactions occurring at one time.

4.6.2 Oxidation

Oxidation processes can be used to selectively break bonds like $\beta - O - 4$, $C - C$, or aryl ether bonds in the lignin polymer structure[122]. The $\beta - O - 4$ bond is targeted for lignin depolymerization due to the abundance of the linkage in lignin[122]. There are many different oxidants that have been employed in lignin oxidation such as chlorines, nitrobenzene, ionic liquids, and metal catalysts[97,106,122,123]. Oxidation is generally performed at mild conditions which makes it an attractive upgrading option. However, one of the difficulties of oxidation is limiting the reaction for partial oxidation of the bonds[124].

There are several oxidants that can be employed for oxidation of lignin and one way to differentiate them is by strength: strong and mild[106]. Strong oxidants will disrupt the aromatic ring such as hydrogen peroxide[125]. Mild oxidants keep the aromatic ring intact such as air[126], oxygen[127], and nitrobenzene[128]. Hydrogen peroxide is highly efficient, inexpensive, and may have industrial applications but can cause the products not to have an aromatic ring[129]. Air is sustainable, very low cost, and is green; however, it may not yield the best results. Pure oxygen or oxygen enriched air is a low cost, green, and sustainable that can give improved results over air, though it presents increased hazards. The improved results may still not be selective enough or have high enough conversions. Nitrobenzene can be used which has resulted in higher yields and more selective to aldehydes while keeping the aromatic ring intact[130]. Nitrobenzene is a harmful chemical

and may present issues during separations though. Oxidants influence product selectivity and yield which depending on the situation will be another variable to consider in the lignin valorization puzzle.

In the process of oxidation, radicals form which can cause the reaction to be reversible. In addition, the radicals can cause compounds to polymerize with each other creating products that are not desirable. An additional challenge is to ensure that the product doesn't over oxidize and break additional bonds. However, if these effects can be minimized, oxidation is a viable pathway to convert lignin into value-added products such as phenolic monomers.

Phenolic monomers are a value-added product that can be made through selective oxidation of lignin. Lancefield et al. investigated targeting the $\beta - O - 4$ bond using 2,3-dichloro-5,6-dicyano-1,4-benzoquinone (DDQ) and zinc to oxidize the bond and depolymerize lignin[123]. DDQ was able to selectively oxidize lignin $\beta - O - 4$ model polymers at 80 °C with success of 99% conversion at 20 mol% DDQ and 20 mol% tert buty nitrite (tBuONO). The oxidized model compound was then treated with excess amounts of zinc and NH_4Cl for selective degradation. The selective degradation gave some good product yields with several model compounds being in the 80 to 90% range. Lancefield used both DDQ and Zinc to depolymerize birch lignin. The oxidation method produced a 5 wt% yield of an isolated phenolic monomer: 3-Hydroxy-1-(4-hydroxy-3,5-dimethoxyphenyl)-1-propanone[123]. Oxidation was shown to work at mild conditions-80 °C-in both lignin and model lignin compounds to achieve phenolic products.

Au, Pd, and Au/Pd over graphite catalysts were used to oxidize glycerol[97]. Pd had a higher activity than Au where at 50 °C with double the activity; 319.8 TOF to 151.7 TOF, respectively. Pd was slightly more selective to glyceric acid at 80.2% and was within 1% selectivity of glycolic acid and tartronic acid. The Au catalyst had an additional by-product of hydroxypruvic acid as a by-product. With the combination of Au/Pd supported on graphite the catalytic activity was significantly higher than in either Au or Pd monometallic catalyst. The catalytic activity was 674.8 TOF h^{-1} which is more than double Pd and more than quadruple Au at 50 °C[97]. The selectivity of the catalyst was similar to that of the Pd catalyst with a conversion higher than 50%. The synergy between the two metals markedly helped the catalyst reaction.

The use of multiple catalysts in a tandem fashion to depolymerize and valorize lignin has been used. Ru/CeO$_2$ and CuCl$_2$ were combined to react with Organosolv poplar lignin to form phenols. The Ru/CeO$_2$ cleaves the C – O bond through hydrogenolysis while the CuCl$_2$ oxidizes the C$_{aryl}$ – C$_\alpha$ bond. When used in unison, this produced 13 wt% yield of phenol and 2 wt% guaiacol and 0.5 wt% syringol. When Ru/CeO$_2$ is used without CuCl$_2$ no phenols were yielded. And when CuCl$_2$ was used without Ru/CeO$_2$ only 2.6 wt% of phenol was yielded[131]. This strategy of combining multiple catalysts to perform different cleavages could be a key to unlocking the full potential of lignin.

Partial pressure effects were tested using Pd/γ-Al$_2$O$_3$ for the catalytic wet air oxidation of sugar cane bagasse. Maintaining a total pressure of 20 bar, the oxygen partial pressure was varied from 2, 5, and 10 bar to see how it would influence the results. The 5 bar had the highest mass fractions of the aldehydes: vanillin, syringaldehyde, and p-

hydroxybenzaldehyde. In each case, duration of the reaction would cause a peak for each aldehyde. This indicates partial pressure of oxygen has an influence on the maximum yields as a function of reaction time[132].

4.7 Support Effects

It is ideal that the support of a catalyst has a high surface area to maximize the number of active sites available for the reaction[133]. The support can also influence the catalytic activity through steric and electronic effects. Almost any material that is thermally stable and relatively inert can be used as a support, however, not all materials are created equal[134]. One of the most common supports for biomass upgrading is activated carbon due to its high surface area and microporosity. Expensive noble metals can be easily recovered from spent carbon making it an even more attractive option[134]. Some other common supports include Al_2O_3, TiO_2, ZrO_3, SiO_2, and SiO_2-Al_2O_3. Al_2O_3 due to its mesopores, high thermal stability, and its ability to be shaped into different structures[134]. Additionally, supports may exhibit support effects where the metal-support interaction can influence the rates of conversion, selectivity, and products[135,136].

Carbon can come in many forms and each form can have different support effects. Carbon nanotubes, oxidized carbon nanotubes, and thermally-treated activated carbon were impregnated with Ni and tested for the conversion of guaiacol[137]. The carbon nanotubes had the highest conversion followed by the oxidized carbon nanotubes, and the activated carbon had the lowest conversion. Hydrogenation was prevalent in all of the supports with the main products all being cyclohexane, cyclohexanol, and methylcyclohexane. The oxidized carbon nanotube catalyst was the only one to have

anisole in more than trace amounts in the product, meaning the oxidization could have modified the active sites thus limiting hydrogenation and promoting hydrogenolysis in a limited capacity. In addition, the oxidized carbon nanotube support had considerable amounts of methoxycyclohexanol indicating that not all $C - O$ bonds had been cleaved. The main product of the activated carbon support had the methoxycyclohexanol followed by cyclohexanol which could indicate that hydrogenolysis is inefficient on activated carbon. The carbon nanotube support promoted both hydrogenation and hydrogenolysis. When compared to the oxidized nanotube support, the results indicate that the presence of acid sites is important in the promotion of hydrogenolysis[137]. Clearly, certain forms of the carbon support are more suited for depolymerization and aromatic products.

The acidity or basicity of the support can affect the products that are formed. The bimetallic catalyst RuW with different supports was used to depolymerize Kraft lignin after it was found to perform better than its monometallic counterparts. Neutral activated carbon, acidic ZSM-5, and basic supports $MgO-La_2O_3$ (ML), $MgO-CeO_2$ (MC), & $MgO-ZrO_2$ (MZ) were used with supercritical methanol in the depolymerization. The acidic ZSM-5 produced the least amount of methanol soluble solids at 40 wt% and the highest char at 30 wt%. The neutral activated carbon produced the highest methanol soluble solids at 82 wt% followed closely by the basic ML at 80 wt% each without any char formed. As the basic supports became more acidic the methanol soluble solid yields dropped to 75 wt% and 68 wt% for MC and MZ, respectively. MZ also had some char formation at 4 wt% which may be attributed to it being the least basic/most acidic of the basic supports. The number of acidic and basic sites on the surface of each catalyst were tested using NH_3- temperature

123

programmed desorption (TPD) and CO_2-TPD, respectively. ZSM-5 had the highest acidic sites with 507 μmol g^{-1} and no basic sites. Activated carbon had small amounts of acidic, 18.6 μmol g^{-1}, and basic site, 0.6 μmol g^{-1}. ML, MC, and MZ each had no acidic sites and decreasing basic sites with 291 μmol g^{-1}, 188.3 μmol g^{-1}, and 104.7 μmol g^{-1}, respectively[138]. In the depolymerization of Kraft lignin using RuW[138], the more acidic support was worse while in Ma's paper[139], the support with the most Lewis acidic sites was the best. This could indicate that each case is unique with support effects and will need to be determined on a case by case basis.

Some additional examples of the use of the support include, Ru/C and Ru/Al$_2$O$_3$ on steam exploded corn stover, had different conversion and major products[101]. Ru/C had a lower conversion at 34% compared to Ru/Al$_2$O$_3$ 61%. Ru/C created 25% toluene, and 23% methylcyclohexane while Ru/Al$_2$O$_3$ created toluene, 18%, and coumaran, 29%. The carbon support was more selective towards toluene and promoted hydrogenation to form methylcyclohexane as well. While the Al$_2$O$_3$ support preferentially promoted hydrogenolysis to form coumaran and toluene.[101] This suggests that the manner of adsorption of the aromatic rings to the supported noble metal surface plays an important role in the selectivity. If the aromatic ring is planar to the support, as in the case with carbon, then it will hydrogenate the ring, but if it is vertical to the support, as in the case with Al$_2$O$_3$, then it will cleave bonds using hydrogenolysis[101].

Ru catalysts on various NbO$_x$ supports were used in the depolymerization of corncob lignin. The mole yields of arenes and cycloalkanes were 91.1% for Nb$_2$O$_5$, 67.5% for HY-340 (commercial niobic acid), and 69.2% for niobium phosphate from the

Comphania Brasileira de Metalurgica e Mineracao (NbPO-CBMM). There is a correlation between selectivity and quantity of Lewis acid sites, which followed the order Nb_2O_5 > HY-340 > NbPO-CBMM. The more Lewis acid sites, the more selective the catalyst was towards aromatic products and the higher the yield of total depolymerized yield including phenolic monomers. There was significantly more hydrogenation with HY-340 and NbPO-CBMM which indicates there must be another definitive factor. Particle size and dispersion of Ru were investigated; interestingly enough, Nb_2O_5 had the highest dispersion and smallest particle size. Large particles can absorb benzene easier and thus lead to more hydrogenation than smaller particles. The smaller particle size of Nb_2O_5 grabs onto the oxygen atom rather than the benzene thus allowing for more selective cleaving of the C – O bonds. Ma et al. tested this with p-cresol to remove some of the complexities, and when they tested a Nb_2O_5 with larger Ru particles they had more hydrogenation and less conversion[139]. Therefore, Lewis acid sites and particle size can have large influences on Nb supported catalysts regarding selectivity and conversion.

Support effects of ReO_x catalyst was tested with 7 different supports (activated carbon, γ-Al_2O_3, SiO_2, CeO_2, TiO_2, ZnO, and MgO)[140] to depolymerize BPE. The acidic ReO_x/Al_2O_3 had the highest conversion with 97.4%, but the selectivity towards toluene and phenol was poor, 1.7% and 20.3% yields, respectively. SiO_2 had a conversion of 50.3% with a very low selectivity towards toluene and phenol. Both Al_2O_3 and SiO_2 created many other products such as 2-benzylphenol, cyclohexanol, and diphenylmethane, which were most likely created by consecutive reactions of radicals. Acidic ReO_x/AC had a high conversion of 84.5% and yielded 80.3% toluene and 62.5 phenol. The non-acidic and basic

catalysts (CeO_2, TiO_2, ZnO, and MgO) all had low conversion and limited hydrogenolysis[140].

Pore size is another factor to be considered when selecting the support. Pores are classified in 3 major groups micropores (< 2 nm), mesopores (between 2 nm and 50 nm), and micropores (> 50 nm)[141]. Zeolite catalysts have been utilized for lignin depolymerization due its microporous structure, size selectivity, and catalytic activity[142,143]. Zeolites have very precise shape and sizes of the pores to allow certain reactants to enter, products to be formed, and/or products to exit the pores, which can make for highly selective catalysts. However, the active sites are predominantly present inside the micropores, and larger biomass molecules may not be able to access the active site or if they can could be significantly limited by mass transfer[144]. Though this leads to poor performance, a possible solution is to combine micropores and mesopores also known as hierarchical zeolites. Hierarchical zeolites allow for bigger molecules to reach more active sites, improve product selectivity for said molecules, and enhance active site accessibility as the larger molecules are less hindered by mass transfer properties[144].

HZSM-5 is a common zeolite used in the petroleum industry, and it can be turned into a hierarchical zeolite. Mesoporous and cerium doped mesoporous HZSM-5 was compared to HZSM-5 in the fast pyrolysis of glucose. HZSM-5 is selective to BTX and when tested had a selectivity of 76.7% and formed 34 wt% coke. The mesoporous HZSM-5 had a selectivity towards BTX of 57.9%, but instead produced more acetaldehyde, furan, and acetone with selective yields of 16.6%, 6.2%, and 8.1% respectively. Cerium doped mesoporous had even lower selectivity towards BTX at 39.4%, in turn, it was more

selective towards acetaldehyde, furan, and acetone at 25%, 12.5% and 9.5%, respectively. In addition to being more selective towards different products, the hierarchical zeolites formed less coked with Meso-HZSM-5 at 25 wt% and Meso-Ce-HZSM-5 at 20 wt%[145]. The hierarchical catalysts were more selective towards different molecules and produced less coked than the microporous HZSM-5 which could be attributed to minimizing diffusion limitations. Hick et al. also used hierarchical HZSM-5 in model lignin compound reactions, which enhanced the production of liquids in comparison to the microporous material. The accessibility to the pores in the hierarchical played a more pronounced role than BET surface area or mesopore size[146]. While pore size is a key component, limitations must be noted as well and depending on the desired products could be tailored to the reaction.

The support can also play a role in hydrophobicity and hydrophilicity which can alter the products formed. Lignin exhibits both hydrophobic and hydrophilic properties and the surface of the catalyst being hydrophobic or hydrophilic can be used to optimize catalytic activity and selectivity[147]. Hydrophilic substrates generally attach to hydrophilic surfaces and can be reacted to remove oxygen to become more hydrophobic. The effects of hydrophobicity were tested using CoS_2-MoS_2 catalysts by adding polyvinylpyrrolidone (PVP) during catalyst preparation; increasing PVP increased the hydrophobicity. These catalysts were used to perform HDO on 4-ethylphenol and the one with no PVP had the lowest conversion at 85.1% and lowest selectivity towards ethylbenzene. As the amount of PVP increased in the catalyst so did conversion and selectivity towards ethylbenzene with the Co-Mo-S-0.4 catalyst performing at 96.6% conversion and 99.3% selectivity[148]. The

enhanced hydrophobicity could help prevent sulfur loss and improve stability of the catalyst thus allowing it to perform better.

4.8 Solvent Effects

The solvent used for the chemical conversion of lignin polymers and monomers also play a role in the desired product distribution. Ni/C was compared using many different solvents to depolymerize birch sawdust. Methanol had the highest conversion at 54%. However, the highest selectivity towards Propyl syringol (PS) was a mix of 25% methanol and the rest water at 75%. The highest selectivity towards Propyl guaiacol (PG) was 1% methanol and the rest water at 31%[102]. The solvent effect was also tested on RuW/C for the conversion of BPE. Methanol, 1,4-dioxane, and THF were all solvents that underperformed with conversions of 5.9%, 43.6% and 36.7%, respectively. This performance could be attributed to strong interactions on the surface of RuW/C and the solvent's high Lewis basicity. Isopropyl alcohol, a hydrogen-donor solvent, was shown to have higher conversion than the other solvents at 62.7%, but it promoted the hydrogenation of the aromatic rings. The two best solvents were n-hexane and cyclohexane, both dipolar aprotic solvents. Cyclohexane had a conversion of 92% and n-hexane had a conversion of 99.7%; each with higher product yields to toluene and phenol than the others. Neither solvents have Lewis basicity and are not hydrogen-donors, thus having the best results for BPE hydrogenolysis with RuW/C[99]. Many of these solvents were used in BPE depolymerization by ReOx/AC. Water had the highest conversion at 99.9% and the highest phenol yield of 85.7%, however, the yield of toluene was low at 41.8%. n-hexane had the highest yield of toluene at 80.3% along with a high conversion of 84.5% and high yield of

phenol at 62.5%. Cyclohexane also performed well at 66.5% conversion and yields of 63.1% and 43.9% for toluene and phenol, respectively. Similar to the RuW/C, 1,4-dioxane, isopropyl alcohol, methanol, and THF did not perform as well as the apolar solvents, n-hexane and cyclohexane. For the hydrogenolysis of BPE by ReOx/AC, n-hexane was the optimized solvent as it has high conversion and high selectivity towards toluene and phenol[140].

The properties of the solvents used for the reaction medium was also studied with Raney Ni for the hydrogenolysis of diphenyl ether. Four major groups were tested: Protic solvents displaying Lewis basicity, Protic solvents displaying no Lewis basicity, Aprotic polar solvents, and Aprotic nonpolar solvents. The aprotic nonpolar solvents and protic solvents displaying no Lewis basicity have the highest conversions with > 99%, and the products were almost all fully saturated. n-Heptane was the only solvent from the groups with no Lewis basicity to have an aromatic product, 1.5% benzene. The two groups with Lewis basicity didn't have as high of a conversion ranging from 72.7% 2-propanol to 12.4% methanol. The Lewis basicity reduced hydrogenation, with methanol having the highest selectivity towards aromatic products[149]. A comparative analysis between Wang et al.[149], using Raney Ni, and Ji et al.[99], using RuW/C, showed the opposite trends where Lewis basicity promoted hydrogenolysis for Raney Ni but promoted hydrogenation for RuW/C. Showing that the effect is different for the heterogeneous catalyst used and must be taken into account for the development of processes that influence lignin depolymerization.

Lignin isolated from Willow *T*. ramosissima was depolymerized with several different solvents to see which yielded the best results. The experiments were carried out with a MoO_x catalyst on carbon nanotube support under a hydrogen environment. Methanol, ethanol, isopropyl alcohol, ethylene glycol, water, and several combinations were screened, with methanol producing the best results. Methanol yielded 33 wt% phenolic monomers whereas ethanol and isopropyl yielded 21 wt% and 30 wt%, respectively. Ethylene glycol was lower with 14 wt% and interestingly enough, no guaiacyl monomers were formed. Water significantly dropped the yield to 7 wt%, possibly due the lack of lignin solubility. But when combined with ethanol it was able to yield 27 wt%; however, methanol by itself still yielded the highest monomer yield[150]. The ideal solvent choice for lignin valorization will vary between the type of catalysts used and the source and type of biomass feedstock.

The solvent can also be a reactant and can contribute to the formation of additional products. Super critical ethanol has been shown to react with catalysts and form different hydrocarbons, alcohols, esters, and more. CuMgAl catalysts were used to depolymerize soda lignin with super critical ethanol which resulted in some cases having greater than 100 wt% yield. The same reactions were carried out without lignin and this yielded many C_4^+ products. The more basic sites the catalyst had the more products were yielded from ethanol. The combination of Cu and basic sites dehydrogenates ethanol which produces hydrogen. This additional hydrogen can increase hydrogenolysis and help facilitate the depolymerization of lignin into monomers with a higher deoxygenated fraction[151]. Molybdenum-based catalysts with super critical ethanol for the depolymerization of Kraft

lignin also resulted in yields higher than 100 wt%. The α-molybdenum carbide catalyst had a high yield of 1.64 g/g lignin with no char formed. Ethanol was the best solvent for Kraft lignin conversion over carbide catalysts; water, methanol, and isopropyl alcohol were tested and produced low yields[152]. The solvent choice is important not only for the solubility of lignin, but it can also play a role as a reactant.

4.9 Caveats and Pitfalls

There has been a large amount of information presented in this review, but not all the research in the lignin valorization literature can be compared easily, and some studies fail to characterize the kinetics, mass transfer and materials properties of the catalyst used for depolymerization. Mass transfer limitations are often overlooked and can be ruled out with additional characterization[153,154]. Neglecting mass transfer limitations may impede accurate comparisons between catalysts especially those reactions with seemingly high conversion. As mentioned earlier in the discussion of support effects, the pore structure is a very important parameter to accurately determine if solubilized lignin is able to diffuse and interact with active sites in the micropores. Zhai et al. compared multiple catalysts near iso-conversion conditions for the depolymerization of Organosolv birch lignin and thus was able to determine when mass transfer limitations was prevalent[104]. The group also studied the influence of the reaction temperature and pressure on the conversion and selectivity. Dimitratos et al. effectively tested for diffusion limitations to study the activity of Au-Pd catalysts before mass transfer limitations prevailed[155]. The group varied mass loading and measured conversion and TOFs in order to test for mass transfer limits.

131

Another common pitfall is the confluence of weight percentages to the actual number and quantity of active sites on the catalyst. The use of weight percentages for the concentration of the metals does not easily detail the number of atoms and molar amounts which can vary for monometallic and bimetallic systems. For example, Ji et al. compared 1 wt% Ru, 101 amu, to 1 wt% Pt, 195 amu, which had comparable performances although Pt has half as many atoms[99]. This leads for some additional characterizations to be desired, such as a dispersion and chemisorption studies to determine how the number of active sites influences the activity. Another pitfall is the inadequate characterization of the bimetallic synergistic interactions. There needs to be a delineation between whether metals formed a solid solution in the form of alloys or core-shells or are two distinct neighboring entities on the surface. A combination of select characterization methods can be utilized to confirm the orientation of the metals such as absorption studies, high-angular annular dark-field imaging scanning transmission electron microscopy (HADDF-STEM) energy dispersive X-ray spectroscopy (EDX), X-ray absorption near edge structure (XANES), Fourier transform infrared spectroscopy (FT-IR), and/or in-situ x-ray photoelectron spectroscopy (XPS). For example, a study by Zhang et al. characterized NiAu using HAADF-STEM, EDX spectrum, HRTEM, XRD, and XANES[156]. This group used iso-conversion conditions to compare monometallic and bimetallic catalysts in the depolymerization of Organosolv birch lignin. The reader should be aware that the bimetallic characteristics of the developed catalysts for some studies may have not been characterized thoroughly to draw conclusions from simple conversions.

Lastly, scaling developed processes from the lab to the industrial scale has additional challenges for lignin valorization. The quality and structure of extracted lignin can differ from the controlled environment of the lab to the same process used in an industrial setting. For example, Deuss et al. compared 27 lignin samples; 18 of the 27 were isolated in the lab through Organosolv pretreatment, while the other 9 were separated using commercial and industrial processes[39]. Overall, the Organosolv pretreated lignin in the laboratory had more β-aryl bonds and yielded more phenolic acetyl products when depolymerized[39]. The lignin from industrial scale Organosolv process incurred structural damage that limited its yield. Thus scaling complications with pretreatment and depolymerization strategies must be done carefully to ensure high quality lignin is maintained to make fungible chemical products that is competitive against petrochemicals.

4.10 Conclusion

The world has an abundance of lignocellulosic biomass that can be used as a renewable alternative to petrochemical feedstocks. However, most conversion strategies focus on a fraction of the available carbon content utilizing mostly cellulose and hemicellulose which is not sufficient for the development of economical strategies to supplant conventional feedstocks. Furthermore, strategies should be developed for the efficient upgrading of the aromatic polymeric structure of lignin. A possible solution is the realization of the integrated biorefinery strategies that utilize homogeneous pretreatment methods with heterogeneous catalysis for lignin valorization. However, as this review stressed, the valorization of lignin must take ques from material science with the selection of metals, supports and solvents to develop successful strategies.

Depolymerization and polymerization through heterogeneous catalytic pathways require further development before lignin valorization is commercially viable. Determining the ideal combination of catalyst metal(s) with support can be difficult depending on the phenotype of the biomass feedstock, quality of the lignin source, and the desired final products. This review covered many different material design principles, with a particular focus on the use of bimetallics, support and solvent effects to modulate the activity and selectivity. The choice and ratio of the catalyst metals are a key attribute for the selective depolymerization of the lignin polymeric structure. One can choose from cheap transition metals like Ni, W or Fe that can be coupled or alloyed with more expensive precious metals like Pd or Ru. Alloying of the metals can potentially improve the activity, and/or selectivity than the respective monometallic catalysts components for a desired product. In addition to the type of metal, the support of the catalyst can influence the activity through steric and electronic effects. Additional factors to consider include the hydrophobicity or hydrophilicity of the support surface as well as the pore size distributions and acid or base characteristics.

Most studies rely on the optimization of catalyst processes with studies on model lignin compounds to mimic common linkages in lignin. The ad hoc study of trends is easier to observe due to its simplicity in comparison to the complicated polymeric structure of raw lignin. However, there are additional factors to consider when dealing with raw lignin where the biomass and phenotype source, historical conditions, and pretreatment method must be considered. The polymeric structure of lignin can vary from corn stover, sugar

beets bagasse, and birch, thus complicating the comparison of heterogeneous catalytic conversion strategies from different laboratories.

Lignin valorization strategies have made many strides in the development of catalytic processes, but additional milestones must be achieved before the realization of an economical strategy. There is a need for more fundamental research that can thoroughly characterize and identify trends in how the lignin structure influences conversion strategies. Additional efforts must be made to characterize lignin polymeric structure from different biomass sources and develop trends on how external factors influence the surface structure. The use of bimetallic heterogeneous catalysts has shown great success in achieving high yields and selectivity and is a promising step in the biomass conversion field. The in-depth studies of heterogeneous catalysts will further push the design of better catalysts and integrated processes to help solve many of our chemical and fuel issues.

4.11 Conflict of Interest

The authors declare no conflict of interest

4.12 Acknowledgements

4.13 Figures and Tables
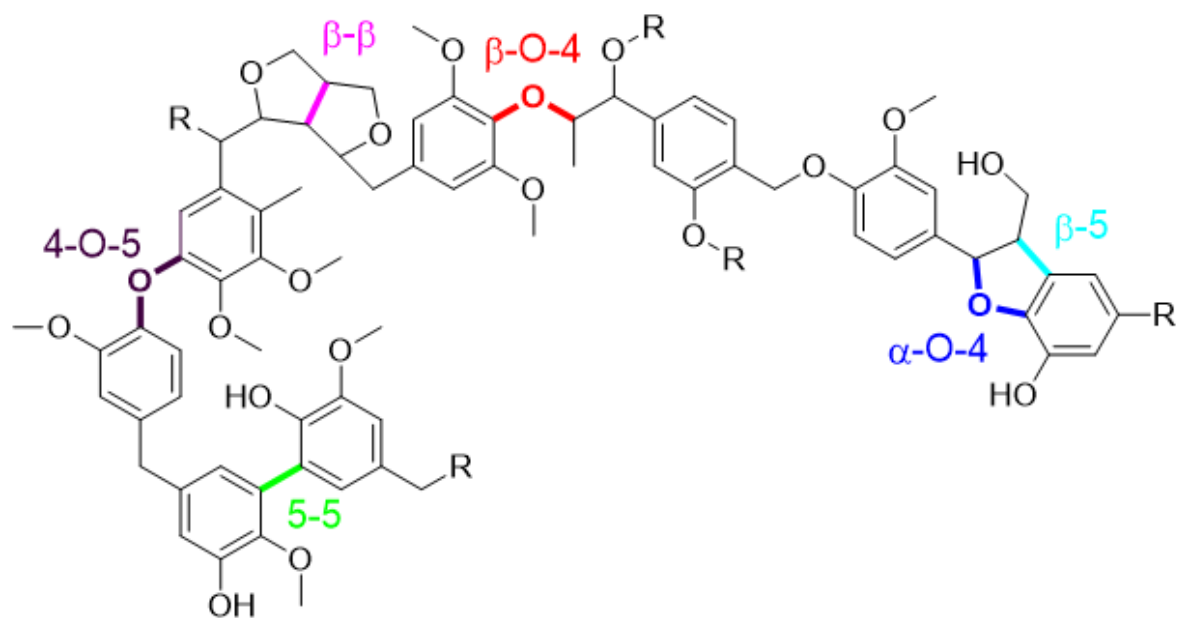
Figure 4.1 Typical structure of lignin, with some common linkages highlighted
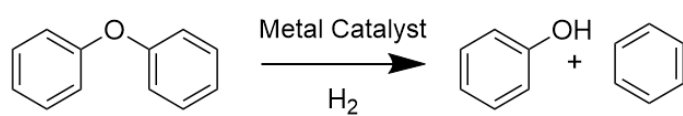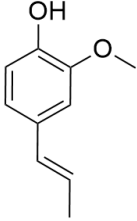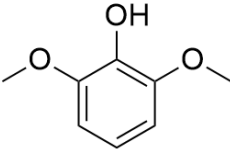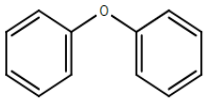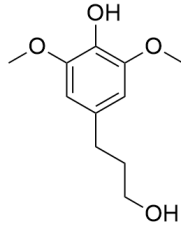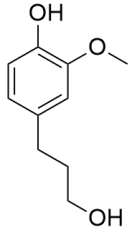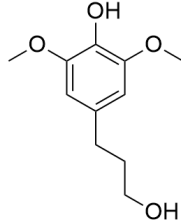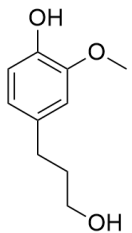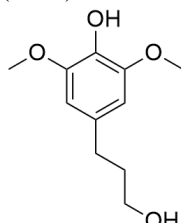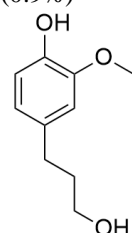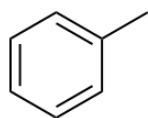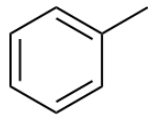
Figure 4.2 Hydrogenolysis of diphenyl ether as a model compound for one of the common building blocks in lignin
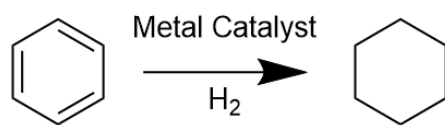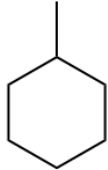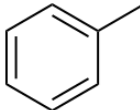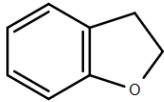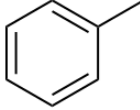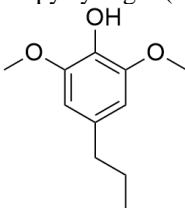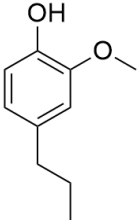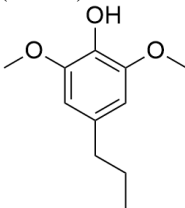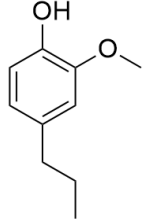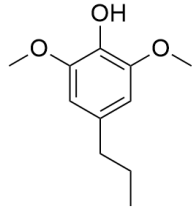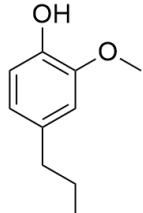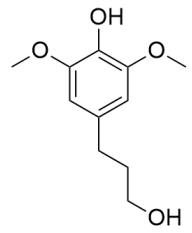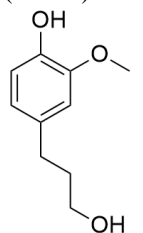
Figure 4.3 Example of a hydrogenation reaction in which benzene is converted into cyclohexane

Table 4.4.1 Depolymerization of extracted or real lignin
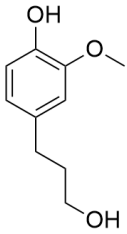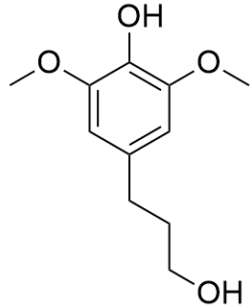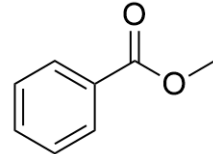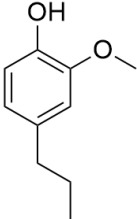
Catalyst	T(°C)	P	Time	Conversion	Feed	Products	Ref
RuW/AC	260	0.7 MPa	10 h	47.3%	Organosolv Poplar Lignin	2-Methoxy-4-(propenyl) phenol (48.4%) 2,6-Dimethoxyphenol (15.8%) Oxydibenzene (18.7%)	99
$Ni_{85}Rh_{15}$	130	1 MPa	12 h	3.6%	Organosolv *Betula platyphylla suk* (Birch) Lignin	4-(3-hydroxypropyl)-2,6-dimethoxyphenol (PS-OH) (2.2%) 4-(3-hydroxypropyl)-2-methoxyphenol (PG-OH) (0.7%)	100
$Ni_{85}Ru_{15}$	130	1 MPa	12 h	6.8%	Organosolv *Betula platyphylla suk* (Birch) Lignin	4-(3-hydroxypropyl)-2,6-dimethoxyphenol (PS-OH) (1.4%)	100

Catalyst	Temp	Pressure	Time	Yield	Feedstock	Product	Ref
						4-(3-hydroxypropyl)-2-methoxyphenol (PG-OH) (5.0%)	
Ni₈₅Pd₁₅	130	1 MPa	12 h	4.6%	Organosolv *Betula platyphylla suk* (Birch) Lignin	4-(3-hydroxypropyl)-2,6-dimethoxyphenol (PS-OH) (3.3%) 4-(3-hydroxypropyl)-2-methoxyphenol (PG-OH) (0.9%)	100
Pt/Al₂O₃	250	4-6 MPa	10 h	45%	Steam Exploded Corn Stover	Toluene (68%)	101
Ru/C	250	4-6 MPa	8 h	34%	Steam Exploded Corn Stover	Toluene (25%)	101
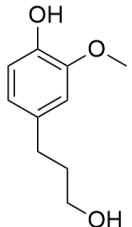
Catalyst	Temp (°C)	Pressure	Time	Yield	Feedstock	Products	Ref
						Methylcyclohexane (23%)	
Ru/Al₂O₃	250	4-6 MPa	8 h	61%	Steam Exploded Corn Stover	Toluene (18%) Coumaran (29%)	101
Rh/Al₂O₃	250	4-6 MPa	10 h	49%	Steam Exploded Corn Stover	Toluene (70%)	101
Ni/C	200	0.1 MPa	6 h	54%	Organosolv Birch Sawdust	Propylsyringol (PS) (67%) Propylguaiacol (PG) (22%)	102
Ni₁Fe₁/AC	200	2 MPa	6 h	20.30%	Organosolv Birch Lignin	Propylsyringol (PS) (58.9%) Propylguaiacol (PG) (26.1%)	104

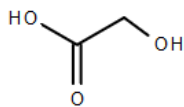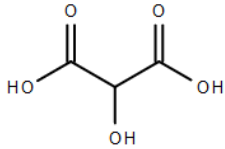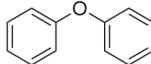|							
						OH structure with methoxy and propyl group	
Ni$_1$Fe$_1$/AC	200	2 MPa	6 h	39.50%	Birch Sawdust (20% Lignin) No Pretreatment	Propylsyringol (PS) (23.70%) Propylguaiacol (PG) (11.06%)	104
Pd/AC	200	2 MPa	6 h	20.10%	Organosolv Birch Lignin	4-(3-hydroxypropyl)-2,6-dimethoxyphenol (PS-OH) (42.9%) 4-(3-hydroxypropyl)-2-methoxyphenol (PG-OH) (13.8%)	104
Ni/Al$_2$O$_3$	250	3 MPa	3 h	36%	Extracted Birch Sawdust (19.5 wt%	4-(3-hydroxypropyl)-2,6-dimethoxyphenol (PS-OH) (21%)	111
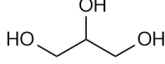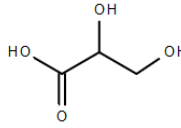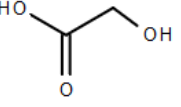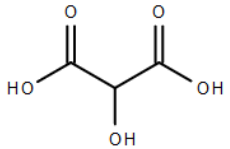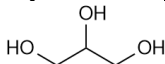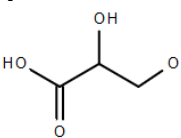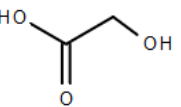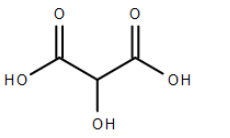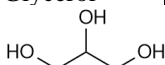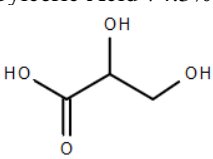
					Klason Lignin)		
Ru/CeO$_2$	200	3 MPa	6 h	-	Organosolv Poplar Lignin	Phenol (0 wt%) 	131
CuCl$_2$	200	3 MPa	6 h	-	Organosolv Poplar Lignin	Phenol (2.6 wt%) 	131
Ru/CeO$_2$ + CuCl$_2$	200	3 MPa	6 h	-	Organosolv Poplar Lignin	Phenol (13 wt%) Guaiacol (2 wt%) Syringol (0.5 wt%) 	131
Ni$_7$Au$_3$	170	1 MPa	12 h	14%	Organosolv Birch Sawdust Lignin	4-(3-hydroxypropyl)-2,6-dimethoxyphenol (PS-OH) (9.3%) 4-(3-hydroxypropyl)-2-methoxyphenol (PG-OH) (3.2%)	156
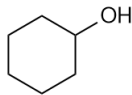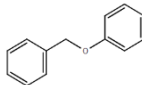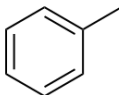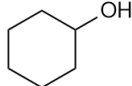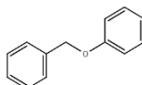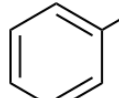
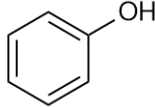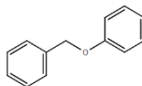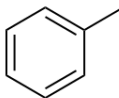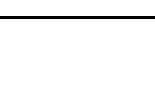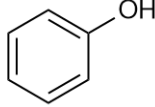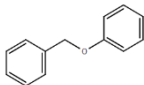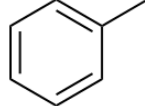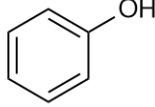|							
TiN (Urea Glass)	300	Super critical Ethanol	-	61 wt% THF-soluble	P1000 Soda Lignin	Monomer yield (12 wt%) THF-soluble (61 wt%)	157
TiN (Urea Glass)	340	Super critical Ethanol	-	51 wt% THF-soluble	P1000 Soda Lignin	Monomer yield (19 wt%) THF-soluble (51 wt%)	157
Pd/C+H_3PO_4	180	3 MPa	3 h	37%	Organosolv Birch Wood Meal Lignin	4-(3-hydroxypropyl)-2,6-dimethoxyphenol (PS-OH) (18.2%)	158
Zr-KIT-5	250	In acetic acid	5 h	11.8%	Organosolv Corn Stover Lignin	Phenyl acetate (Percentage unknown)	159
$Cu_{20}PMO$	310	MeOH	N.R.	48.3%	Organosolv Candlenut Lignin	Phenolics, aromatics	160
ZnPd/C	150	2 MPa	2 h	100%	β-O-4 Synthetic Lignin Polymer	Propylguaiacol (PG) (56%) 4-(3-hydroxypropyl)-2-methoxyphenol (PG-OH) (44%)	161

						OH, O, OH (2-methoxy-4-(3-hydroxypropyl)phenol structure)	
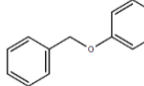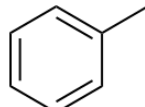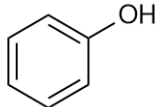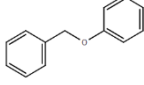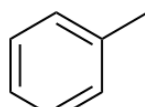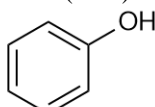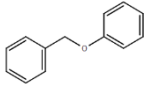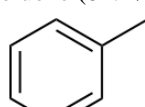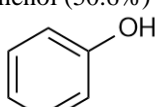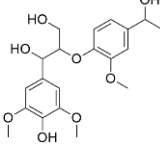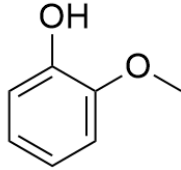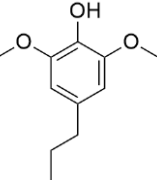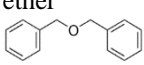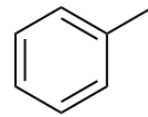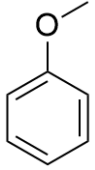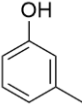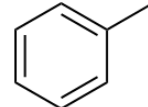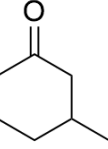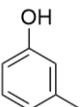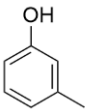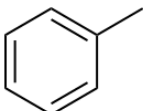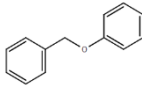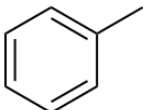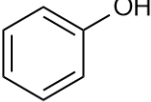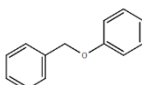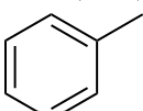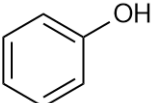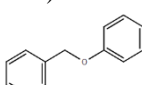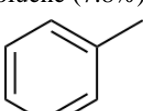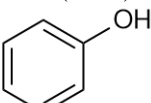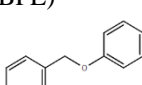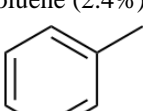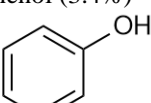
Table 4.4.2 Model Lignin Compounds Depolymerization
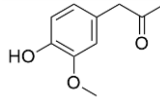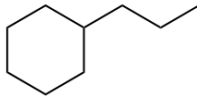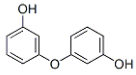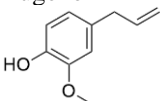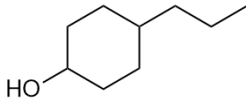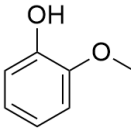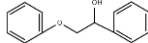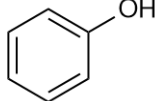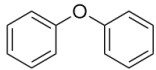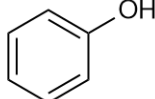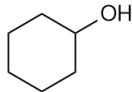
Catalyst	T(°C)	P	Time	Conversion	Feed	Products	Ref
1% Au/G	50	0.3 MPa	Varied	@50%	Glycerol	Gylceric Acid 78.5% Glycolic Acid 8.4% Tartronic Acid 10.4%	[97]
1% Pd/G	50	0.3 MPa	Varied	@50%	Glycerol	Gylceric Acid 80.2% Glycolic Acid 9% Tartronic Acid 10.8%	[97]
1% (AuPd)/ G	50	0.3 MPa	Varied	@50%	Glycerol	Gylceric Acid 74.3% Glycolic Acid 9.6%	[97]

						HO—CH₂—OH structure Tartronic Acid 11.6% malonic acid structure	
NiPd/C	240	1 MPa	90 Min	96%	Diphenyl Ether	Benzene (45%) Cyclohexanol (46%)	98
Pd/AC	260	0.7 MPa	10 h	99.7%	Benzyl phenyl ether (BPE)	Toluene (89.0%) Cyclohexanol (36.5%)	99
Pt/AC	260	0.7 MPa	10 h	89.2%	Benzyl phenyl ether (BPE)	Toluene (60.5%) Phenol (36.5%)	99
Ru/AC	260	0.7 MPa	10 h	94.2%	Benzyl phenyl ether (BPE)	Toluene (81.4%) Phenol (48.6%)	99

						OH	
W/AC	260	0.7 MPa	10 h	79.5%	Benzyl phenyl ether (BPE)	Toluene (40.3%) Phenol (33.8%) OH	99
RuW/AC	260	0.7 MPa	10 h	99.7%	Benzyl phenyl ether (BPE)	Toluene (92.6%) Phenol (61.5%) OH	99
PdW/AC	260	0.7 MPa	10 h	100%	Benzyl phenyl ether (BPE)	Toluene (100%) Phenol (29%) OH	99
PtW/AC	260	0.7 MPa	10 h	98.9%	Benzyl phenyl ether (BPE)	Toluene (82.4%) Phenol (50.6%) OH	99

NiFe/C	200	2 MPa	6 h	100%	1-(4-hydroxy-3,5-dimethoxyphenyl)-2-(2-methoxyphenoxy)propane-1,3-diol	Guaiacol (100%) Propylsyringol (88%)	104
FeS$_2$/AC	250	10 MPa	2 h	98%	Dibenzyl ether	Toluene (100%)	105
Ni$_{13.3}$Cu$_{11.8}$/ Al$_2$O$_3$	300	1 MPa	Continuous	70.3%	Anisole	Benzene (42.2%) Cyclohexane (27.7%)	107
Pt/C	200	3.6 MPa	~3 h	8.3%	*m*-cresol	Toluene (62%) 3- methylcyclo-hexanone (23%)	110
WO$_x$/C	200	3.6 MPa	~3 h	0%	*m*-cresol	None	110

Catalyst	Temp	Pressure	Time	Yield	Substrate	Product	Ref
PtWO$_x$	200	3.6 MPa	~3 h	61%	*m*-cresol	Toluene (98%)	[110]
ReO$_x$/AC	200	3 MPa	5 h	84.5%	Benzyl phenyl ether (BPE)	Toluene (80.3%) Phenol (62.5%)	[140]
ReO$_x$/Al2O3	200	3 MPa	5 h	97.4%	Benzyl phenyl ether (BPE)	Toluene (1.7%) Phenol (20.3%)	[140]
ReOx/SiO2	200	3 MPa	5 h	50.3%	Benzyl phenyl ether (BPE)	Toluene (7.8%) Phenol (9.5%)	[140]
ReO$_x$/CeO$_2$	200	3 MPa	5 h	4.7%	Benzyl phenyl ether (BPE)	Toluene (2.4%) Phenol (3.4%)	[140]

Catalyst	Temp	Pressure	Time	Conversion	Substrate	Product	Ref
Pd/C + H₃PO₄	250	5 MPa	2h	100%	4-Hydroxy-3-methoxyphenylacetone	Propylcyclohexane (71%)	[162]
Ru/HZSM-5	200	5 MPa	4h	97%	3,3′-Oxydiphenol	Cyclohexane (100%)	[163]
Co/TiO₂	200	1 MPa	2h	100%	Eugenol	4-propylcyclohexanol	[164]
NiCuLa/ZrO₂−SiO2	320	17 MPa	1h	85.6%	Guaiacol	cyclohexane (63%)	[165]
Ni₇Au₃/NaOH	100	1 MPa	0.5 h	33.6%	2-phenoxy-1-phenylethanol	Phenol (15%)	[166]
Ni₇Au₃/NaOH	100	1 MPa	15 h	37.2%	Diphenyl Ether	Phenol (6.5%) Cyclohexanol (12.3%)	[166]

4.14 References

(1)   Subburaj, A. S.; Pushpakaran, B. N.; Bayne, S. B. Overview of Grid Connected Renewable Energy Based Battery Projects in USA. *Renew. Sustain. Energy Rev.* **2015**, *45*, 219–234. https://doi.org/10.1016/j.rser.2015.01.052.

(2)   Seemala, B.; Meng, X.; Parikh, A.; Nagane, N.; Kumar, R.; Wyman, C. E.; Ragauskas, A.; Christopher, P.; Cai, C. M. Hybrid Catalytic Biorefining of Hardwood Biomass to Methylated Furans and Depolymerized Technical Lignin. *ACS Sustain. Chem. Eng.* **2018**, *6* (8), 10587–10594. https://doi.org/10.1021/acssuschemeng.8b01930.

(3)   Ragauskas, A. J.; Beckham, G. T.; Biddy, M. J.; Chandra, R.; Chen, F.; Davis, M. F.; Davison, B. H.; Dixon, R. A.; Gilna, P.; Keller, M.; et al. Lignin Valorization: Improving Lignin Processing in the Biorefinery. *Science (80-.).* **2014**, *344* (6185), 1246843-1–10. https://doi.org/10.1126/science.1246843.

(4)   Chheda, J. N.; Huber, G. W.; Dumesic, J. A. Liquid-Phase Catalytic Processing of Biomass-Derived Oxygenated Hydrocarbons to Fuels and Chemicals. *Angew. Chemie - Int. Ed.* **2007**, *46* (38), 7164–7183. https://doi.org/10.1002/anie.200604274.

(5)   Huber, G. W.; Iborra, S.; Corma, A. Synthesis of Transportation Fuels from Biomass: Chemistry, Catalysts, and Engineering. *Chem. Rev.* **2006**, *106* (9), 4044–4098. https://doi.org/10.1021/cr068360d.

(6)   Saha, B.; Abu-Omar, M. M. Current Technologies, Economics, and Perspectives for 2,5-Dimethylfuran Production from Biomass-Derived Intermediates. *ChemSusChem* **2015**, *8* (7), 1133–1142. https://doi.org/10.1002/cssc.201403329.

(7)   Saha, B.; Klein, I.; Parsell, T.; Abu-Omar, M. M. Catalytic Hydrodeoxygenation of Lignin Model Compounds. In *Reaction Pathways and Mechanisms in Thermocatalytic Biomass Conversion II*; Springer, Singapore, 2016; pp 119–129. https://doi.org/https://doi.org/10.1007/978-981-287-769-7_6.

(8)   He, J.; Huang, K.; Barnett, K. J.; Krishna, S. H.; Alonso, D. M.; Brentzel, Z. J.; Burt, S. P.; Walker, T.; Banholzer, W. F.; Maravelias, C. T.; et al. New Catalytic Strategies for α,ω-Diols Production from Lignocellulosic Biomass. *Faraday Discuss.* **2017**, *202*, 247–267. https://doi.org/10.1039/c7fd00036g.

(9)   Gallo, J. M. R.; Alamillo, R.; Dumesic, J. A. Acid-Functionalized Mesoporous Carbons for the Continuous Production of 5-Hydroxymethylfurfural. *J. Mol. Catal. A Chem.* **2016**, *422*, 13–17. https://doi.org/10.1016/j.molcata.2016.01.005.

(10)   Yang, B.; Tao, L.; Wyman, C. E. Strengths, Challenges, and Opportunities for

Hydrothermal Pretreatment in Lignocellulosic Biorefineries. *Biofuels, Bioprod. Biorefining* **2018**, *12* (1), 125–138. https://doi.org/10.1002/bbb.1825.

(11) Bin Yang; Ziyu Dai; Shi-You Ding; Charles E Wyman. Enzymatic Hydrolysis of Cellulosic Biomass. *Biofuels* **2011**, *2* (4), 421–449. https://doi.org/10.4155/BFS.11.116.

(12) Cai, C. M.; Zhang, T.; Kumar, R.; Wyman, C. E. Integrated Furfural Production as a Renewable Fuel and Chemical Platform from Lignocellulosic Biomass. *J. Chem. Technol. Biotechnol.* **2014**, *89* (1), 2–10. https://doi.org/10.1002/jctb.4168.

(13) Liu, Z. H.; Le, R. K.; Kosa, M.; Yang, B.; Yuan, J.; Ragauskas, A. J. Identifying and Creating Pathways to Improve Biological Lignin Valorization. *Renew. Sustain. Energy Rev.* **2019**, *105* (January), 349–362. https://doi.org/10.1016/j.rser.2019.02.009.

(14) Deuss, P. J.; Barta, K.; De Vries, J. G. Homogeneous Catalysis for the Conversion of Biomass and Biomass-Derived Platform Chemicals. *Catal. Sci. Technol.* **2014**, *4* (5), 1174–1196. https://doi.org/10.1039/c3cy01058a.

(15) Schutyser, W.; Renders, T.; Van Den Bosch, S.; Koelewijn, S. F.; Beckham, G. T.; Sels, B. F. Chemicals from Lignin: An Interplay of Lignocellulose Fractionation, Depolymerisation, and Upgrading. *Chem. Soc. Rev.* **2018**, *47* (3), 852–908. https://doi.org/10.1039/c7cs00566k.

(16) Sun, Z.; Fridrich, B.; De Santi, A.; Elangovan, S.; Barta, K. Bright Side of Lignin Depolymerization: Toward New Platform Chemicals. *Chem. Rev.* **2018**, *118* (2), 614–678. https://doi.org/10.1021/acs.chemrev.7b00588.

(17) McKendry, P. Energy Production from Biomass (Part 1): Overview of Biomass. *Bioresour. Technol.* **2002**, *83* (1), 37–46. https://doi.org/10.1016/S0960-8524(01)00118-3.

(18) Lynd, L. R.; Cushman, J. H.; Nichols, R. J.; Wyman, C. E. Fuel Ethanol from Cellulosic Biomass. *Science (80-.).* **1991**, *251* (4999), 1318–1323. https://doi.org/10.1126/science.251.4999.1318.

(19) Gírio, F. M.; Fonseca, C.; Carvalheiro, F.; Duarte, L. C.; Marques, S.; Bogel-Łukasik, R. Hemicelluloses for Fuel Ethanol: A Review. *Bioresour. Technol.* **2010**, *101* (13), 4775–4800. https://doi.org/10.1016/j.biortech.2010.01.088.

(20) Demirbaş, A. Bioethanol from Cellulosic Materials: A Renewable Motor Fuel from Biomass. *Energy Sources* **2005**, *27* (4), 327–337. https://doi.org/10.1080/00908310390266643.

(21)　Wyman, C. E. Cellulose and Biomass Conversion Technology and Its Application to Ethanol Production from Corn. *Fuel Reformul.* **1993**, No. March/April, 67–74.

(22)　Bond, J. Q.; Upadhye, A. A.; Olcay, H.; Tompsett, G. A.; Jae, J.; Xing, R.; Alonso, D. M.; Wang, D.; Zhang, T.; Kumar, R.; et al. Production of Renewable Jet Fuel Range Alkanes and Commodity Chemicals from Integrated Catalytic Processing of Biomass. *Energy Environ. Sci.* **2014**, *7* (4), 1500–1523. https://doi.org/10.1039/c3ee43846e.

(23)　Dodds, D. R.; Gross, R. A. Chemicals from Biomass. *Science* **2007**, *318*, 1250–1251. https://doi.org/10.1126/science.1146356.

(24)　Wyman, C. E.; Decker, S. R.; Himmel, M. E.; Brady, J. W.; Skopec, C. E. Hydrolysis of Cellulose and Hemicellulose. In *Polysaccharides: Structural Diversity and Functional Versatility, 2nd Edition,*; 2004; pp 955–1033.

(25)　Schutt, B. D.; Serrano, B.; Cerro, R. L.; Abraham, M. A. Production of Chemicals from Cellulose and Biomass-Derived Compounds through Catalytic Sub-Critical Water Oxidation in a Monolith Reactor. *Biomass and Bioenergy* **2002**, *22* (5), 365–375. https://doi.org/10.1016/S0961-9534(02)00010-7.

(26)　Mascal, M.; Nikitin, E. B. Comment on Processes for the Direct Conversion of Cellulose or Cellulosic Biomass into Levulinate Esters. *ChemSusChem* **2010**, *3* (12), 1349–1351. https://doi.org/10.1002/cssc.201000326.

(27)　Mascal, M.; Nikitin, E. B. High-Yield Conversion of Plant Biomass into the Key Value-Added Feedstocks 5-(Hydroxymethyl)Furfural, Levulinic Acid, and Levulinic Esters via 5-(Chloromethyl)Furfural. *Green Chem.* **2010**, *12* (3), 370–373. https://doi.org/10.1039/b918922j.

(28)　Jones, L.; Ennos, A. R.; Turner, S. R. Cloning and Characterization of Irregular Xylem4 (Irx4): A Severely Lignin-Deficient Mutant of Arabidopsis. *Plant J.* **2001**, *26* (2), 205–216. https://doi.org/10.1046/j.1365-313X.2001.01021.x.

(29)　Demirbaş, A. Relationships between Lignin Contents and Heating Values of Biomass. *Energy Convers. Manag.* **2001**, *42*, 183–188. https://doi.org/10.1016/S0196-8904(00)00050-9.

(30)　Guerra, A.; Filpponen, I.; Lucia, L. A.; Argyropoulos, D. S. Comparative Evaluation of Three Lignin Isolation Protocols for Various Wood Species. *J. Agric. Food Chem.* **2006**, *54* (26), 9696–9705. https://doi.org/10.1021/jf062433c.

(31)　Vanholme, R.; Demedts, B.; Morreel, K.; Ralph, J.; Boerjan, W. Lignin Biosynthesis and Structure. *Plant Physiol.* **2010**, *153* (3), 895–905. https://doi.org/10.1104/pp.110.155119.

(32) Irvine, G. M. The Significance of the Glass Transition of Lignin in Thermomechanical Pulping. *Wood Sci. Technol.* **1985**, *19* (2), 139–149. https://doi.org/10.1007/BF00353074.

(33) Petridis, L.; Schulz, R.; Smith, J. C. Simulation Analysis of the Temperature Dependence of Lignin Structure and Dynamics. *J. Am. Chem. Soc.* **2011**, *133* (50), 20277–20287. https://doi.org/10.1021/ja206839u.

(34) Pan, Y.; Birdsey, R. A.; Phillips, O. L.; Jackson, R. B. The Structure, Distribution, and Biomass of the World's Forests. *Annu. Rev. Ecol. Evol. Syst.* **2013**, *44* (1), 593–622. https://doi.org/10.1146/annurev-ecolsys-110512-135914.

(35) Woodcock, B. A.; Redhead, J.; Vanbergen, A. J.; Hulmes, L.; Hulmes, S.; Peyton, J.; Nowakowski, M.; Pywell, R. F.; Heard, M. S. Impact of Habitat Type and Landscape Structure on Biomass, Species Richness and Functional Diversity of Ground Beetles. *Agric. Ecosyst. Environ.* **2010**, *139* (1–2), 181–186. https://doi.org/10.1016/j.agee.2010.07.018.

(36) Chakar, F. S.; Ragauskas, A. J. Review of Current and Future Softwood Kraft Lignin Process Chemistry. *Ind. Crops Prod.* **2004**, *20* (2), 131–141. https://doi.org/10.1016/j.indcrop.2004.04.016.

(37) Yuan, T. Q.; Sun, S. N.; Xu, F.; Sun, R. C. Characterization of Lignin Structures and Lignin-Carbohydrate Complex (LCC) Linkages by Quantitative 13C and 2D HSQC NMR Spectroscopy. *J. Agric. Food Chem.* **2011**, *59* (19), 10604–10614. https://doi.org/10.1021/jf2031549.

(38) Dorrestijn, E.; Laarhoven, L.; Arends, I. W. C. E.; Mulder, P. The Occurrence and Reactivity of Phenoxyl Linkages in Lignin and Low Rank Coal. *J. Anal. Appl. Pyrolysis* **2000**, *54* (1–2), 153–192. https://doi.org/https://doi.org/10.1016/S0165-2370(99)00082-0.

(39) Deuss, P. J.; Lancefield, C. S.; Narani, A.; De Vries, J. G.; Westwood, N. J.; Barta, K. Phenolic Acetals from Lignins of Varying Compositions via Iron(III) Triflate Catalysed Depolymerisation† Peter. *Green Chem.* **2017**, *19* (12), 2774–2782. https://doi.org/10.1039/c7gc00195a.

(40) Da Silva, A. S. A.; Inoue, H.; Endo, T.; Yano, S.; Bon, E. P. S. Milling Pretreatment of Sugarcane Bagasse and Straw for Enzymatic Hydrolysis and Ethanol Fermentation. *Bioresour. Technol.* **2010**, *101* (19), 7402–7409. https://doi.org/10.1016/j.biortech.2010.05.008.

(41) Lin, Z.; Huang, H.; Zhang, H.; Zhang, L.; Yan, L.; Chen, J. Ball Milling Pretreatment of Corn Stover for Enhancing the Efficiency of Enzymatic Hydrolysis. *Appl. Biochem. Biotechnol.* **2010**, *162* (7), 1872–1880.

https://doi.org/10.1007/s12010-010-8965-5.

(42)   Haghighi Mood, S.; Hossein Golfeshan, A.; Tabatabaei, M.; Salehi Jouzani, G.;
         Najafi, G. H.; Gholami, M.; Ardjmand, M. Lignocellulosic Biomass to Bioethanol,
         a Comprehensive Review with a Focus on Pretreatment. *Renew. Sustain. Energy
         Rev.* **2013**, *27*, 77–93. https://doi.org/10.1016/j.rser.2013.06.033.

(43)   Yang, B.; Wyman, C. E. Effect of Xylan and Lignin Removal by Batch and
         Flowthrough Pretreatment on the Enzymatic Digestibility of Corn Stover
         Cellulose. *Biotechnol. Bioeng.* **2004**, *86* (1), 88–95.
         https://doi.org/10.1002/bit.20043.

(44)   Beckham, G. T.; Johnson, C. W.; Karp, E. M.; Salvachúa, D.; Vardon, D. R.
         Opportunities and Challenges in Biological Lignin Valorization. *Curr. Opin.
         Biotechnol.* **2016**, *42* (March), 40–53.
         https://doi.org/10.1016/j.copbio.2016.02.030.

(45)   Duff, S. J. B.; Murray, W. D. Bioconversion of Forest Products Industry Waste
         Cellulosics to Fuel Ethanol: A Review. *Bioresour. Technol.* **1996**, *55* (1), 1–33.
         https://doi.org/10.1016/0960-8524(95)00122-0.

(46)   Seidl, P. R.; Goulart, A. K. Pretreatment Processes for Lignocellulosic Biomass
         Conversion to Biofuels and Bioproducts. *Curr. Opin. Green Sustain. Chem.* **2016**,
         2, 48–53. https://doi.org/10.1016/j.cogsc.2016.09.003.

(47)   Guo, G. L.; Chen, W. H.; Chen, W. H.; Men, L. C.; Hwang, W. S. Characterization
         of Dilute Acid Pretreatment of Silvergrass for Ethanol Production. *Bioresour.
         Technol.* **2008**, *99* (14), 6046–6053.
         https://doi.org/10.1016/j.biortech.2007.12.047.

(48)   Kumar, R.; Hu, F.; Sannigrahi, P.; Jung, S.; Ragauskas, A. J.; Wyman, C. E.
         Carbohydrate Derived-Pseudo-Lignin Can Retard Cellulose Biological
         Conversion. *Biotechnol. Bioeng.* **2013**, *110* (3), 737–753.
         https://doi.org/10.1002/bit.24744.

(49)   Shinde, S. D.; Meng, X.; Kumar, R.; Ragauskas, A. J. Recent Advances in
         Understanding the Pseudo-Lignin Formation in a Lignocellulosic Biorefinery.
         Green Chem. **2018**, *20* (10), 2192–2205. https://doi.org/10.1039/c8gc00353j.

(50)   Zhao, X.; Cheng, K.; Liu, D. Organosolv Pretreatment of Lignocellulosic Biomass
         for Enzymatic Hydrolysis. *Appl. Microbiol. Biotechnol.* **2009**, *82* (5), 815–827.
         https://doi.org/10.1007/s00253-009-1883-1.

(51)   Yasuda, S.; Fukushima, K.; Kakehi, A. Formation and Chemical Structures of
         Acid-Soluble Lignin I: Sulfuric Acid Treatment Time and Acid-Soluble Lignin

Content of Hardwood. *J. Wood Sci.* **2001**, *47* (1), 69–72. https://doi.org/10.1007/BF00776648.

(52) Kim, J. S.; Lee, Y. Y.; Kim, T. H. A Review on Alkaline Pretreatment Technology for Bioconversion of Lignocellulosic Biomass. *Bioresour. Technol.* **2016**, *199*, 42–48. https://doi.org/10.1016/j.biortech.2015.08.085.

(53) Jung, H. G.; Mertens, D. R.; Payne, A. J. Correlation of Acid Detergent Lignin and Klason Lignin with Digestibility of Forage Dry Matter and Neutral Detergent Fiber. *J. Dairy Sci.* **2010**, *80* (8), 1622–1628. https://doi.org/10.3168/jds.s0022-0302(97)76093-4.

(54) Wallberg, O.; Jönsson, A. S.; Wimmerstedt, R. Fractionation and Concentration of Kraft Black Liquor Lignin with Ultrafiltration. *Desalination* **2003**, *154* (2), 187–199. https://doi.org/10.1016/S0011-9164(03)80019-X.

(55) Pan, X.; Xie, D.; Yu, R. W.; Lam, D.; Saddler, J. N. Pretreatment of Lodgepole Pine Killed by Mountain Pine Beetle Using the Ethanol Organosolv Process: Fractionation and Process Optimization. *Ind. Eng. Chem. Res.* **2007**, *46* (8), 2609–2617. https://doi.org/10.1021/ie061576l.

(56) Pan, X.; Gilkes, N.; Kadla, J.; Pye, K.; Saka, S.; Gregg, D.; Ehara, K.; Xie, D.; Lam, D.; Saddler, J. Bioconversion of Hybrid Poplar to Ethanol and Co-Products Using an Organosolv Fractionation Process: Optimization of Process Yields. *Biotechnol. Bioeng.* **2006**, *94* (5), 851–861. https://doi.org/10.1002/bit.20905.

(57) Nguyen, T. Y.; Cai, C. M.; Osman, O.; Kumar, R.; Wyman, C. E. CELF Pretreatment of Corn Stover Boosts Ethanol Titers and Yields from High Solids SSF with Low Enzyme Loadings. *Green Chem.* **2016**, *18* (6), 1581–1589. https://doi.org/10.1039/c5gc01977j.

(58) Cai, C. M.; Zhang, T.; Kumar, R.; Wyman, C. E. THF Co-Solvent Enhances Hydrocarbon Fuel Precursor Yields from Lignocellulosic Biomass. *Green Chem.* **2013**, *15* (11), 3140–3145. https://doi.org/10.1039/c3gc41214h.

(59) Pu, Y.; Jiang, N.; Ragauskas, A. J. Ionic Liquid as a Green Solvent for Lignin. *J. Wood Chem. Technol.* **2007**, *27* (1), 23–33. https://doi.org/10.1080/02773810701282330.

(60) Xu, A.; Guo, X.; Zhang, Y.; Li, Z.; Wang, J. Efficient and Sustainable Solvents for Lignin Dissolution: Aqueous Choline Carboxylate Solutions. *Green Chem.* **2017**, *19* (17), 4067–4073. https://doi.org/10.1039/c7gc01886j.

(61) Schuerch, C. The Solvent Properties of Liquids and Their Relation to the Solubility, Swelling, Isolation and Fractionation of Lignin. *J. Am. Chem. Soc.*

1952, *74* (20), 5061–5067. https://doi.org/10.1021/ja01140a020.

(62) Sun, N.; Rahman, M.; Qin, Y.; Maxim, M. L.; Rodríguez, H.; Rogers, R. D. Complete Dissolution and Partial Delignification of Wood in the Ionic Liquid 1-Ethyl-3-Methylimidazolium Acetate. *Green Chem.* **2009**, *11* (5), 646–655. https://doi.org/10.1039/b822702k.

(63) Pan, X.; Gilkes, N.; Kadla, J.; Pye, K.; Saka, S.; Gregg, D.; Ehara, K.; Xie, D.; Lam, D.; Saddler, J. Bioconversion of Hybrid Poplar to Ethanol and Co-Products Using an Organosolv Fractionation Process: Optimization of Process Yields. *Biotechnol. Bioeng.* **2006**, *94* (5), 851–861. https://doi.org/10.1002/bit.20905.

(64) Chum, H. L.; Johnson, D. K.; Black, S. K.; Overend, R. P. Pretreatment-Catalyst Effects and the Combined Severity Parameter. *Appl. Biochem. Biotechnol.* **1990**, *24–25* (1), 1–14. https://doi.org/10.1007/BF02920229.

(65) Chum, H. L.; Johnson, D. K.; Black, S.; Baker, J.; Grohmann, K.; Sarkanen, K. V.; Wallace, K.; Schroeder, H. A. Organosolv Pretreatment for Enzymatic Hydrolysis of Poplars: I. Enzyme Hydrolysis of Cellulosic Residues. *Biotechnol. Bioeng.* **1988**, *31* (7), 643–649. https://doi.org/doi:10.1002/bit.260310703.

(66) Jiménez, L.; De La Torre, M. J.; Maestre, F.; Ferrer, J. L. Organosolv Pulping of Wheat Straw by Use of Acetone-Water Mixtures. *Process Biochem.* **1998**, *33* (4), 401–408. https://doi.org/10.1016/S0032-9592(98)00001-6.

(67) Sadeghifar, H.; Wells, T.; Le, R. K.; Sadeghifar, F.; Yuan, J. S.; Jonas Ragauskas, A. Fractionation of Organosolv Lignin Using Acetone:Water and Properties of the Obtained Fractions. *ACS Sustain. Chem. Eng.* **2017**, *5* (1), 580–587. https://doi.org/10.1021/acssuschemeng.6b01955.

(68) Sidiras, D. K.; Salapa, I. S. Organosolv Pretreatment As a Major Step of Lignocellulosic Biomass Refining Organosolv Pretreatment As a Major Step of Lignocellulosic Biomass Refining. In *Biorefinery I: Chemicals and Materials From Thermo-Chemical Biomass Conversion and Related Processes*; 2015.

(69) Lam, H. Q.; Bigot, Y. Le; Delmas, M.; Avignon, G. G. Formic Acid Pulping of Rice Straw. *Ind. Crops Prod.* **2001**, *14* (1), 65–71. https://doi.org/10.1016/S0926-6690(00)00089-3.

(70) Wettstein, S. G.; Alonso, D. M.; Chong, Y.; Dumesic, J. A. Production of Levulinic Acid and Gamma-Valerolactone (GVL) from Cellulose Using GVL as a Solvent in Biphasic Systems. *Energy Environ. Sci.* **2012**, *5* (8), 8199–8203. https://doi.org/10.1039/c2ee22111j.

(71) Gosselink, R. J. A.; De Jong, E.; Guran, B.; Abächerli, A. Co-Ordination Network

for Lignin - Standardisation, Production and Applications Adapted to Market Requirements (EUROLIGNIN). *Ind. Crops Prod.* **2004**, *20* (2), 121–129. https://doi.org/10.1016/j.indcrop.2004.04.015.

(72)   Dehne, L.; Vila Babarro, C.; Saake, B.; Schwarz, K. U. Influence of Lignin Source and Esterification on Properties of Lignin-Polyethylene Blends. *Ind. Crops Prod.* **2016**, *86*, 320–328. https://doi.org/10.1016/j.indcrop.2016.04.005.

(73)   L'udmila, H.; Michal, J.; Andrea, Š.; Aleš, H. Lignin, Potential Products and Their Market Value. *Wood Res.* **2015**, *60* (6), 973–986.

(74)   Smolarski, N. High-Value Opportunities for Lignin: Unlocking Its Potential Lignin Potential. *Frost & Sullivan* **2012**, 1–15. https://doi.org/10.1007/s00216-010-3562-6.

(75)   Cheng, F.; Brewer, C. E. Producing Jet Fuel from Biomass Lignin: Potential Pathways to Alkyl-Benzenes and Cycloalkanes. *Renew. Sustain. Energy Rev.* **2017**, *72*, 673–722. https://doi.org/10.1016/j.rser.2017.01.030.

(76)   Shen, R.; Tao, L.; Yang, B. Techno-Economic Analysis of Jet-Fuel Production from Biorefinery Waste Lignin. *Biofuels, Bioprod. Biorefining* **2019**, *13* (3), 486–501. https://doi.org/10.1002/bbb.1952.

(77)   Shyamala, B. N.; Madhava Naidu, M.; Sulochanamma, G.; Srinivas, P. Studies on the Antioxidant Activities of Natural Vanilla Extract and Its Constituent Compounds through in Vitro Models. *J. Agric. Food Chem.* **2007**, *55* (19), 7738–7743. https://doi.org/10.1021/jf071349+.

(78)   Borges da Silva, E. A.; Zabkovaa, M.; Araújoa, J. D.; Catetob, C. A.; Barreiro, M. F.; Elgacem, M. N.; Rodrigues, A. E. An Integrated Process to Produce Vanillin and Lignin-Based Polyurethanes from Kraft Lignin. *Chem. Eng. Res. Des.* **2009**, *7* (April), 1276–1292. https://doi.org/10.1016/j.cherd.2009.05.008.

(79)   Baker, D. A.; Rials, T. G. Recent Advances in Low-Cost Carbon Fiber Manufacture from Lignin. *Appl. Polym. Sci.* **2013**, *130* (2), 713–728. https://doi.org/10.1002/app.39273.

(80)   Kadla, J. F.; Kubo, S.; Venditti, R. A.; Gilbert, R. D.; Compere, A. L.; Groffith, W. Lignin-Based Carbon Fibers for Composite Fiber Applications. *Carbon N. Y.* **2002**, *40* (15), 2913–2920. https://doi.org/https://doi.org/10.1016/S0008-6223(02)00248-8.

(81)   Kumar, V.; Kumari, M. Recent Advances in Green Hydrogels from Lignin : A Review. *Int. J. Biol. Macromol.* **2015**, *72*, 834–847. https://doi.org/10.1016/j.ijbiomac.2014.09.044.

(82)   Doherty, W. O. S.; Mousavioun, P.; Fellows, C. M. Value-Adding to Cellulosic Ethanol: Lignin Polymers. *Ind. Crops Prod.* **2011**, *33* (2), 259–276. https://doi.org/10.1016/j.indcrop.2010.10.022.

(83)   Scheibel, J. J. Household Cleaning and/or Laundry Detergent Compositions Comprising Lignin-Derived Materials. US 6,689,737 B2, 2004.

(84)   Sarkar, S.; Adhikari, B. Jute Felt Composite From Lignin Modified Phenolic Resin. *Polym. Compos.* **2001**, *22* (4), 518–527. https://doi.org/https://doi.org/10.1002/pc.10556.

(85)   Çetin, N.; Özmen, N. Use of Organosolv Lignin in Phenol – Formaldehyde Resins for Particleboard Production I. Organosolv Lignin Modified Resins. *Ind. J. Adhes. Adhes.* **2002**, *22* (6), 477–480. https://doi.org/https://doi.org/10.1016/S0143-7496(02)00058-1.

(86)   Sahoo, S.; Misra, M.; Mohanty, A. K. Enhanced Properties of Lignin-Based Biodegradable Polymer Composites Using Injection Moulding Process. *Compos. Part A* **2011**, *42* (11), 1710–1718. https://doi.org/10.1016/j.compositesa.2011.07.025.

(87)   Miller, S. A. Sustainable Polymers: Opportunities for the next Decade. *ACS Macro Lett.* **2013**, *2* (6), 550–554. https://doi.org/10.1021/mz400207g.

(88)   Laurichesse, S.; Avérous, L. Chemical Modification of Lignins: Towards Biobased Polymers. *Prog. Polym. Sci.* **2014**, *39* (7), 1266–1290. https://doi.org/10.1016/j.progpolymsci.2013.11.004.

(89)   Zhao, S.; Abu-omar, M. M. Renewable Thermoplastics Based on Lignin-Derived Polyphenols. *Macromolecules* **2017**, *50* (9), 3573–3581. https://doi.org/10.1021/acs.macromol.7b00064.

(90)   Liu, W. J.; Jiang, H.; Yu, H. Q. Thermochemical Conversion of Lignin to Functional Materials: A Review and Future Directions. *Green Chem.* **2015**, *17* (11), 4888–4907. https://doi.org/10.1039/c5gc01054c.

(91)   Bridgwater, A. V; Peacocke, G. V. C. Fast Pyrolysis Processes for Biomass. *Renew. Sustain. Energy Rev.* **2000**, *4* (1), 1–73. https://doi.org/https://doi.org/10.1016/S1364-0321(99)00007-6.

(92)   Xiu, S.; Shahbazi, A. Bio-Oil Production and Upgrading Research : A Review. *Renew. Sustain. Energy Rev.* **2012**, *16* (7), 4406–4414. https://doi.org/10.1016/j.rser.2012.04.028.

(93)   Mortensen, P. M.; Grunwaldt, J.; Jensen, P. A.; Knudsen, K. G.; Jensen, A. D. A

Review of Catalytic Upgrading of Bio-Oil to Engine Fuels. *Appl. Catal. A, Gen.* **2011**, *407* (1–2), 1–19. https://doi.org/10.1016/j.apcata.2011.08.046.

(94) Hu, B.; Antonietti, M.; Wu, L.; Yu, S.-H.; Wang, K.; Titirici, M.-M. Engineering Carbon Materials from the Hydrothermal Carbonization Process of Biomass. *Adv. Mater.* **2010**, *22* (7), 813–828. https://doi.org/10.1002/adma.200902812.

(95) Demir, M.; Kahveci, Z.; Aksoy, B.; Palapati, N. K. R.; Subramanian, A.; Cullinan, H. T.; El-Kaderi, H. M.; Harris, C. T.; Gupta, R. B. Graphitic Biocarbon from Metal-Catalyzed Hydrothermal Carbonization of Lignin. *Ind. Eng. Chem. Res.* **2015**, *54* (43), 10731–10739. https://doi.org/10.1021/acs.iecr.5b02614.

(96) Xiao, L. P.; Shi, Z. J.; Xu, F.; Sun, R. C. Hydrothermal Carbonization of Lignocellulosic Biomass. *Bioresour. Technol.* **2012**, *118*, 619–623. https://doi.org/10.1016/j.biortech.2012.05.060.

(97) Dimitratos, N.; Porta, F.; Prati, L. Au, Pd (Mono and Bimetallic) Catalysts Supported on Graphite Using the Immobilisation Method Synthesis and Catalytic Testing for Liquid Phase Oxidation of Glycerol. *Appl. Catal. A Gen.* **2005**, *291* (1–2), 210–214. https://doi.org/10.1016/j.apcata.2005.01.044.

(98) Mauriello, F.; Paone, E.; Pietropaolo, R.; Balu, A. M.; Luque, R. Catalytic Transfer Hydrogenolysis of Lignin-Derived Aromatic Ethers Promoted by Bimetallic Pd/Ni Systems. *ACS Sustain. Chem. Eng.* **2018**, *6* (7), 9269–9276. https://doi.org/10.1021/acssuschemeng.8b01593.

(99) Ji, J.; Guo, H.; Li, C.; Qi, Z.; Zhang, B.; Dai, T.; Jiang, M.; Ren, C.; Wang, A.; Zhang, T. Tungsten-Based Bimetallic Catalysts for Selective Cleavage of Lignin C−O Bonds. *ChemCatChem* **2018**, *10* (2), 415–421. https://doi.org/10.1002/cctc.201701240.

(100) Zhang, J.; Teo, J.; Chen, X.; Asakura, H.; Tanaka, T.; Teramura, K.; Yan, N. A Series of NiM (M = Ru, Rh, and Pd) Bimetallic Catalysts for Effective Lignin Hydrogenolysis in Water. *ACS Catal.* **2014**, *4* (5), 1574–1583. https://doi.org/10.1021/cs401199f.

(101) Laskar, D. D.; Helms, G. L.; Chen, X.; Tucker, M. P.; Yang, B. Noble-Metal Catalyzed Hydrodeoxygenation of Biomass-Derived Lignin to Aromatic Hydrocarbons. *Green Chem.* **2013**, *16* (2), 897. https://doi.org/10.1039/c3gc42041h.

(102) Song, Q.; Wang, F.; Cai, J.; Wang, Y.; Zhang, J.; Yu, W.; Xu, J. Lignin Depolymerization (LDP) in Alcohol over Nickel-Based Catalysts via a Fragmentation-Hydrogenolysis Process. *Energy Environ. Sci.* **2013**, *6* (3), 994–1007. https://doi.org/10.1039/c2ee23741e.

(103) Liu, X.; Li, H.; Xiao, L. P.; Sun, R. C.; Song, G. Chemodivergent Hydrogenolysis of Eucalyptus Lignin with Ni@ZIF-8 Catalyst. *Green Chem.* **2019**, *21* (6), 1498–1504. https://doi.org/10.1039/c8gc03511c.

(104) Zhai, Y.; Xu, G.; Zhang, Y.; Liu, X.; Ma, Y.; Li, C. Depolymerization of Lignin via a Non-Precious Ni–Fe Alloy Catalyst Supported on Activated Carbon. *Green Chem.* **2017**, *19* (8), 1895–1903. https://doi.org/10.1039/c7gc00149e.

(105) Ji, N.; Wang, X.; Weidenthaler, C.; Spliethoff, B.; Rinaldi, R. Iron(II) Disulfides as Precursors of Highly Selective Catalysts for Hydrodeoxygenation of Dibenzyl Ether into Toluene. *ChemCatChem* **2015**, *7* (6), 960–966. https://doi.org/10.1002/cctc.201500041.

(106) Villar, J. C.; Caperos, A.; García-Ochoa, F. Oxidation of Hardwood Kraft-Lignin to Phenolic Derivatives. Nitrobenzene and Copper Oxide as Oxidants. *J. Wood Chem. Technol.* **1997**, *17* (3), 259–285. https://doi.org/10.1007/s002260100089.

(107) Ardiyanti, A. R.; Khromova, S. A.; Venderbosch, R. H.; Yakovlev, V. A.; Heeres, H. J. Catalytic Hydrotreatment of Fast-Pyrolysis Oil Using Non-Sulfided Bimetallic Ni-Cu Catalysts on a δ -Al 2 O 3 Support. "*Applied Catal. B, Environ.* **2012**, *117–118*, 105–117. https://doi.org/10.1016/j.apcatb.2011.12.032.

(108) Sinfelt, J. H. Catalysis by Alloys and Bimetallic Clusters. *Acc. Chem. Res.* **1977**, *10* (1), 15–20. https://doi.org/10.1021/ar50109a003.

(109) Connor, R.; Adkins, H. Hydrogenolysis of Oxygenated Organic Compounds. *J. Am. Chem. Soc.* **1932**, *54* (12), 4678–4690. https://doi.org/10.1021/ja01351a026.

(110) Wang, C.; Mironenko, A. V; Raizada, A.; Chen, T.; Mao, X.; Padmanabhan, A.; Vlachos, D. G.; Gorte, R. J.; Vohs, J. M. Mechanistic Study of the Direct Hydrodeoxygenation of M-Cresol over WOx-Decorated Pt/C Catalysts. *ACS Catal.* **2018**, *8*, 7749–7759. https://doi.org/10.1021/acscatal.8b01746.

(111) Bosch, S. Van Den; Renders, T.; Kennis, S.; Koelewijn, S.; Bossche, G. Van Den; Vangeel, T.; Deneyer, A.; Depuydt, D.; Courtin, C. M.; Thevelein, J. M.; et al. Integrating Lignin Valorization and Bio-Ethanol Production: On the Role of Ni-Al2O3 Catalyst Pellets during Lignin-First Fractionation. *Green Chem.* **2017**, *19*, 3313–3326. https://doi.org/10.1039/c7gc01324h.

(112) Renders, T.; Van Den Bosch, S.; Koelewijn, S. F.; Schutyser, W.; Sels, B. F. Lignin-First Biomass Fractionation: The Advent of Active Stabilisation Strategies. *Energy Environ. Sci.* **2017**, *10* (7), 1551–1557. https://doi.org/10.1039/c7ee01298e.

(113) Verboekend, D.; Liao, Y.; Schutyser, W.; Sels, B. F. Alkylphenols to Phenol and

Olefins by Zeolite Catalysis: A Pathway to Valorize Raw and Fossilized Lignocellulose. *Green Chem.* **2016**, *18* (1), 297–306. https://doi.org/10.1039/c5gc01868d.

(114) Ma, H.; Li, H.; Zhao, W.; Li, L.; Liu, S.; Long, J.; Li, X. Selective Depolymerization of Lignin Catalyzed by Nickel Supported on Zirconium Phosphate. *Green Chem.* **2019**, *21* (3), 658–668. https://doi.org/10.1039/c8gc03617a.

(115) Li, T.; Lin, H.; Ouyang, X.; Qiu, X.; Wan, Z. In Situ Preparation of Ru@N-Doped Carbon Catalyst for the Hydrogenolysis of Lignin to Produce Aromatic Monomers. *ACS Catal.* **2019**, *9*, 5828–5836. https://doi.org/10.1021/acscatal.9b01452.

(116) Rautiainen, S.; Di Francesco, D.; Katea, S. N.; Westin, G.; Tungasmita, D. N.; Samec, J. S. M. Lignin Valorization by Cobalt-Catalyzed Fractionation of Lignocellulose to Yield Monophenolic Compounds. *ChemSusChem* **2019**, *12* (2), 404–408. https://doi.org/10.1002/cssc.201802497.

(117) Guo, H.; Zhang, B.; Qi, Z.; Li, C.; Ji, J.; Dai, T.; Wang, A.; Zhang, T. Valorization of Lignin to Simple Phenolic Compounds over Tungsten Carbide: Impact of Lignin Structure. *ChemSusChem* **2017**, *10* (3), 523–532. https://doi.org/10.1002/cssc.201601326.

(118) Cui, X.; Surkus, A.; Junge, K.; Topf, C.; Radnik, J.; Kreyenschulte, C.; Beller, M. Highly Selective Hydrogenation of Arenes Using Nanostructured Ruthenium Catalysts Modified with a Carbon–Nitrogen Matrix. *Nat. Commun.* **2016**, *7*, 1–8. https://doi.org/10.1038/ncomms11326.

(119) Wang, Y.; Ling, L.; Jiang, H. Selective Hydrogenation of Lignin to Produce Chemical Commodities by Using a Biochar Supported Ni–Mo2C Catalyst Obtained from Biomass†. *Green Chem.* **2016**, *18*, 4032–4041. https://doi.org/10.1039/c6gc00247a.

(120) Wan, H.; Chaudhari, R. V.; Subramaniam, B. Aqueous Phase Hydrogenation of Acetic Acid and Its Promotional Effect on P-Cresol Hydrodeoxygenation. *Energy and Fuels* **2012**, *27* (1), 487–493. https://doi.org/10.1021/ef301400c.

(121) McVeigh, A.; Bouxin, F. P.; Jarvis, M. C.; Jackson, S. D. Catalytic Depolymerisation of Isolated Lignin to Fine Chemicals: Part 2-Process Optimisation. *Catal. Sci. Technol.* **2016**, *6* (12), 4142–4150. https://doi.org/10.1039/c5cy01896j.

(122) Dai, J.; Patti, A. F.; Saito, K. Recent Developments in Chemical Degradation of Lignin: Catalytic Oxidation and Ionic Liquids. *Tetrahedron Lett.* **2016**, *57* (45),

4945–4951. https://doi.org/10.1016/j.tetlet.2016.09.084.

(123) Lancefield, C. S.; Ojo, O. S.; Tran, F.; Westwood, N. J. Isolation of Functionalized Phenolic Monomers through Selective Oxidation and CO Bond Cleavage of the β-O-4 Linkages in Lignin. *Angew. Chemie - Int. Ed.* **2015**, *54* (1), 258–262. https://doi.org/10.1002/anie.201409408.

(124) Dawange, M.; Galkin, M. V; Samec, J. S. M. Selective Aerobic Benzylic Alcohol Oxidation of Lignin Model Compounds : Route to Aryl Ketones. *ChemCatChem* **2015**, *7* (3), 401–404. https://doi.org/10.1002/cctc.201402825.

(125) He, W.; Gao, W.; Fatehi, P. Oxidation of Kraft Lignin with Hydrogen Peroxide and Its Application as a Dispersant for Kaolin Suspensions. *ACS Sustain. Chem. Eng.* **2017**, *5* (11), 10597–10605. https://doi.org/10.1021/acssuschemeng.7b02582.

(126) Magallanes, G.; Kärkäs, M. D.; Bosque, I.; Lee, S.; Maldonado, S.; Stephenson, C. R. J. Selective C-O Bond Cleavage of Lignin Systems and Polymers Enabled by Sequential Palladium-Catalyzed Aerobic Oxidation and Visible-Light Photoredox Catalysis. *ACS Catal.* **2019**, *9* (3), 2252–2260. https://doi.org/10.1021/acscatal.8b04172.

(127) Bozell, J. J.; Hames, B. R.; Dimmel, D. R. Cobalt-Schiff Base Complex Catalyzed Oxidation of Para-Substituted Phenolics. Preparation of Benzoquinones. *J. Org. Chem.* **1995**, *60* (8), 2398–2404. https://doi.org/10.1021/jo00113a020.

(128) Min, D.; Xiang, Z.; Liu, J.; Jameel, H.; Chiang, V.; Jin, Y.; Chang, H. M. Improved Protocol for Alkaline Nitrobenzene Oxidation of Woody and Non-Woody Biomass. *J. Wood Chem. Technol.* **2014**, *35* (1), 52–61. https://doi.org/10.1080/02773813.2014.902965.

(129) Maziero, P.; Neto, M. de O.; Machado, D.; Batista, T.; Cavalheiro, C. C. S.; Neumann, M. G.; Craievich, A. F.; Rocha, G. J. de M.; Polikarpov, I.; Gonçalves, A. R. Structural Features of Lignin Obtained at Different Alkaline Oxidation Conditions from Sugarcane Bagasse. *Ind. Crops Prod.* **2012**, *35* (1), 61–69. https://doi.org/10.1016/j.indcrop.2011.06.008.

(130) Villar, J. C.; Caperos, A.; García-Ochoa, F. Oxidation of Hardwood Kraft-Lignin to Phenolic Derivatives with Oxygen as Oxidant. *Wood Sci. Technol.* **2001**, *35* (3), 245–255. https://doi.org/10.1007/s002260100089.

(131) Wang, M.; Liu, M.; Li, H.; Zhao, Z.; Zhang, X.; Wang, F. Dealkylation of Lignin to Phenol via Oxidation–Hydrogenation Strategy. *ACS Catal.* **2018**, *8*, 6837–6843. https://doi.org/10.1021/acscatal.8b00886.

(132) Sales, F. G.; Maranhão, L. C. A.; Lima Filho, N. M.; Abreu, C. A. M. Kinetic

Evaluation and Modeling of Lignin Catalytic Wet Oxidation to Selective Production of Aromatic Aldehydes. *Ind. Eng. Chem. Res.* **2006**, *45* (20), 6627–6631. https://doi.org/10.1021/ie0601697.

(133) Sakata, Y.; Tamaura, Y.; Imamura, H.; Watanabe, M. *Preparation of a New Type of CaSiO 3 with High Surface Area and Property as a Catalyst Support*; Elsevier Masson SAS, 2006; Vol. 162. https://doi.org/10.1016/S0167-2991(06)80924-9.

(134) Chorkendorff, I.; Niemantsverdriet, J. W. *Concepts of Modern Catalysis and Kinetics*, 3rd, Compl ed.; Wiley-VCH, 2013.

(135) Zhang, X.; Tang, W.; Zhang, Q.; Wang, T.; Ma, L. Hydrodeoxygenation of Lignin-Derived Phenoic Compounds to Hydrocarbon Fuel over Supported Ni-Based Catalysts. *Appl. Energy* **2018**, *227*, 73–79. https://doi.org/10.1016/j.apenergy.2017.08.078.

(136) Jung, K. Bin; Lee, J.; Ha, J. M.; Lee, H.; Suh, D. J.; Jun, C. H.; Jae, J. Effective Hydrodeoxygenation of Lignin-Derived Phenols Using Bimetallic RuRe Catalysts: Effect of Carbon Supports. *Catal. Today* **2018**, *303*, 191–199. https://doi.org/10.1016/j.cattod.2017.07.027.

(137) Dongil, A. B.; Ghampson, I. T.; García, R.; Fierro, J. L. G.; Escalona, N. Hydrodeoxygenation of Guaiacol over Ni/Carbon Catalysts: Effect of the Support and Ni Loading †. *RSC Adv.* **2016**, *6* (4), 2611–2623. https://doi.org/10.1039/c5ra22540j.

(138) Narani, A.; Chowdari, R. K.; Cannilla, C.; Bonura, G.; Frusteri, F.; Heeres, H. J.; Barta, K. Efficient Catalytic Hydrotreatment of Kraft Lignin to Alkylphenolics Using Supported NiW and NiMo Catalysts in Supercritical Methanol†. *Green Chem.* **2015**, *17*, 5046–5057. https://doi.org/10.1039/c5gc01643f.

(139) Ma, D.; Lu, S.; Liu, X.; Guo, Y.; Wang, Y. Depolymerization and Hydrodeoxygenation of Lignin to Aromatic Hydrocarbons with a Ru Catalyst on a Variety of Nb-Based Supports. *Chinese J. Catal.* **2019**, *40* (4), 609–617. https://doi.org/10.1016/S1872-2067(19)63317-6.

(140) Zhang, B.; Qi, Z.; Li, X.; Ji, J.; Luo, W.; Li, C.; Wang, A.; Zhang, T. ReOx/AC-Catalyzed Cleavage of C-O Bonds in Lignin Model Compounds and Alkaline Lignins. *ACS Sustain. Chem. Eng.* **2019**, *7* (1), 208–215. https://doi.org/10.1021/acssuschemeng.8b02929.

(141) Rouquerol, J.; Baron, G.; Denoyel, R.; Giesche, H.; Groen, J.; Klobes, P.; Levitz, P.; Neimark, A. V; Rigby, S.; Skudas, R.; et al. Recommendations for the Characterization of Porous Solids. *Pure Appl. Chem.* **1994**, *66* (8), 1739–1758. https://doi.org/10.1351/pac199466081739.

(142) Yu, Y.; Li, X.; Su, L.; Zhang, Y.; Wang, Y.; Zhang, H. The Role of Shape Selectivity in Catalytic Fast Pyrolysis of Lignin with Zeolite Catalysts. *Appl. Catal. A Gen.* **2012**, *447–448*, 115–123. https://doi.org/10.1016/j.apcata.2012.09.012.

(143) Luo, Z.; Wang, S.; Guo, X. Selective Pyrolysis of Organosolv Lignin over Zeolites with Product Analysis by TG-FTIR. *J. Anal. Appl. Pyrolysis* **2012**, *95*, 112–117. https://doi.org/10.1016/j.jaap.2012.01.014.

(144) Sudarsanam, P.; Peeters, E.; Makshina, E. V.; Parvulescu, V. I.; Sels, B. F. Advances in Porous and Nanoscale Catalysts for Viable Biomass Conversion. *Chem. Soc. Rev.* **2019**, *48* (8), 2366–2421. https://doi.org/10.1039/c8cs00452h.

(145) Neumann, G. T.; Hicks, J. C. Novel Hierarchical Cerium-Incorporated MFI Zeolite Catalysts for the Catalytic Fast Pyrolysis of Lignocellulosic Biomass. *ACS Catal.* **2012**, *2*, 642–646. https://doi.org/10.1021/cs200648q.

(146) Neumann, G. T.; Pimentel, B. R.; Rensel, D. J.; Hicks, J. C. Catalysis Science & Technology in the Catalytic Fast Pyrolysis of Lignin Model Compounds Containing β – O – 4 Linkages †. *Catal. Letters* **2014**, *4*, 3953–3963. https://doi.org/10.1039/c4cy00569d.

(147) Rinaldi, R.; Sch, F. Design of Solid Catalysts for the Conversion of Biomass. *Energy Environ. Sci.* **2009**, *2* (6), 610–626. https://doi.org/10.1039/b902668a.

(148) Wang, W.; Wu, K.; Tan, S.; Yang, Y. Hydrothermal Synthesis of Carbon-Coated CoS 2 − MoS 2 Catalysts with Enhanced Hydrophobicity and Hydrodeoxygenation Activity. *ACS Sustain. Chem. Eng.* **2017**, *5* (10), 8602–8609. https://doi.org/10.1021/acssuschemeng.7b01087.

(149) Wang, X.; Rinaldi, R. Solvent Effects on the Hydrogenolysis of Diphenyl Ether with Raney Nickel and Their Implications for the Conversion of Lignin. *ChemSusChem* **2012**, *5* (8), 1455–1466. https://doi.org/10.1002/cssc.201200040.

(150) Xiao, L.; Wang, S.; Li, H.; Li, Z.; Shi, Z.; Xiao, L.; Sun, R.; Fang, Y.; Song, G. Catalytic Hydrogenolysis of Lignins into Phenolic Compounds over Carbon Nanotube Supported Molybdenum Oxide. *ACS Catal.* **2017**, *7*, 7535–7542. https://doi.org/10.1021/acscatal.7b02563.

(151) Huang, X.; Atay, C.; Korányi, T. I.; Boot, M. D.; Hensen, E. J. M. Role of Cu-Mg-Al Mixed Oxide Catalysts in Lignin Depolymerization in Supercritical Ethanol. *ACS Catal.* **2015**, *5* (12), 7359–7370. https://doi.org/10.1021/acscatal.5b02230.

(152) Ma, X.; Ma, R.; Hao, W.; Chen, M.; Yan, F.; Cui, K.; Tian, Y.; Li, Y. Common Pathways in Ethanolysis of Kraft Lignin to Platform Chemicals over

Molybdenum-Based Catalysts. *ACS Catal.* **2015**, *5*, 4803–4813. https://doi.org/10.1021/acscatal.5b01159.

(153) Kramm, U. I.; Marschall, R.; Rose, M. Pitfalls in Heterogeneous Thermal, Electro- and Photocatalysis. *ChemCatChem* **2019**, *11* (11), 2563–2574. https://doi.org/10.1002/cctc.201900137.

(154) Schüth, F.; Ward, M. D.; Buriak, J. M. Common Pitfalls of Catalysis Manuscripts Submitted to Chemistry of Materials. *Chem. Mater.* **2018**, *30* (11), 3599–3600. https://doi.org/10.1021/acs.chemmater.8b01831.

(155) Dimitratos, N.; Villa, A.; Prati, L. Liquid Phase Oxidation of Glycerol Using a Single Phase (Au-Pd) Alloy Supported on Activated Carbon: Effect of Reaction Conditions. *Catal. Letters* **2009**, *133* (3–4), 334–340. https://doi.org/10.1007/s10562-009-0192-8.

(156) Zhang, J.; Asakura, H.; Rijn, J. Van; Yang, J.; Duchesne, P.; Zhang, B.; Chen, X.; Zhang, P.; Saeys, M.; Yan, N. Highly Efficient, NiAu-Catalyzed Hydrogenolysis of Lignin into Phenolic Chemicals. *Green Chem.* **2014**, *16*, 2432–2437. https://doi.org/10.1039/c3gc42589d.

(157) Chen, L.; Kora, I.; Hensen, E. J. M. Transition Metal (Ti, Mo, Nb, W) Nitride Catalysts for Lignin Depolymerisation †. *Chem. Commun.* **2016**, *52* (60), 9375–9378. https://doi.org/10.1039/c6cc04702e.

(158) Kumaniaev, I.; Subbotina, E.; Sävmarker, J.; Larhed, M.; Galkin, M. V; Samec, J. S. M. Lignin Depolymerization to Monophenoliccompounds in a Flow-through System. *Green Chem.* **2017**, *19* (24, 2017), 5767–5771. https://doi.org/10.1039/c7gc02731a.

(159) Nandiwale, K.; Danby, A.; Anand, R.; Chaudhari, R.; Subramaniam, B. Dual Function Lewis Acid Catalyzed Depolymerization of Industrial Corn Stover Lignin into Stable Monomeric Phenols. *ACS Sustain. Chem. Eng.* **2018**, *7*, 1362–1371. https://doi.org/10.1021/acssuschemeng.8b05077.

(160) Warner, G.; Hansen, T. S.; Riisager, A.; Beach, E. S.; Barta, K.; Anastas, P. T. Depolymerization of Organosolv Lignin Using Doped Porous Metal Oxides in Supercritical Methanol. *Bioresour. Technol.* **2014**, *161*, 78–83. https://doi.org/10.1016/j.biortech.2014.02.092.

(161) Parsell, T. H.; Owen, B. C.; Klein, I.; Jarrell, T. M.; Marcum, C. L.; Haupert, L. J.; Amundson, L. M.; Ribeiro, F.; Kenttamaa, H. I.; Miller, T. J.; et al. Cleavage and Hydrodeoxygenation (HDO) of C–O Bonds Relevant to Lignin Conversion Using Pd/Zn Synergistic Catalysis. *Chem. Sci.* **2013**, *4*, 806–813. https://doi.org/10.1039/c2sc21657d.

(162) Zhao, C.; Kou, Y.; Lemonidou, A. A.; Li, X.; Lercher, J. A. Highly Selective Catalytic Conversion of Phenolic Bio-Oil to Alkanes. *Angew. Chemie - Int. Ed.* **2009**, *48*, 3987–3990. https://doi.org/10.1002/anie.200900404.

(163) Zhang, W.; Chen, J.; Liu, R.; Wang, S.; Chen, L.; Li, K. Hydrodeoxygenation of Lignin-Derived Phenolic Monomers and Dimers to Alkane Fuels over Bifunctional Zeolite-Supported Metal Catalysts. *ACS Sustain. Chem. Eng.* **2014**, *2*, 683–691. https://doi.org/10.1021/sc400401n.

(164) Liu, X.; Jia, W.; Xu, G.; Zhang, Y.; Fu, Y. Selective Hydrodeoxygenation of Lignin-Derived Phenols to Cyclohexanols over Co-Based Catalysts. *ACS Sustain. Chem. Eng.* **2017**, *5*, 8594–8601. https://doi.org/10.1021/acssuschemeng.7b01047.

(165) Bykova, M. V; Ermakov, D. Y.; Kaichev, V. V; Bulavchenko, O. A.; Saraev, A. A.; Lebedev, M. Y.; Yakovlev, V. A. Environmental Ni-Based Sol – Gel Catalysts as Promising Systems for Crude Bio-Oil Upgrading : Guaiacol Hydrodeoxygenation Study. *"Applied Catal. B, Environ.* **2012**, *113–114*, 296–307. https://doi.org/10.1016/j.apcatb.2011.11.051.

(166) Konnerth, H.; Zhang, J.; Ma, D.; Prechtl, M. H. G.; Yan, N. Base Promoted Hydrogenolysis of Lignin Model Compounds and Organosolv Lignin over Metal Catalysts in Water. *Chem. Eng. Sci.* **2015**, *123*, 155–163. https://doi.org/10.1016/j.ces.2014.10.045.

Chapter 5 Alternative Idle Resource Projects

5.1 Abstract

Idle resource conversion has many approaches to finding solutions. This chapter discusses Soxhlet extraction, polyvinyl chloride (PVC) upcycling and biochar derived from orange peel. Soxhlet extraction of algae to produce bio-oil derived from nannochloropsis and chlorella strands was found to be ineffective. However, the use of Soxhlet extraction was found to be useful in the removal of bio-oils from biochar as well as creating a potentially upgraded precursor to activated carbon for the adsorption of vanillin.

Dehydrochlorination is an important step to PVC plastic upcycling as it removes the chlorine, a toxic compound which poses many challenges when working with PVC. Temperatures lower than 400 °C will be important for dechlorination as that is when the majority of HCl gas comes off due to thermal degradation. The combination of La_2O_3 and silica alumina catalyst allowed for HCl to be removed a lower temperature range starting at 210 °C. Lower temperatures will allow for less energy required to dechlorinate which can translate to lower costs.

Scale up of biochar production allowed production to go from 1g to 40g per run using a Parr reactor. Using a 300 mL vessel at 250 C for 1 hour dwell time allowed for a 53% recovery of biochar from initial feedstock of dried orange peel. The biochar will be probed from soil amendment and plant growth by the Pagliaccia lab.

5.2 Introduction

Multiple methods need to be explored to fully utilize idle resources. In this chapter, Soxhlet extraction, polyvinyl chloride (PVC) upcycling, and orange peel biochar are researched. The current dependence on fossil fuels is an unsustainable practice. Algae oil

has been researched to produce biodiesel which can be an alternative to fossil fuels[1,2]. Algae has the potential to produce more oil per acre than any other feedstock being used to produce biodiesel[3]. Algae is an underutilized resource with great potential to solve many challenges facing the world. Algae oil can be extracted with n-hexane as the solvent and then be upgraded to produce biodiesel[3,4]. Soxhlet extraction is a technique where solvent is continuously leaching from the sample and recirculating through boiling and condensing[5]. Soxhlet extraction has been used for algae oil extraction[4]. However, Soxhlet extraction has other applications. During the production of biochar, bio-oils can be trapped inside the pores and the oils may contain polycyclic aromatic hydrocarbons (PAHs)[6]. Utilizing a combination of polar and nonpolar solvents have been employed at removing oils[6,7]. This has also been shown to produce upgraded activated carbon.

Besides combining plastic and biomass to utilize waste plastic, one can look to upcycle plastic by itself. Polyvinyl chloride (PVC) is the third most produced plastic in the world[8]. Plastic recycling faces many challenges that make it uneconomical and thus not a feasible strategy to reducing our plastic pollution. The chlorine in PVC makes it particularly challenging to work with and recycle as it creates toxic emissions[9]. PVC is heavily saturated with chlorine, 58%, and this chlorine can produce toxic emissions like HCl[10]. These toxic emissions can harm human health and have adverse effects to the environment thus causing significant concern. Removing the chlorine needs to be one of the first steps to work safely and reuse PVC. Catalytic de(hydro)chlorination of PVC is viewed as a potential practical way to remove the chlorine. Some of the challenges associated with catalytic dechlorination include chlorine poisoning leading to deactivated

catalysts, low product selectivity, and high cost of precious metals that some catalysts utilize. Bimetallic alloys on catalysts can create a synergistic effect that can improve not only conversion but selectively as well[11]. Once the chlorine has been removed, the PVC can then be turned into numerous products. One of the potential products is jet fuel, which primarily consists of hydrocarbons, namely: C_9-C_{16} paraffins, naphthenes, aromatics, and olefins[12].

The final portion of this chapter is the carbonization of orange peels into biochar for plant growth. In California, citrus production is valued at 3.6 billion USD[13]. The citrus peel is agricultural waste in the production of citrus and juicing. During citrus processing, 50-60% of the citrus is consider waste[14]. Utilization of local wastes can help reduce transportation pollution and provide an economic benefit for the community. Biochar has been demonstrated as a soil amendment with its ability to suppress disease, remediate heavy metals and organic pollutants, and revitalize soil properties[15–17]. Biochar from orange peels will be researched for soil amendment.

5.3 Materials and Methods

5.3.1 Solvent Extraction

A Soxhlet Extraction was setup with a glass thimble to hold the feedstock. 150 mL of solvents were added to a 250 mL round bottom flask which was heated to the solvent's boiling point. A condensing unit was attached to the extracting unit to allow for a continuous leaching process. For the algae oil extraction, 50 g of algae powder, either nannochloropsis or chlorella, was added to the glass thimble- filled completely. Extraction of algae oil used Hexanes as the solvent for 4 hours. Solvent was rotovaped to collect algae

oil. Soxhlet extraction of the bio-oil from biochar involved sequential solvent extraction. The order began with hexanes (non-polar solvent), followed by a mixture of hexanes and ethanol (1:1), and finished up with ethanol (polar solvent). Each solvent ran for 3 hours and was rotovaped afterwards to collect the bio-oil. The solid char was dried in an oven at 105 °C overnight.

5.3.2 PVC Dechlorination and Upgrading

A Hidden Analytical CATLAB-PCS with attached QGA is used for the PVC Dechlorination experiments. PVC in a powder form is utilized in 100 mg batches and will be combined with the catalyst. Multiple catalysts will be studied, with a comparison between basic supports like La_2O_3, and acidic supports like silica alumina. The supports will be wet impregnated with metals including Ni, Fe, and Pd. After the reaction run has occurred, the spent catalyst and remaining PVC will be collected and characterized. The CATLAB microreactor has a mass spectrometer downstream and will be able to analyze the gases released in real time. This will allow us to study the hydrocarbons and chlorine species that are removed. The catalysts and absorbent materials will be characterized using XRD, BET, STEM, and NH_3 temperature programmed desorption (TPD).

5.3.3 Orange Peel Biochar

A 300 mL Series 4561 Bench Parr Reactor was used for the orange peel biochar experiments. Orange peel was sourced from the juicing production at Gless Ranch in Riverside, CA. Orange peel was dried in a dehydrator for 8.5 hours at 65 °C. 75 g of dried orange peel was put into the reactor and purged with nitrogen for 10 minutes. The reactor was heated to 250 °C and held for 1 hour. Once finished, the reactor was submerged in ice

water to stop the reaction. The biochar was rinsed with a 1:1 mixture of hexanes and ethanol and vacuumed filtered to remove excess biooil. The biochar was then rinsed with water and dried overnight in an oven at 105 °C.

5.4 Results and Discussion

5.4.1 Soxhlet Extraction

Algae oil extraction was the original purpose of using Soxhlet extraction in the lab. High lipid algae were going to be extracted by hexanes; however, when tested with *Nannochloropsis* algae, high lipid algae[18], the amount of oil was minimal. Another high lipid algae, *Chlorella*[19], was extracted with hexanes, but produced the same results. Not enough oil could be produced with a full thimble. A previous study with *Chlorella vulgaris* extracted a yield of 61% oil[4]. The setup was unable to produce any result remotely close to that. A potential reason for this is Abdulah et. al cultured the algae then freeze dried where the algae used in the experiments were commercially dried. Though the knowledge of Soxhlet extraction would prove useful in different experiments.

Soxhlet extraction was experimented with for creating an upgraded biochar and activated carbon in the co-pyrolysis experiments. Biochar from CSPS was extracted with sequential solvent extraction of hexanes and ethanol. Pure hexane was the first solvent in the experiment and no color change was observed in the solvent. This indicated no bio-oil was extracted. The 1:1 ratio of hexanes and ethanol followed, and a dark color was observed in the solvent which indicates the leaching of bio-oil. Then pure ethanol was used which showed no color change during extraction. Previous work indicated increasing polarity during sequential solvent extraction can provide better removal of pyrolysis oil[7].

174

The experiment conducted indicated the mixture of hexanes and ethanol provided the best medium for bio-oil extraction. Table 5.1 shows the surface area of the biochar and activated carbon before and after Soxhlet extraction. The extracted biochar was chemically activated following the same procedure as the non-extracted biochar. The surface area of the biochar and activated increased slightly with extraction. Also, pore size slightly increased. This maybe be due to the removal of ash and bio-oil that could have partially blocked pores. However, this difference is marginally and is within error tolerance. Vanillin adsorption tests showed a larger difference. AC was probed for adsorption with contaminated water of 100 mg/L vanillin concentration. 50 mg of AC was mixed with 50 mL of the contaminated water for the desired time frame. The AC 500 2h 4:1 ratio CSPS removed less than 40% of the contaminates at 30 minutes, 1 hour, and 2 hours. The concentration of vanillin leftover was too high for the machine to read accurately. However, when the Soxhlet extracted AC made from the same biochar precursor was tested, the 1-hour run adsorption reduce the contamination by 59% and the 2-hours run by 63%. Surface functional groups often play a significant role in adsorption of vanillin[20]. The removal of the bio-oil and ash from the biochar prior to activation may have changed the functional groups. FTIR could be used to probe this theory; however, due to the scope of the project further research was not conducted. The use of Soxhlet extraction to improve adsorption properties has potential for future work; the explanation and study of the physiochemical properties can be researched.

175

5.4.2 PVC Degradation

Figure 5.1a shows the thermal degradation of PVC with a focus on HCl and Benzene fractions. The initial data on thermal degradation of PVC shows at 280 °C chlorine starts to be removed at HCl. The majority of the HCl gas found is prior to 400 °C, indicating that range is going to be important to dechlorination. While there is some Cl_2, vinyl chloride, and carbon tetrachloride detected these have relatively low values compared to HCl. The chain of PVC is also starting to break down as benzene and propane are coming off at 250 °C and 220 °C, respectively.

Figure 5.1b shows the isothermal degradation of PVC at 300 ℃ and 400 ℃ for 30 minutes, respectively. HCl is a primary product of thermal cracking and is the major chloro-species that comes off. When solely PVC, HCl comes off between 250 ℃ and 300 ℃. When La_2O_3 is added, 1:1 ratio, the amount of HCl comes off is reduced, however, it comes off at a higher temperature 260 ℃ to 300 ℃. Though when combined with silica alumina and La_2O_3, the HCl starts to come off around 210 ℃. A grant proposal was submitted for this work; however, this was not funded thus not continued. PVC upcycling will play an important role in the solution of plastic waste.

5.4.3 Orange Peel Biochar

The biochar for orange peel is a collaboration project with the Pagliaccia's Lab. The Abdul-Aziz lab will produce the biochar from orange peels, while the Pagliaccia's lab will probe the biochar for soil amendment while ensuring active growth. The goal was to produce 2 kg of biochar for plant growth testing, which is significant scale up for biochar

production. The original setup for biochar was producing around 1-2g of biochar per run and to meet the needs of the project, scale up was needed.

The scale up would be comprised of multiple parameters including temperature, duration, and volume of the reactor. From corn stover experiments, a lower temperature will increase the output of biochar[20]. At 250 °C, the biochar accounts for 53% of the original dried orange peel mass whereas higher temperatures such as 500 °C more the biomass would be converted to gas and liquid phases. For corn stover experiments, this can be seen when temperature was probed, at 400 °C 33.4% of biochar was recovered whereas at 500 °C 29.1% was recovered. For duration, a similar trend was observed, where longer durations would cause for more of the biomass to be converted to the gas and liquid phase. A duration of 1 hour was chosen to ensure carbonization but maximize production. For volume, a larger vessel will allow for more production. A Parr reactor with a volume of 300 mL was employed to increase production. After experimenting, the Parr reactor setup could produce 40g of biochar at 250 °C and 1 hour dwell.

The bio-oil is separated with a 1:1 mixture of hexanes and ethanol. Hexanes (nonpolar) and ethanol (polar) are combined due to previous research on sequential solvent extraction of corn stover biochar using Soxhlet extraction, showing improved removal of bio-oil. This project is ongoing and can be used as a project for another graduate student in the Abdul-Aziz lab. At time of this dissertation, the Pagliaccia's lab will be probing for plant growth and soil amendment. Future work will involve employing larger reactor sizes to improve scale up and probing physiochemical properties of the biochar and relating to soil amendment.

5.5 Conclusion

Soxhlet extraction, PVC dehydrochlorination, and orange peel biochar experiments were conducted; however, they were not pursed for various reasons including not securing funding. Soxhlet extraction was found to be ineffective for algae oil extraction, but useful for bio-oil removal in biochar. PVC dehydrochlorination may play a crucial role in upcycling PVC. Orange peel biochar production was scaled up and will be tested for plant growth and soil amendment. Each of these projects can be developed further by future graduate students.

5.6 Conflict of Interest

There are no conflicts of interest to declare.

5.7 Acknowledgements

5.8 Figures and Tables
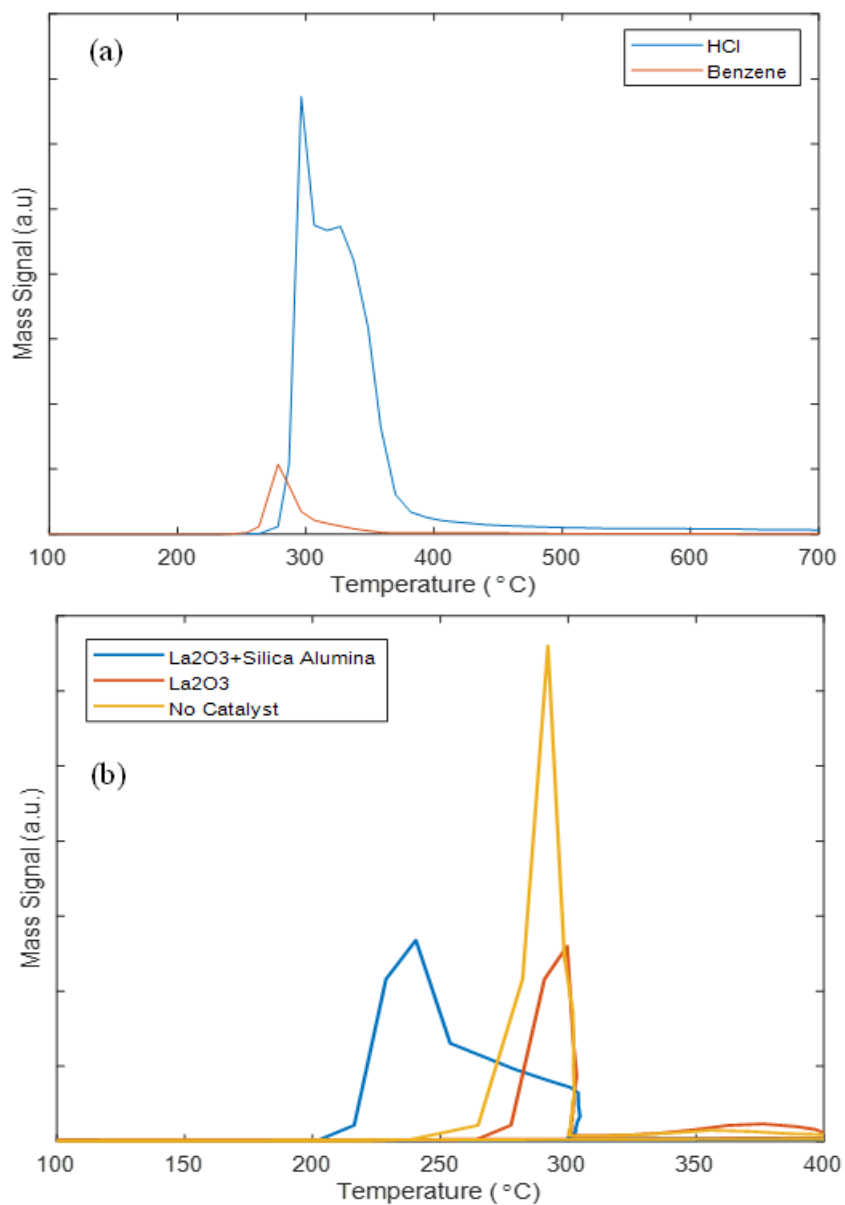
Figure 5.1 (a) Thermal degradation of PVC to 700 °C. (b) Formation of HCl from PVC in a two-stage study. First stage 300 °C and second stage 400 °C each for 30 minutes

Table 5.1 Surface area and pore size of biochar and activated carbon with and without Soxhlet extraction treatment

Sample 500 °C 2h 4:1 ratio CSPS	Surface Area (m^2/g)	Pore Size (nm)
Biochar	8.9	29.6
Soxhlet Biochar	9.8	30.0
AC	477.0	4.1
AC Soxhlet	497.9	4.4

5.9 References

(1)   Giridharan, R.; Rajan, A. V.; Krishnan, B. R. Performance and Emission
       Characteristics of Algae Oil in Diesel Engine. *Mater. Today Proc.* **2021**, *37*, 576–
       579. https://doi.org/10.1016/j.matpr.2020.05.591.

(2)   Haik, Y.; Selim, M. Y. E.; Abdulrehman, T. Combustion of Algae Oil Methyl
       Ester in an Indirect Injection Diesel Engine. *Energy* **2010**, *36* (3), 1827–1835.
       https://doi.org/10.1016/j.energy.2010.11.017.

(3)   Demirbas, A.; Demirbas, M. F. Importance of Algae Oil as a Source of Biodiesel.
       Energy Convers. Manag. **2011**, *52* (1), 163–170.
       https://doi.org/10.1016/j.enconman.2010.06.055.

(4)   Abdullah, N.; Amran, N. A.; Yasin, N. H. M. ALGAE OIL EXTRACTION
       FROM FRESHWATER MICROALGAE Chlorella Vulgaris. *Malaysian J. Anal.
       Sci.* **2017**, *21* (3), 735–744.

(5)   Castro, M. D. L. De; Priego-Capote, F. Soxhlet Extraction : Past and Present
       Panacea. *J. Chromatogr. A* **2010**, *1217* (16), 2383–2389.
       https://doi.org/10.1016/j.chroma.2009.11.027.

(6)   Fabbri, D.; Rombolà, A. G.; Torri, C.; Spokas, K. A. Determination of Polycyclic
       Aromatic Hydrocarbons in Biochar and Biochar Amended Soil. *J. Anal. Appl.
       Pyrolysis* **2013**, *103*, 60–67. https://doi.org/10.1016/j.jaap.2012.10.003.

(7)   Bernardo, M.; Lapa, N.; Gonçalves, M.; Mendes, B.; Pinto, F.; Fonseca, I.; Lopes,
       H. Physico-Chemical Properties of Chars Obtained in the Co-Pyrolysis of Waste
       Mixtures. *J. Hazard. Mater.* **2012**, *219–220*, 196–202.
       https://doi.org/10.1016/j.jhazmat.2012.03.077.

(8)   Halsband, C.; Allan, I. J.; Thomas, K. V. *Report Made for the Norwegian
       Environment Agency : Microplastics in Marine Microplastics in Marine
       Environments : Occurrence , Distribution and Effects*; 2014.

(9)   Stec, A. A.; Readman, J.; Blomqvist, P.; Gylestam, D.; Karlsson, D.; Wojtalewicz,
       D.; Dlugogorski, B. Z. Chemosphere Analysis of Toxic Effluents Released from
       PVC Carpet under Different Fire Conditions. *Chemosphere* **2013**, *90* (1), 65–71.
       https://doi.org/10.1016/j.chemosphere.2012.07.037.

(10)   Verma, R.; Vinoda, K. S.; Papireddy, M.; Gowda, A. N. S. Toxic Pollutants from
       Plastic Waste- A Review. *Procedia Environ. Sci.* **2016**, *35*, 701–708.
       https://doi.org/10.1016/j.proenv.2016.07.069.

(11)   Gale, M.; Cai, C. M.; Gilliard-Abdul-Aziz, K. L. Heterogeneous Catalyst Design

Principles for the Conversion of Lignin into High-Value Commodity Fuels and Chemicals. *ChemSusChem* **2020**, *13* (8), 1947–1966. https://doi.org/10.1002/cssc.202000002.

(12)   Pires, A. P. P.; Han, Y.; Kramlich, J.; Garcia-Perez, M. Chemical Composition and Fuel Properties of Alternative Jet Fuels. *BioResources* **2018**, *13* (2), 2632–2657.

(13)   Babcock, B. A. Economic Impact of California's Citrus Industry in 2020. *J. Citrus Pathol.* **2022**, *9* (1), 0–18. https://doi.org/10.5070/c49156433.

(14)   Raimondo, M.; Caracciolo, F.; Cembalo, L.; Chinnici, G.; Pecorino, B.; D'Amico, M. Making Virtue Out of Necessity: Managing the Citrus Waste Supply Chain for Bioeconomy Applications. *Sustainability* **2018**, *10* (12), 4821. https://doi.org/10.3390/su10124821.

(15)   Jaiswal, A. K.; Elad, Y.; Graber, E. R.; Frenkel, O. Rhizoctonia Solani Suppression and Plant Growth Promotion in Cucumber as Affected by Biochar Pyrolysis Temperature, Feedstock and Concentration. *Soil Biol. Biochem.* **2014**, *69*, 110–118. https://doi.org/10.1016/j.soilbio.2013.10.051.

(16)   Jaiswal, A. K.; Frenkel, O.; Elad, Y.; Lew, B.; Graber, E. R. Non-Monotonic Influence of Biochar Dose on Bean Seedling Growth and Susceptibility to Rhizoctonia Solani: The "Shifted Rmax-Effect." *Plant Soil* **2015**, *395* (1–2), 125–140. https://doi.org/10.1007/s11104-014-2331-2.

(17)   Tang, J.; Zhu, W.; Kookana, R.; Katayama, A. Characteristics of Biochar and Its Application in Remediation of Contaminated Soil. *J. Biosci. Bioeng.* **2013**, *116* (6), 653–659. https://doi.org/10.1016/j.jbiosc.2013.05.035.

(18)   Cheng, F.; Cui, Z.; Mallick, K.; Nirmalakhandan, N.; Brewer, C. E. Hydrothermal Liquefaction of High- and Low-Lipid Algae: Mass and Energy Balances. *Bioresour. Technol.* **2018**, *258* (February), 158–167. https://doi.org/10.1016/j.biortech.2018.02.100.

(19)   Li, Z. S.; Yuan, H. L.; Yang, J. S.; Li, B. Z. Optimization of the Biomass Production of Oil Algae Chlorella Minutissima UTEX2341. *Bioresour. Technol.* **2011**, *102* (19), 9128–9134. https://doi.org/10.1016/j.biortech.2011.07.004.

(20)   Gale, M.; Nguyen, T.; Moreno, M.; Gilliard-AbdulAziz, K. L. Physiochemical Properties of Biochar and Activated Carbon from Biomass Residue: Influence of Process Conditions to Adsorbent Properties. *ACS Omega* **2021**, *6* (15), 10224–10233. https://doi.org/10.1021/acsomega.1c00530.

Chapter 6 Conclusion

Conclusion

The overall goal of this research is to analyze different techniques to convert idle resources into value added products. This dissertation focused on the thermal and chemical conversion agricultural and plastic waste into biochar and activated carbon. Hydrothermal Carbonization (HTC) and Slow Pyrolysis (SP) of corn stover were evaluated for the physiochemical properties of the biochar produced. The physiochemical properties of the biochar were further probed during the chemical activation to produce Activated Carbon (AC). Application testing of vanillin adsorption were conducted on the AC produced from HTC, SP, and the direct method. The direct method AC performed the best for the adsorption of vanillin followed by the AC HTC and lastly the AC SP. Properties like surface area, surface function groups, pore size, and pore structure influenced the adsorptive properties. The objective of evaluating the physicochemical properties of biochar and activated carbon from corn stover was completed successfully. The AC produced is a valuable product that can have applications in the water treatment industry.

Co-pyrolysis of corn stover and plastics was evaluated for the physiochemical properties of the biochar and activated carbon. Polystyrene and PET plastics are two common plastics that pose challenges to reuse. PS acts as a hydrogen donor during co-pyrolysis and produces a low oxygen content biochar. Once activated, the surface area and vanillin adsorption performance are worse than AC CS. The biochar of CS-PET produced high surface area; however, microplastics were found on the surface. Thermal degradation produces acids like benzoic acid and polymers, which are attributed with the high surface area of the biochar. When chemically activated with KOH the products of thermal

184

degradation of PET would react with each other creating a lower surface area AC. When the AC CS-PS, CS-PET, and AC CS were compared, the AC-CS had the highest surface area and best vanillin adsorption performance. Co-pyrolysis of corn stover and PS or PET did not produce a beneficial precursor.

A literature review was conducted on heterogenous catalysts for lignin valorization. Full biomass utilization will help build a circular bioeconomy and lignin is a key factor in that goal. Lignin is often considered a waste stream and left unused. This review discusses catalytic design principles and strategies to convert lignin. While utilization of lignin still has many milestones ahead, significant progress has been made with precious metals like Ru and Pd. Bimetallic alloys on catalysts have shown promise as well.

Three other idle resource projects were researched: Soxhlet extraction, PVC upcycling, and orange peel biochar. Soxhlet extraction was conducted on algae and CS-PS biochar for the removal of bio-oils. The algae extraction was unsuccessful, but the biochar extraction showed promise. Further research on the benefits of Soxhlet extraction is needed to determine the viability of producing upgraded biochar as a precursor for activated carbon adsorption applications. Dehydrochlorination will play an important role in PVC upcycling. La_2O_3 and silica alumina showed initial results of lowering the temperature that HCl gas would come off due to thermal decomposition. Lowering the temperature could provide lower cost pathways to PVC upcycling and additional research will be required. Biochar from orange peels was produced for the applications of soil amendment and plant growth. The application testing is being conducted by another research group and is on-

going. The biochar production utilized scale up principles and has promise to be a section

in another graduate student's research.